

# Review of pulsed power-driven high energy density physics research on Z at Sandia <sup>EP</sup>

Cite as: Phys. Plasmas **27**, 070501 (2020); <https://doi.org/10.1063/5.0007476>

Submitted: 17 March 2020 . Accepted: 18 May 2020 . Published Online: 08 July 2020

D. B. Sinars <sup>id</sup>, M. A. Sweeney, C. S. Alexander, D. J. Ampleford <sup>id</sup>, T. Ao, J. P. Apruzese, C. Aragon, D. J. Armstrong <sup>id</sup>, K. N. Austin, T. J. Awe, A. D. Baczewski, J. E. Bailey, K. L. Baker <sup>id</sup>, C. R. Ball, H. T. Barclay <sup>id</sup>, S. Beatty, K. Beckwith, K. S. Bell <sup>id</sup>, J. F. Benage, N. L. Bennett <sup>id</sup>, K. Blaha, D. E. Bliss, J. J. Boerner, C. J. Bourdon, B. A. Branch, J. L. Brown <sup>id</sup>, E. M. Campbell <sup>id</sup>, R. B. Campbell, D. G. Chacon, G. A. Chandler, K. Chandler <sup>id</sup>, P. J. Christenson, M. D. Christison, E. B. Christner, R. C. Clay, K. R. Cochrane, A. P. Colombo, B. M. Cook, C. A. Coverdale, M. E. Cuneo, J. S. Custer, A. Dasgupta, J.-P. Davis <sup>id</sup>, M. P. Desjarlais, D. H. Dolan, J. D. Douglass, G. S. Dunham, S. Duwal, A. D. Edens, M. J. Edwards, E. G. Evstatiev, B. G. Farfan, J. R. Fein <sup>id</sup>, E. S. Field, J. A. Fisher, T. M. Flanagan <sup>id</sup>, D. G. Flicker, M. D. Furnish, B. R. Galloway <sup>id</sup>, P. D. Gard, T. A. Gardiner, M. Geissel <sup>id</sup>, J. L. Giuliani, M. E. Glinsky, M. R. Gomez <sup>id</sup>, T. Gomez, G. P. Grim <sup>id</sup>, K. D. Hahn, T. A. Hail <sup>id</sup>, N. D. Hamlin <sup>id</sup>, J. H. Hammer, S. B. Hansen, H. L. Hanshaw, E. C. Harding, A. J. Harvey-Thompson, D. Headley, M. C. Herrmann, M. H. Hess, C. Highstrete, O. A. Hurricane <sup>id</sup>, B. T. Hutsel <sup>id</sup>, C. A. Jennings, O. M. Johns, D. Johnson, M. D. Johnston, B. M. Jones, M. C. Jones <sup>id</sup>, P. A. Jones, P. E. Kalita, R. J. Kamm, J. W. Kellogg, M. L. Kiefer, M. W. Kimmel, P. F. Knapp <sup>id</sup>, M. D. Knudson, A. Kreft, G. R. Laity, P. W. Lake, D. C. Lamppa, W. L. Langston, J. S. Lash, K. R. LeChien, J. J. Leckbee, R. J. Leeper <sup>id</sup>, G. T. Leifeste, R. W. Lemke <sup>id</sup>, W. Lewis, S. A. Lewis, G. P. Loisel, Q. M. Looker <sup>id</sup>, A. J. Lopez, D. J. Lucero, S. A. MacLaren <sup>id</sup>, R. J. Magyar, M. A. Mangan, M. R. Martin, T. R. Mattsson, M. K. Matzen, A. J. Maurer, M. G. Mazarakis, R. D. McBride <sup>id</sup>, H. S. McLean <sup>id</sup>, C. A. McCoy <sup>id</sup>, G. R. McKee, J. L. McKenney, A. R. Miles, J. A. Mills <sup>id</sup>, M. D. Mitchell, N. W. Moore, C. E. Myers <sup>id</sup>, T. Nagayama, G. Natoni, A. C. Owen, S. Patel, K. J. Peterson <sup>id</sup>, T. D. Pointon, J. L. Porter, A. J. Porwitzky, S. Radovich, K. S. Raman, P. K. Rambo, W. D. Reinhart <sup>id</sup>, G. K. Robertson, G. A. Rochau, S. Root <sup>id</sup>, D. V. Rose, D. C. Rovang, C. L. Ruiz, D. E. Ruiz <sup>id</sup>, D. Sandoval, M. E. Savage, M. E. Sceiford, M. A. Schaeuble, P. F. Schmit <sup>id</sup>, M. S. Schollmeier <sup>id</sup>, J. Schwarz, C. T. Seagle, A. B. Sefkow, D. B. Seidel, G. A. Shipley <sup>id</sup>, J. Shores, L. Shulenburger <sup>id</sup>, S. C. Simpson, S. A. Slutz <sup>id</sup>, I. C. Smith, C. S. Speas, P. E. Specht <sup>id</sup>, M. J. Speir <sup>id</sup>, D. C. Spencer, P. T. Springer, A. M. Steiner, B. S. Stoltzfus, W. A. Stygar, J. Ward Thornhill, J. A. Torres, J. P. Townsend <sup>id</sup>, C. Tyler, R. A. Vesey, P. E. Wakeland, T. J. Webb, E. A. Weinbrecht, M. R. Weis <sup>id</sup>, D. R. Welch, J. L. Wise, M. Wu, D. A. Yager-Elorriaga, A. Yu, and E. P. Yu

## COLLECTIONS

Paper published as part of the special topic on [Papers from the 61st Annual Meeting of the APS Division of Plasma Physics](#)

<sup>EP</sup> This paper was selected as an Editor's Pick



View Online



Export Citation



CrossMark

## ARTICLES YOU MAY BE INTERESTED IN

[Experimental determination of the thermal, turbulent, and rotational ion motion and magnetic field profiles in imploding plasmas](#)

Physics of Plasmas **27**, 060901 (2020); <https://doi.org/10.1063/5.0009432>

Perspectives on the generation of electron beams from plasma-based accelerators and their near and long term applications

Physics of Plasmas **27**, 070602 (2020); <https://doi.org/10.1063/5.0004039>

Hotspot conditions achieved in inertial confinement fusion experiments on the National Ignition Facility

Physics of Plasmas **27**, 050901 (2020); <https://doi.org/10.1063/5.0003298>



**NEW!**

Sign up for topic alerts  
New articles delivered to your inbox

The banner features a dark blue background with abstract, colorful brushstrokes in shades of purple, green, and yellow. A yellow diagonal banner in the top left corner contains the word 'NEW!' in white. The main text is centered in white and yellow. The AIP Publishing logo is in the bottom right corner.

# Review of pulsed power-driven high energy density physics research on Z at Sandia

Cite as: Phys. Plasmas **27**, 070501 (2020); doi: [10.1063/5.0007476](https://doi.org/10.1063/5.0007476)

Submitted: 17 March 2020 · Accepted: 18 May 2020 ·

Published Online: 8 July 2020























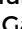
























View Online



Export Citation



CrossMark

D. B. Sinars,<sup>1,a),b)</sup>  M. A. Sweeney,<sup>1</sup> C. S. Alexander,<sup>1</sup> D. J. Ampleford,<sup>1</sup>  T. Ao,<sup>1</sup> J. P. Apruzese,<sup>2</sup> C. Aragon,<sup>1</sup> D. J. Armstrong,<sup>1</sup>  K. N. Austin,<sup>1</sup> T. J. Awe,<sup>1</sup> A. D. Baczewski,<sup>1</sup> J. E. Bailey,<sup>1</sup> K. L. Baker,<sup>3</sup>  C. R. Ball,<sup>1</sup> H. T. Barclay,<sup>1</sup>  S. Beatty,<sup>1</sup> K. Beckwith,<sup>1</sup> K. S. Bell,<sup>1</sup>  J. F. Benage, Jr.,<sup>1</sup> N. L. Bennett,<sup>1</sup>  K. Blaha,<sup>1</sup> D. E. Bliss,<sup>1</sup> J. J. Boerner,<sup>1</sup> C. J. Bourdon,<sup>1</sup> B. A. Branch,<sup>1</sup> J. L. Brown,<sup>1</sup>  E. M. Campbell,<sup>1</sup>  R. B. Campbell,<sup>1</sup> D. G. Chacon,<sup>1</sup> G. A. Chandler,<sup>1</sup> K. Chandler,<sup>1</sup>  P. J. Christenson,<sup>1</sup> M. D. Christison,<sup>1</sup> E. B. Christner,<sup>1</sup> R. C. Clay III,<sup>1</sup> K. R. Cochran,<sup>1</sup> A. P. Colombo,<sup>1</sup> B. M. Cook,<sup>1</sup> C. A. Coverdale,<sup>1</sup> M. E. Cuneo,<sup>1</sup> J. S. Custer,<sup>1</sup> A. Dasgupta,<sup>2</sup> J.-P. Davis,<sup>1</sup>  M. P. Desjarlais,<sup>1</sup> D. H. Dolan III,<sup>1</sup> J. D. Douglass,<sup>1</sup> G. S. Dunham,<sup>1</sup> S. Duwal,<sup>1</sup> A. D. Edens,<sup>1</sup> M. J. Edwards,<sup>3</sup> E. G. Evstatiev,<sup>1</sup> B. G. Farfan,<sup>1</sup> J. R. Fein,<sup>1</sup>  E. S. Field,<sup>1</sup> J. A. Fisher,<sup>1</sup> T. M. Flanagan,<sup>1</sup>  D. G. Flicker,<sup>1</sup> M. D. Furnish,<sup>1</sup> B. R. Galloway,<sup>1</sup>  P. D. Gard,<sup>1</sup> T. A. Gardiner,<sup>1</sup> M. Geissel,<sup>1</sup>  J. L. Giuliani,<sup>2</sup> M. E. Glinsky,<sup>1</sup> M. R. Gomez,<sup>1</sup>  T. Gomez,<sup>1</sup> G. P. Grim,<sup>3</sup>  K. D. Hahn,<sup>1,d)</sup> T. A. Haill,<sup>1</sup>  N. D. Hamlin,<sup>1</sup>  J. H. Hammer,<sup>3</sup> S. B. Hansen,<sup>1</sup> H. L. Hanshaw,<sup>1</sup> E. C. Harding,<sup>1</sup> A. J. Harvey-Thompson,<sup>1</sup> D. Headley,<sup>1</sup> M. C. Herrmann,<sup>1,d)</sup> M. H. Hess,<sup>1</sup> C. Highstrete,<sup>1</sup> O. A. Hurricane,<sup>3</sup>  B. T. Hutsel,<sup>1</sup>  C. A. Jennings,<sup>1</sup> O. M. Johns,<sup>1</sup> D. Johnson,<sup>1</sup> M. D. Johnston,<sup>1</sup> B. M. Jones,<sup>1</sup> M. C. Jones,<sup>1</sup>  P. A. Jones,<sup>1</sup> P. E. Kalita,<sup>1</sup> R. J. Kamm,<sup>1</sup> J. W. Kellogg,<sup>1</sup> M. L. Kiefer,<sup>1</sup> M. W. Kimmel,<sup>1</sup> P. F. Knapp,<sup>1</sup>  M. D. Knudson,<sup>1</sup> A. Kreft,<sup>1</sup> G. R. Laity,<sup>1</sup> P. W. Lake,<sup>1</sup> D. C. Lamma,<sup>1</sup> W. L. Langston,<sup>1</sup> J. S. Lash,<sup>1</sup> K. R. LeChien,<sup>1,3,d)</sup> J. J. Leckbee,<sup>1</sup> R. J. Leeper,<sup>1,e)</sup>  G. T. Leifeste,<sup>1</sup> R. W. Lemke,<sup>1</sup>  W. Lewis,<sup>1</sup> S. A. Lewis,<sup>1</sup> G. P. Loisel,<sup>1</sup> Q. M. Looker,<sup>1</sup>  A. J. Lopez,<sup>1</sup> D. J. Lucero,<sup>1</sup> S. A. MacLaren,<sup>3</sup>  R. J. Magyar,<sup>1,f)</sup> M. A. Mangan,<sup>1</sup> M. R. Martin,<sup>1</sup> T. R. Mattsson,<sup>1</sup> M. K. Matzen,<sup>1</sup> A. J. Maurer,<sup>1</sup> M. G. Mazarakis,<sup>1</sup> R. D. McBride,<sup>1,g)</sup>  H. S. McLean,<sup>3</sup>  C. A. McCoy,<sup>1</sup>  G. R. McKee,<sup>1</sup> J. L. McKenney,<sup>1</sup> A. R. Miles,<sup>3</sup> J. A. Mills,<sup>1</sup>  M. D. Mitchell,<sup>1</sup> N. W. Moore,<sup>1</sup> C. E. Myers,<sup>1</sup>  T. Nagayama,<sup>1</sup> G. Natoni,<sup>1</sup> A. C. Owen,<sup>1</sup> S. Patel,<sup>1</sup> K. J. Peterson,<sup>1</sup>  T. D. Pointon,<sup>1</sup> J. L. Porter,<sup>1</sup> A. J. Porwitzky,<sup>1</sup> S. Radovich,<sup>1</sup> K. S. Raman,<sup>3</sup> P. K. Rambo,<sup>1</sup> W. D. Reinhart,<sup>1</sup>  G. K. Robertson,<sup>1</sup> G. A. Rochau,<sup>1</sup> S. Root,<sup>1</sup>  D. V. Rose,<sup>4</sup> D. C. Rovang,<sup>1</sup> C. L. Ruiz,<sup>1</sup> D. E. Ruiz,<sup>1</sup>  D. Sandoval,<sup>1</sup> M. E. Savage,<sup>1</sup> M. E. Sceiford,<sup>1</sup> M. A. Schaeuble,<sup>1</sup> P. F. Schmit,<sup>1</sup>  M. S. Schollmeier,<sup>1</sup>  J. Schwarz,<sup>1</sup> C. T. Seagle,<sup>1</sup> A. B. Sefkow,<sup>1,c)</sup> D. B. Seidel,<sup>1</sup> G. A. Shipley,<sup>1</sup>  J. Shores,<sup>1</sup> L. Shulenburg,<sup>1</sup>  S. C. Simpson,<sup>1</sup> S. A. Slutz,<sup>1</sup>  I. C. Smith,<sup>1</sup> C. S. Speas,<sup>1</sup> P. E. Specht,<sup>1</sup>  M. J. Speir,<sup>1</sup>  D. C. Spencer,<sup>1</sup> P. T. Springer,<sup>3</sup> A. M. Steiner,<sup>1</sup> B. S. Stoltzfus,<sup>1</sup> W. A. Stygar,<sup>1,d)</sup> J. Ward Thornhill,<sup>2</sup> J. A. Torres,<sup>1</sup> J. P. Townsend,<sup>1</sup>  C. Tyler,<sup>1</sup> R. A. Vesey,<sup>1</sup> P. E. Wakeland,<sup>1</sup> T. J. Webb,<sup>1</sup> E. A. Weinbrecht,<sup>1</sup> M. R. Weis,<sup>1</sup>  D. R. Welch,<sup>4</sup> J. L. Wise,<sup>1</sup> M. Wu,<sup>1</sup> D. A. Yager-Elorriaga,<sup>1</sup> A. Yu,<sup>1</sup> and E. P. Yu<sup>1</sup>

## AFFILIATIONS

<sup>1</sup>Sandia National Laboratories, P.O. Box 5800, Albuquerque, New Mexico 87185, USA

<sup>2</sup>Naval Research Laboratory, 4555 Overlook Avenue SW, Washington, D.C. 20375, USA

<sup>3</sup>Lawrence Livermore National Laboratory, 7000 East Avenue, Livermore, California 94550, USA

<sup>4</sup>Voss Scientific, 418 Washington St., SE, Albuquerque, New Mexico 87108, USA

**Note:** This paper is part of the Special Collection: Papers from the 61st Annual Meeting of the APS Division of Plasma Physics.

**Note:** Paper FR11, Bull. Am. Phys. Soc. **64** (2019).

<sup>a)</sup>Invited speaker.

<sup>b)</sup>Author to whom correspondence should be addressed: [dbsinar@sandia.gov](mailto:dbsinar@sandia.gov)

<sup>c)</sup>Present address: University of Rochester Laboratory for Laser Energetics, 250 E River Rd., Rochester, New York 14623, USA.

<sup>d)</sup>Present address: Lawrence Livermore National Laboratory, 7000 East Avenue, Livermore, California 94550, USA.

<sup>e)</sup>Present address: Los Alamos National Laboratory, P.O. Box 1663, Los Alamos, New Mexico 87545, USA.

<sup>f)</sup>Present address: Northrop Grumman Corporation, Linthicum, Maryland 21090, USA.

<sup>g)</sup>Present address: University of Michigan, 500 S State St., Ann Arbor, Michigan 48109, USA.

## ABSTRACT

Pulsed power accelerators compress electrical energy in space and time to provide versatile experimental platforms for high energy density and inertial confinement fusion science. The 80-TW “Z” pulsed power facility at Sandia National Laboratories is the largest pulsed power device in the world today. Z discharges up to 22 MJ of energy stored in its capacitor banks into a current pulse that rises in 100 ns and peaks at a current as high as 30 MA in low-inductance cylindrical targets. Considerable progress has been made over the past 15 years in the use of pulsed power as a precision scientific tool. This paper reviews developments at Sandia in inertial confinement fusion, dynamic materials science, x-ray radiation science, and pulsed power engineering, with an emphasis on progress since a previous review of research on Z in *Physics of Plasmas* in 2005.

© 2020 Author(s). All article content, except where otherwise noted, is licensed under a Creative Commons Attribution (CC BY) license (<http://creativecommons.org/licenses/by/4.0/>). <https://doi.org/10.1063/5.0007476>

## I. INTRODUCTION

This paper reviews the remarkable progress in high-current pulsed power research at Sandia National Laboratories over the past 15 years. Sandia operates the world’s largest pulsed power accelerator,<sup>1,2</sup> the “Z” facility, which can store up to 22 MJ in its capacitor banks and discharge that energy in a 100-ns, linearly rising pulse with a peak electrical power of 80 TW and a peak current of up to 30 MA.<sup>3</sup> This high electrical power, roughly 15 times the continuous electrical generating capacity of the entire world’s power plants, can be used to compress matter to extreme pressures that greatly exceed  $1 \times 10^6$  times atmospheric pressure (1 Mbar). Plasmas can also be created that are very efficient radiators in the x-ray regime. As such, Z is used for a wide range of high energy density (HED) physics experiments spanning radiation source development, radiation-driven science, dynamic material properties, magneto-inertial fusion (MIF), and inertial confinement fusion (ICF). Z has been an engine of discovery, and even after 23 years of operation in its present configuration, scientists continue to set new facility performance records and to conduct novel experiments in each of these research areas. We survey some of these achievements and conclude with a discussion of research opportunities for the next decade.

Pulsed power can be optimized to produce high-current ( $>10$  MA) or high voltage ( $>10$  MV) and to produce energetic radiation ranging from soft x rays (0.1–1 keV) up through gamma rays (1–20 MeV). Pulsed power accelerators were developed at Sandia and elsewhere during the 1960s to provide laboratory radiation sources for weapon effects studies.<sup>4,5</sup> Laboratory testing was then needed to cost effectively ensure that the electronics in nuclear warheads would not be vulnerable to radiation from other nuclear weapons. Z is one of the three pulsed power facilities at Sandia for this weapon effects mission and can produce 2.6 MJ and  $>330$  TW in soft x rays,<sup>6</sup> 10–400 kJ in 1–10 keV x rays, and 1–10 kJ in 10–100 keV x rays.<sup>7</sup> The Saturn facility<sup>8</sup> is typically used as a bremsstrahlung source of 0.1–1 MeV x rays as well as a soft x-ray source using a gas puff z-pinch system. The High-Energy Radiation Megavolt Electron Source (HERMES) III facility<sup>9</sup> began operating in 1988 and is used as a  $>1$ -MeV gamma ray source.

Sandia began applying pulsed power to inertial confinement fusion in 1971 with an electron beam fusion initiative.<sup>10–12</sup> That effort led to the detection, in 1977, of fusion neutrons on the Rehyd accelerator using a plastic shell target containing a CD<sub>2</sub> fuel wire. This “Phi target” was an early version of a direct drive magneto-inertial fusion target.<sup>13</sup> The pulsed power ICF initiative culminated with construction

of the 20-TW Particle Beam Fusion Accelerator II (PBFA-II) in 1985 with the intent to compress spherical capsules containing fusion fuel to extreme pressures. The accelerator was optimized to drive light ion beams rather than electron beams because of the more favorable target performance based upon predictions of one-dimensional computer simulations.<sup>14,15</sup> Subsequently, record radiation powers were produced in the laboratory in the mid-1990s by vaporizing and compressing very large numbers of fine wires in a cylindrical array on Saturn.<sup>16,17</sup> Such a wire-array implosion is an example of a “z pinch.” Building upon that success, in 1996 PBFA-II was converted to Z to demonstrate the scaling of z-pinch radiation sources, resulting in then-record soft x-ray outputs from pulsed power ( $\sim 2$  MJ and 200 TW).<sup>18</sup> In the late 1990s, Sandia scientists began using the extreme magnetic pressures on Z to compress matter directly to the 1–5 Mbar range as a dynamic material platform and using Z’s powerful radiation sources to drive additional experiments located around the x-ray sources. The early research program on Z from 1996 to 2004 is well documented in a previous review paper.<sup>19</sup>

This paper reviews the last 15 years of HED research on Z. During that period, the pulsed power components of Z were refurbished to double the stored energy, new record facility outputs in radiation sources were achieved (2.6 MJ and 330 TW of soft x rays;  $>10$  cal/cm<sup>2</sup> at 10 keV), improved materials research platforms were developed to enable increasingly sophisticated measurements at facility record pressures ( $>40$  km/s flyer plates, up to 10 Mbar in mm-scale samples), and a major shift occurred with an emphasis on direct drive ICF rather than indirect drive (i.e., radiation-driven) ICF. Today, Z is renowned for being used to study a wide range of nuclear weapon-relevant materials (e.g., 52-year-old plutonium samples taken directly from the U.S. stockpile), demonstrating the key tenets of magneto-inertial fusion in the laboratory for the first time, and x-ray-driven experiments capable of reproducing astrophysical conditions from the Sun’s core to the photospheres of white dwarf stars. More recently, novel tools in power flow physics are being developed and next-generation pulsed power technology is being improved. Scientists today are looking at the opportunities that may be present on next-generation laboratory pulsed power facilities, which are also briefly discussed here.

## II. Z PULSED POWER FACILITY COMPLEX

Z operates by storing energy in a ring of Marx-generator capacitor banks around its perimeter, as illustrated in Fig. 1. Each of the 36 Marx generators is composed of 60 2.6-microfarad capacitors. When



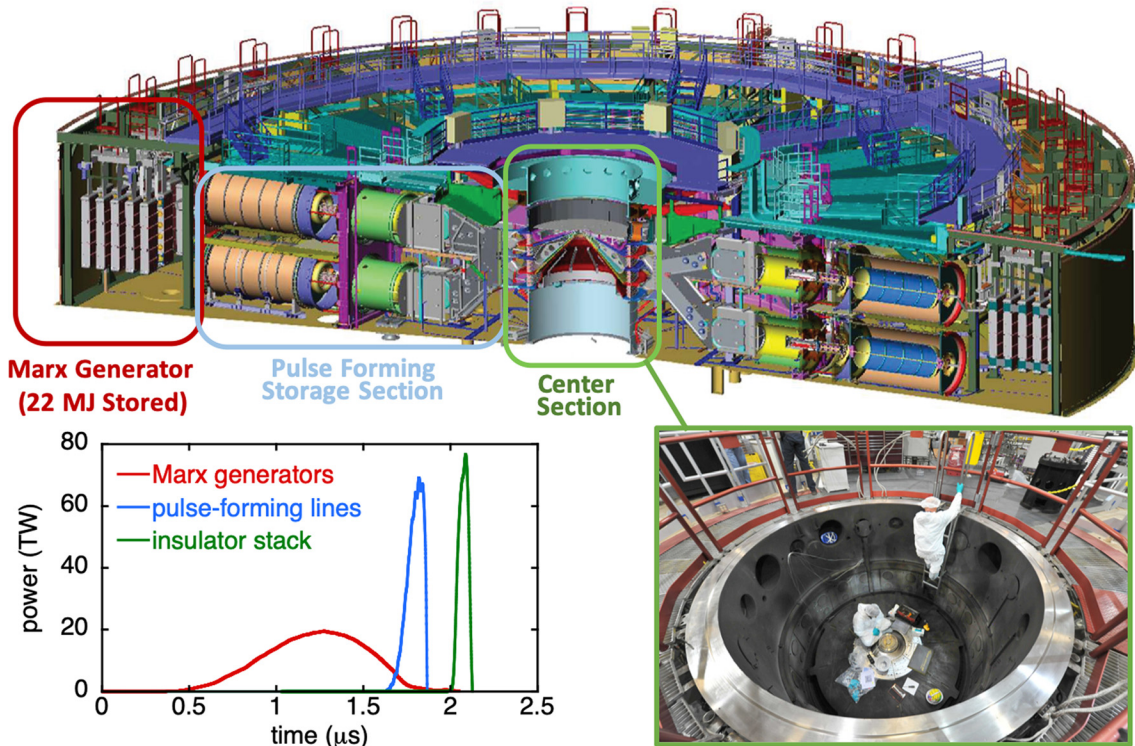


**FIG. 1.** Cross-section of Z showing various stages of pulse compression. The diameter of the outer tank wall is about 33 m. As indicated by the plot at lower left, peak electrical power entering vacuum insulator stack can reach about 80 TW. Photo at lower right taken from above Z insulator stack center section showing (for scale) two workers loading hardware.

charged to  $\pm 90$  kV, each will store 632 kJ, for a total of  $>22$  MJ stored energy. While most short-pulse experiments use 85–95 kV charge voltages, some pulse-shaped dynamic materials experiments use voltages as low as 50–60 kV. The energy stored in the Marx generators can be discharged in as short as  $1.3 \mu\text{s}$  into the pulse forming section. There, a series of switches and low-inductance transmission lines compress the electrical energy in time, so the peak electrical power delivered to the vacuum insulator stack at the accelerator center can be as high as 80 TW in a linearly rising, 100-ns current pulse. The specific peak current delivered to the target at the center of Z varies with the inductance of the target and the surrounding load hardware. Z was optimized to drive the z-pinch dynamic *Hohlraum* load described later and reproducibly delivers 26 MA to this target with negligible current loss in the last stages of current delivery. More specific details of the pulsed power hardware, which we refurbished in 2006–2007, can be found in other publications.<sup>3,20,21</sup>

In a separate building south of Z (Fig. 2) is the Z-Backlighter laser facility, which contains three high-energy lasers: Z-Beamlet laser, Z-Petawatt laser, and Chaco.<sup>22,23</sup> The first two are kJ-class lasers that can be directed down a 70-m transport tube to a final optics assembly above the Z center section and focused down to targets within Z. These lasers generate independent multi-keV x-ray sources for radiography<sup>24–26</sup> and x-ray diffraction<sup>27</sup> and can heat plasmas in some fusion experiments, as described later. We can also direct them to standalone target chambers to develop diagnostics or conduct laser heating

experiments independent of Z, as the lasers have a significantly higher shot rate (about three times a day) than Z (about once a day). The 50-J Chaco laser, which can execute up to 60 shots a day, is used for laser-matter interaction studies and development of laser-based diagnostics independent of Z.

Z can deliver  $\sim 3$  MJ to a target and its surrounding load hardware. The specific amount varies with the Marx charge voltage and the inductance of the load hardware. This energy release is equivalent to that from a few sticks of dynamite, so the debris generated is considerable, as illustrated in Fig. 3. This debris introduces some level of complexity for the diagnostics and laser hardware used in the facility, which must be protected from that debris. The debris also introduces challenges when hazardous materials are used, such as beryllium and plutonium. For high-hazard materials, explosively driven containment systems are used to prevent the material from being dispersed within the Z center section.

### III. SCIENCE RESEARCH ON Z

#### A. Overview

The energy from Z is typically concentrated in “targets” or “samples” located in the center of Z, which can vary from  $0.3$  to  $25 \text{ cm}^3$  in volume, depending on the experiment. The most natural geometry is a cylinder. A nominal peak current of 26 MA, delivered to a radius of 1 mm, can produce  $\sim 100$  Mbar pressures on the surface of

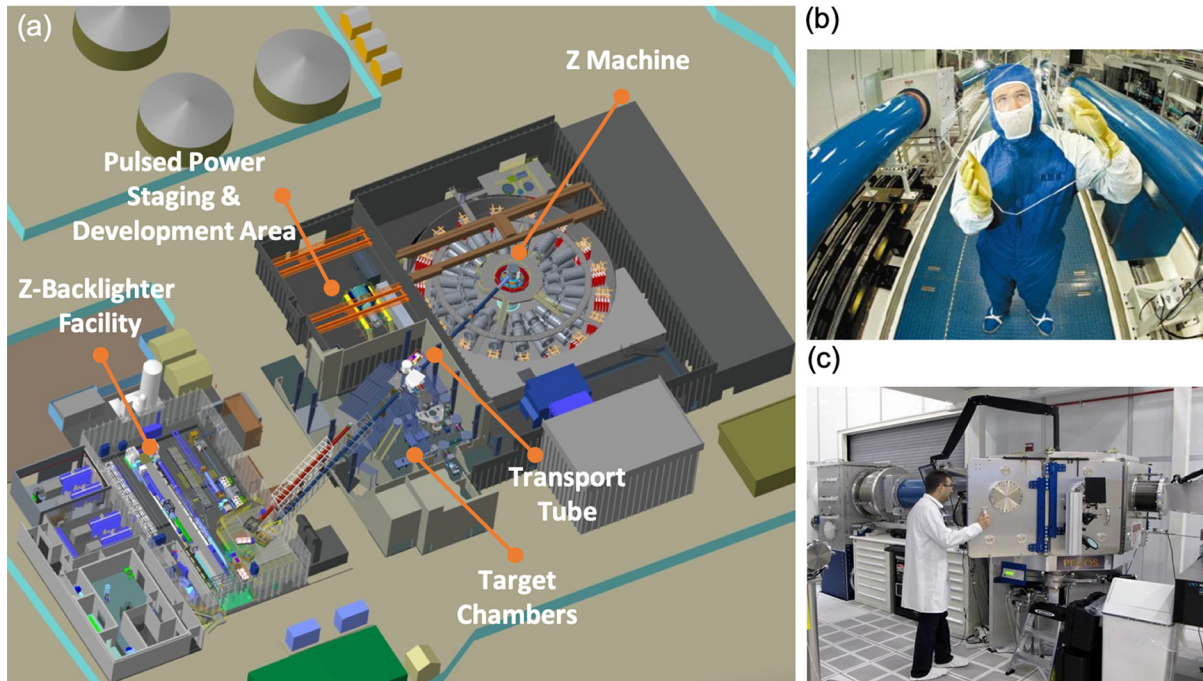


**FIG. 2.** (a) Diagram of Z facility complex, which includes Z, multi-kJ Z-Backlighter facility, standalone target chambers for lasers, 70-m transport tube from Z-Backlighter lasers to Z center section, and pulsed power staging and development area. (b) The Z-Beamlet laser beam is 31 cm × 31 cm in area until focused to a target, requiring large optics as illustrated by a photo. (c) Example photo of one of the standalone laser target chambers, which are used to develop laser-based diagnostics or study plasma heating in fusion targets independent of Z.

a cylinder. This pressure can be used to compress material samples directly to  $\sim 1$  to 10 Mbar over time scales in excess of  $1 \mu\text{s}$  or to accelerate matter to high velocities (100–1000 km/s) in a convergent geometry in  $\sim 1$  ns to achieve the more extreme pressures needed for ICF.

The three general classes of targets on Z are plasma radiation sources, dynamic materials samples, and magnetic direct drive targets, as illustrated in Fig. 4. Radiation sources are generally produced by large-diameter ( $\sim 4$ -cm) wire arrays or gas puffs arranged in a cylindrically symmetric configuration. These are optimized to provide

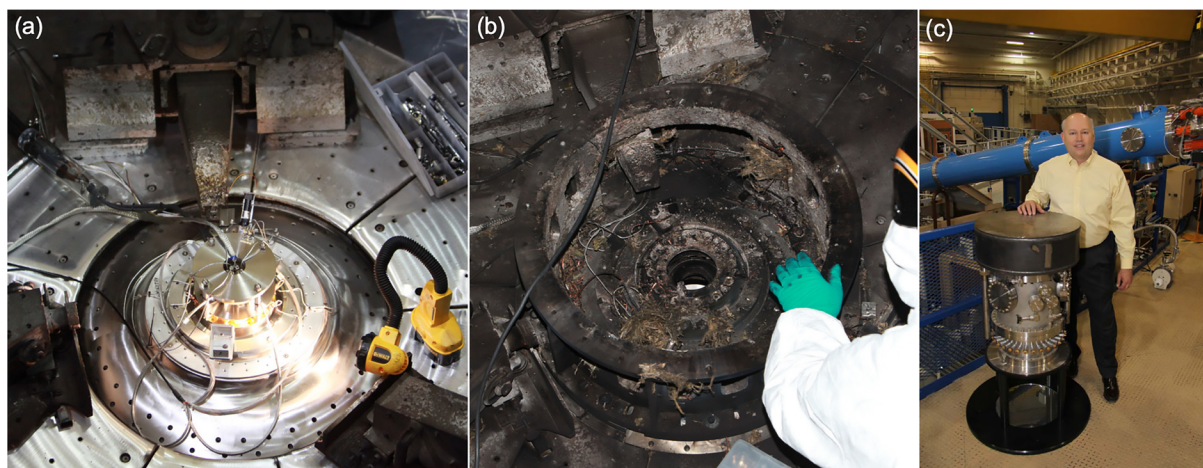


**FIG. 3.** (a) Pre-shot photo during hardware installation of target assembly in the Z center section for a magnetized liner inertial fusion experiment. (b) Post-shot photo of the same experiment illustrating debris generated through release of several MJ energy in load hardware. (c) Photo of the explosively driven containment system used on hazardous dynamic material experiments.



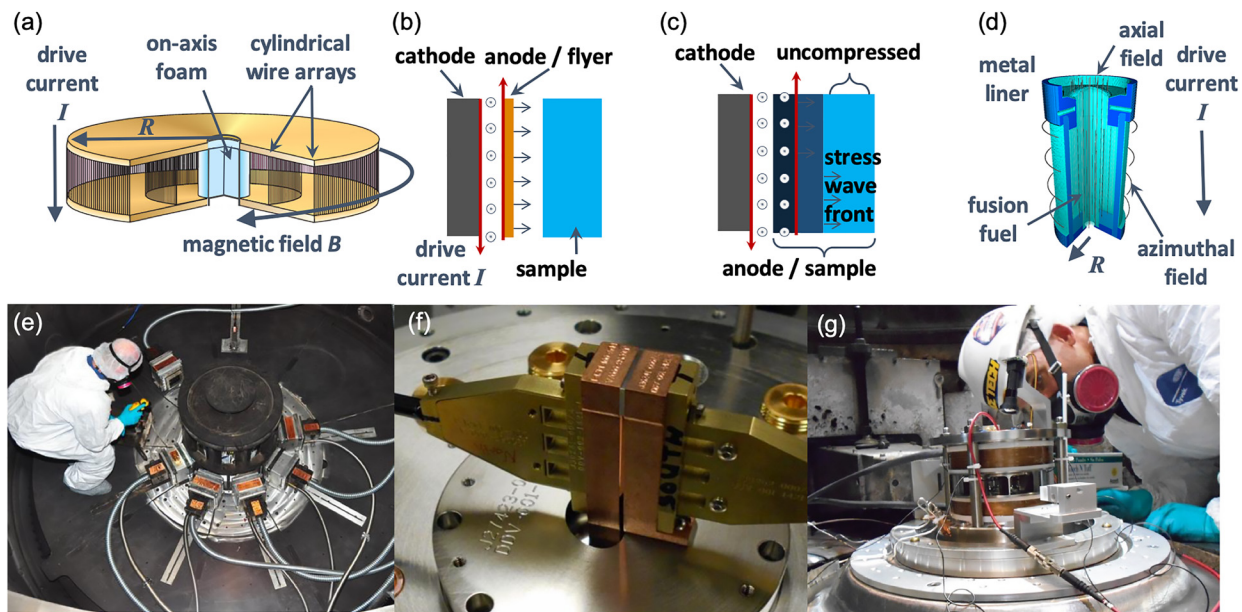


**FIG. 4.** Overview of types of research platforms fielded on Z. (a) Diagram of example wire-array radiation source. (b) Diagram of example planar flyer shock geometry for dynamic material experiments. (c) Diagram of example planar quasi-isentropic compression experiment geometry for dynamic material experiments. (d) Diagram of nominal magnetic direct drive fusion target. (e) Z center section photo for the radiation experiment showing test cassettes outside debris containment shield, surrounding x-ray source. (f) Photo of the planar material hardware set, showing optical probe hookups looking at back side of each sample. (g) Photo of magnetized liner inertial fusion hardware including external magnetic field coils to generate an axial field.

100–1000 km/s implosions that result in high-temperature plasmas emitting short ( $\sim 1$  ns) bursts of x-ray radiation. A dynamic material sample is usually in planar geometry. Z's magnetic pressure accelerates a thin metal sheet (also known as a “flyer plate”) up to 40 km/s, which then collides with a sample and drives a strong shock in the material. Alternatively, we can carefully shape the Z current pulse for up to  $\sim 1$   $\mu$ s by distributing the timing of laser-triggered gas switches in each of the 36 magnetically insulated transmission lines (MITLs) to ramp up the pressure directly without driving a strong shock in the material. We can also combine these two techniques to drive a small shock that heats the sample and then ramp compresses it to high pressure and density. These platforms allow us to study Hugoniot or quasi-isentropic compression loading paths throughout a material's phase space. The third class of targets on Z today is fusion targets, which are typically small-diameter ( $\sim 0.6$ -cm) metal cylinders (also known as “liners”) that reach implosion velocities of  $\sim 100$  km/s.

We fielded 152 experiments on Z in 2018. Of these, 32 were categorized as radiation experiments, 54 as dynamic materials experiments, 49 as fusion-related experiments, and 17 in other categories (e.g., power flow physics or fundamental science). Five dynamic materials experiments used hazardous materials and were fielded in a containment geometry [Fig. 3(c)].

The National Nuclear Security Administration (NNSA) funds most Z research. The NNSA research is driven by our mission to address key nuclear weapons stockpile stewardship science questions. One way to characterize the Z research is to consider the two axes of “Pasteur's Quadrant,”<sup>28</sup> which categorize research according to (a) scientific novelty and (b) its relevance to a specific application. In the case of Z, we consider three categories: basic science (high novelty,

weak tie to the NNSA mission), applied science (relatively low novelty, strong tie to NNSA mission), or use-inspired (high novelty, strong tie to mission). In 2018, the Z shot distribution across these categories was roughly 15% basic, 40% applied, and 45% use-inspired. The use-inspired category is important in the context of common scientific practice and cost efficiency. Many applied Z experiments are complex, costly, and involve non-publishable research. The basic and use-inspired research allows for peer review of scientific methods that build confidence in the application of our experimental methods. Novel techniques or diagnostics are typically matured on the less-costly, use-inspired experiments before being applied to high-consequence, applied experiments. It is also important to note that many of the applied and use-inspired missions have fostered fertile experimental platforms for wide-ranging and unprecedented discoveries in the field of high energy density science.

## B. Radiation science

### 1. Development of radiation sources

Z provides unique capabilities to generate remarkably intense radiation environments at 0.1–100 keV photon energy. We are assessing bright x-ray sources to understand the response of materials and complex systems to powerful radiation bursts and to study opacity and radiation flow. This section discusses research on Z to create these bright x-ray sources and experiments that elucidate the properties of astrophysical plasmas and their interactions with radiation.

Pulsed power provides an energy-rich approach to generating x-ray radiation environments. Magnetically driven implosions are an extremely efficient technique to couple kinetic energy into an

imploding plasma,<sup>29</sup> with the wall-plug electrical energy being converted to x rays with an efficiency as high as  $\sim 15\%$ .<sup>30</sup> As the material stagnates on the axis of symmetry, the kinetic energy is efficiently thermalized to create a hot dense plasma that effectively radiates. Depending on the kinetic energy per ion and the material imploded, the radiated spectrum can either be dominated by broad-band quasi-Planckian emission<sup>16,17</sup> or by line emission from highly charged ions (i.e., K-shell emission).<sup>31,32</sup>

The enhanced stored energy in the refurbished Z, combined with our improved physics understanding, simulation tools, and diagnostics, has allowed advances in the sources available, both in radiated energies (and the resultant fluences on a test article) and photon energies, as summarized in Fig. 5.

To provide bright sources in the sub-keV photon energy range, z-pinch x-ray sources aim to couple the maximum energy from an implosion such that the energy, when stagnated, is radiated. Use of a high atomic number material, such as tungsten, maximizes the atomic transitions available to produce self-emission and provides an efficient quasi-Planckian radiator. We have improved the radiated power and energy in dynamic *Hohlraum* experiments as the result of the increased current and the choice of wire-array masses that implode efficiently with that current.<sup>33</sup> On separate experiments, we increased the wire-array z-pinch diameter and the mass, resulting in record soft x-ray powers and x-ray energy output (i.e.,  $>330$  TW and 2.6 MJ, respectively).<sup>6</sup> This is the power and output from the most energetic laboratory x-ray burst in the world. By incorporating diagnostic improvements, we also enhanced the characterization of the radiation compared to earlier experiments.<sup>6</sup>

Z pinches can radiate efficiently in the 1–15 keV spectral range for highly ionized, mid-atomic-number materials (i.e., aluminum to krypton). To achieve this enhanced radiation, an implosion must have sufficient kinetic energy per ion (i.e., velocity) such that, when the kinetic energy is thermalized, a fraction of the mass will be ionized to the K-shell.<sup>34,35</sup>

Given a fixed minimum current rise time, with increasing atomic number the implosion velocity can be increased by increasing the initial z-pinch diameter.<sup>7,32</sup> In addition, as we increase the atomic

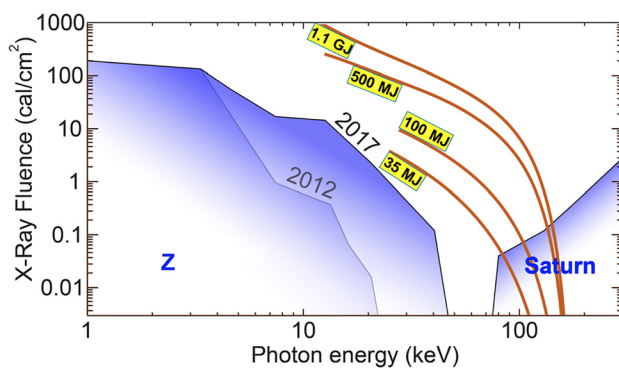


**FIG. 5.** Summary of the x-ray radiation output from Z as applied to samples in a test article. Shaded regions illustrate experimentally demonstrated results from Z or Saturn. Orange curves represent spectra from a magnetized liner inertial fusion plasma on a notional future facility producing the deuterium–tritium output yields noted.

number (and the photon energy of the highly ionized spectral lines), energy is lost to ionization and thermal energy, thus reducing the radiated energy in the K-shell spectral lines. The K-shell x-ray yields achieved at Z include  $>400$  kJ for Al near 1.7 keV and  $>300$  kJ for argon near 3-keV photon energy, tens of kilojoules for iron and copper, and several kilojoules for Kr near 13 keV.<sup>7</sup> Design of experiments and estimates of K-shell yield have used thin-shell models to calculate the coupled energy.<sup>36</sup> The models have advanced in recent years to provide more physically complete two-dimensional (2D)<sup>37,38</sup> and three-dimensional (3D)<sup>39,40</sup> radiation magnetohydrodynamic (MHD) simulations that include the effects of instability growth on stagnation dynamics and of non-local thermodynamic equilibrium atomic physics on various opacity treatments to calculate the emitted x-ray power.

To access a broad range of photon energies, implosions are used to generate K-shell radiation corresponding to the atomic number of the radiating material. Both metal and gas targets are imploded at Z using wire-array and gas puff z pinches, respectively. We have improved the fidelity of wire-array z-pinch experiments through pre-shot characterization of individual few- $\mu\text{m}$ -scale wires.<sup>41</sup> To perform gas puff experiments on Z, we established a gas puff system<sup>42,43</sup> paired with detailed pre-shot characterization of the gas density profiles<sup>44</sup> and hydrodynamic modeling to design the gas nozzle configurations.<sup>40</sup>

In the 1990s, wire-array experiments proved to be a breakthrough for fast z pinches, demonstrating high total x-ray power from nested tungsten wire arrays and paving the way for K-shell x-ray source development on Z. Aluminum wire-array z pinches have been studied on pulsed power facilities for decades, including initial studies that indicated very high x-ray powers could be achieved using high-wire-number arrays with optimized inter-wire gaps.<sup>45</sup> On Z, spectra from Al wire-array z pinches provided Doppler signatures that, for the first time, directly diagnosed implosion velocities  $>500$  km/s in z pinches.<sup>46</sup> More recent experiments on Z showed that, for the plasma densities reached, opacity effects had to be mitigated when optimizing Al line emission; the data indicated that a highly structured stagnation column created optimal emission rather than a uniform stagnation column.<sup>47</sup>

To provide radiation sources at 5–8 keV, we studied stainless steel wire-array z pinches in detail on Z. To understand the trade-offs in optimization, we varied the wire-array diameter,<sup>48</sup> the exact configuration of the nested wire array,<sup>36</sup> and the length of the z pinch.<sup>49</sup> Experiments to optimize emission from the stainless steel wire arrays indicated a direct connection between implosion velocity and radiated energy and achieved 80 kJ radiated at  $>5$  keV with a peak power of  $>30$  TW.<sup>50</sup> Similar optimization of copper wire arrays achieved  $\sim 35$  kJ radiated at  $>7$  keV<sup>7,49</sup> and provided rich spectral data for comparison to atomic modeling.<sup>51–54</sup>

Gas puff z pinches, in which the current pulse flows through a jet of supersonic gas rather than an array of fine wires, can access K-shell radiation at additional photon energies by using Ar or Kr as the radiating material. Radiation MHD simulations, coupled to tabular collisional radiative equilibrium atomic kinetics at NRL<sup>37,55</sup> and Sandia,<sup>43</sup> were key to rapid progress in Ar gas puffs. The initial experiments achieved  $>300$  kJ radiated at  $>3$  keV with  $<10\%$  shot-to-shot variability.<sup>56</sup> Following earlier work on several facilities,<sup>57</sup> other experiments increased the radiated power from Ar gas puffs<sup>58</sup> and showed the impact of low-level dopants in the gas puffs through radiative cooling.<sup>59</sup> The progressive improvement in gas puff K-shell radiation



source development, as described in a comprehensive 2015 review,<sup>60</sup> culminated with experiments on Z (see pp. 2428 and 2442–2443 of that review).

Kr gas puffs represent the limit of the photon energies where line emission from highly ionized (K-shell) ions has been accessed on Z. To reach high temperatures for effective emission, large initial diameters are required; most experiments use 12-cm-diameter gas puff nozzles. Implosions from these diameters are highly susceptible to the magnetic Rayleigh–Taylor (MRT) instability. To limit MRT growth, we used an idealized gas density profile<sup>61</sup> that minimizes acceleration in the experiments. Using hydrodynamic simulations of cold gas flow coupled to the MHD simulations, we developed realistic configurations for exploration on Z.<sup>40</sup> The Z experiments, with appropriate mitigation of MRT growth, radiated 9 kJ at >10-keV.<sup>40,62</sup>

Radiation sources at >15 keV from highly ionized charge states are not practical on Z because the specific energy requirement to ionize to the K shell drives the wire arrays to diameters so large that the implosion is too unstable to form a high-density stagnated column. Instead, we have characterized the K- $\alpha$  spectral lines that are collisionally excited by electron beams or non-thermal tail populations in this region.<sup>7,63</sup> A specific challenge with higher photon energies is that the Z diagnostic suite has historically targeted the <10-keV range. In the last few years, we have developed a suite of diagnostics for >10-keV radiation sources. These include time-integrated<sup>64</sup> and time-resolved<sup>65</sup> transmission crystal spectrometers, diodes optimized for this spectral range,<sup>66</sup> high-energy pinhole cameras,<sup>67</sup> and a high-resolution monochromatic Wolter imager.<sup>68–70</sup> Even for sources in the 1–25 keV range, characterizing the continuum emission at >25 keV and even at >100 keV can be critical to understand the experimental uncertainties driven by the radiation source; we have developed a number of capabilities to characterize this portion of the spectrum.<sup>71,72</sup> An additional challenge in designing >15-keV x-ray sources is the lack of a mature numerical design tool that can capture the kinetic effects of electron beam formation and excitation of K- $\alpha$  emission. Hybrid particle-in-cell (PIC) codes<sup>73–75</sup> are candidates to address these effects; however, such codes must be validated in high-density z-pinch stagnation plasma regimes and coupled to atomic models to predict the radiation output.

## 2. Application of radiation sources

X-ray-driven experiments on Z provide unprecedented capability for HED physics. Creating extreme conditions has been routine for several decades, but our understanding has been hindered by the need to concentrate energy in sub-mm spatial scales for sub-ns durations. This has led to non-uniform plasmas, under-resolved and/or incomplete data, and irreproducible results. Yet Z has been transformational for HED physics because its enormous x-ray output energy of >1 MJ allows us to heat macroscopic quantities of matter long enough for detailed studies of extreme plasma states.

A second feature of our success is the capability to conduct multiple physics experiments on a single Z shot. For example, the Z Astrophysical Plasma Properties (ZAPP) collaboration<sup>33</sup> has routinely conducted four simultaneous, independent experiments. Simultaneous magnetic direct drive fusion and radiation-heated matter experiments are another example.<sup>76</sup> This unique capability expands access to a precious scientific resource, promotes reproducibility and accuracy, and fosters rapid progress. Reproducibility tests are especially notable, since HED physics faces the dilemma that reaching extreme conditions requires large facilities with limited opportunities to repeat experiments. Plasma physics experiments are known to provide surprises relative to expectations, and one of the best methods to ensure reliable results is repeatability.

There are three main approaches to x-ray-driven experiments at Z. The first measures fundamental material properties such as stellar interior opacity,<sup>77,78</sup> line broadening in white dwarf photospheres,<sup>79</sup> and continuum lowering for iron at supra-solid density.<sup>80</sup> The second approach measures absorption or emission spectra from HED plasmas at known conditions and uses these spectra to test spectral synthesis models that are essential to interpret astronomical observations or laboratory diagnostic signatures. This approach includes spectral emission and absorption from photoionized plasmas that are ubiquitous in accretion-powered objects such as black holes and x-ray binaries.<sup>81–83</sup> The third approach measures x-ray drive and the validity of hydrodynamic simulations to test predictions based on estimates of stellar opacity data from Z experiments.<sup>84,85</sup>

The ZAPP experiments use the Z dynamic *Hohlraum* x-ray source,<sup>86–88</sup> as shown in Fig. 6. The 26-MA peak current implodes

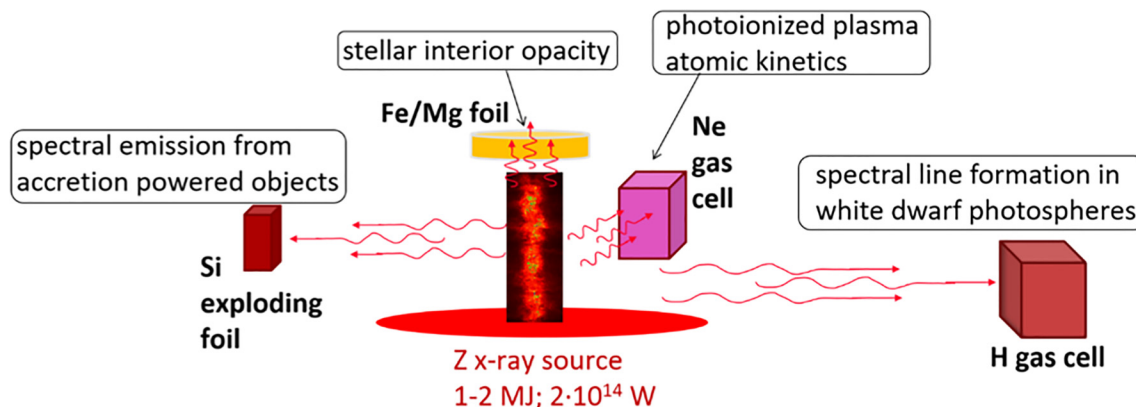


**FIG. 6.** The Z Astrophysical Plasma Properties (ZAPP) collaboration uses x rays to drive four separate laboratory astrophysics experiments simultaneously. Conditions for each are optimized by adjusting distance from the x-ray source and sample composition, density, and size.

annular cylindrical tungsten wire arrays onto a 14 mg/cc CH foam that converts the implosive energy to x rays. The stellar opacity sample is 1–2 mm above the source, while four other samples are arranged at different side-on azimuthal locations 4–30 cm away.<sup>33</sup> The location, sample design, and diagnostics are separately optimized to address different physics objectives. The stellar opacity experiment<sup>89</sup> seeks to answer the question: Why can we not accurately predict helioseismology observations for the Sun? Two different photoionization experiments<sup>90–92</sup> address the question: How does ionization and spectral line formation in accretion-powered objects occur? The white dwarf photosphere experiment<sup>93–95</sup> targets the question: Why does fitting photosphere spectra not provide accurate properties for white dwarf stars? In this review paper, we use the stellar opacity experiment to illustrate the opportunities and challenges associated with this type of research. Readers interested in the other topics are referred to the publications cited above.

How does energy propagate from the solar core to the surface of the Sun, where it emerges to warm the Earth? How old are the stellar systems that host the numerous exoplanets that have been discovered outside our solar system? How does radiation penetrate and heat an inertial fusion capsule? The answers to these three questions hinge on knowledge of the fundamental material property (i.e., opacity) that controls absorption of radiation.<sup>77</sup> A specific question arose about 15 years ago<sup>96</sup> when refined analysis of solar photosphere spectra led to reduced abundances for certain elements in the Sun. Solar energy transport depends on how much of each element is present and the nature of individual elemental opacities. Thus, these composition revisions altered the internal structure calculated with the Standard Solar Model, and the model predictions now disagree with helioseismology observations.<sup>97</sup> This issue can be resolved by an arbitrary increase in

the calculated solar matter opacity used as input for the Standard Solar Model.<sup>98</sup> The question is whether this is the right explanation.

HED opacity experiments volumetrically heat a sample with x rays and measure the transmission with spectrometers that view a bright backlighter through the sample. Requirements for opacity experiments were developed over the last 30 years,<sup>78,99,100</sup> but the high temperature and density inside stars precluded measurements at those conditions until now. Both the energy required to heat a sample uniformly and the backlighter brightness required to overwhelm the sample self-emission increase with sample temperature. These challenges were surmounted in Z experiments<sup>101</sup> beginning around 2005. X rays from the dynamic *Hohlraum* x-ray source heat an opacity sample located above the cylindrical source over  $\sim 10$  ns and the convergence on axis generates a backlighter with radiation temperatures  $> 350$  eV over  $\sim 3$  ns. These characteristics, developed over a decade, enabled the first iron opacity data at solar interior conditions.<sup>89</sup> Iron contributes significantly to solar opacity; the relatively large number of bound electrons makes iron more susceptible to model uncertainty. We found that opacity models were accurate at 150–160 eV temperatures and  $7 \times 10^{21}$  electrons/cc, but the model predictions were lower than our opacity data when the temperatures and densities were increased to solar interior values (Fig. 7).

The higher-than-predicted Z iron opacity data<sup>89</sup> account for about half the increase needed to resolve the Standard Solar Model discrepancy. However, the question remains: Why are the model predictions lower than our measurements? This question is critical because, if the data are correct, our understanding of photon absorption in HED matter must be revised. This would have far-reaching consequences for astrophysics and terrestrial HED science. For example, a widely used method to estimate stellar ages depends on opacity, and

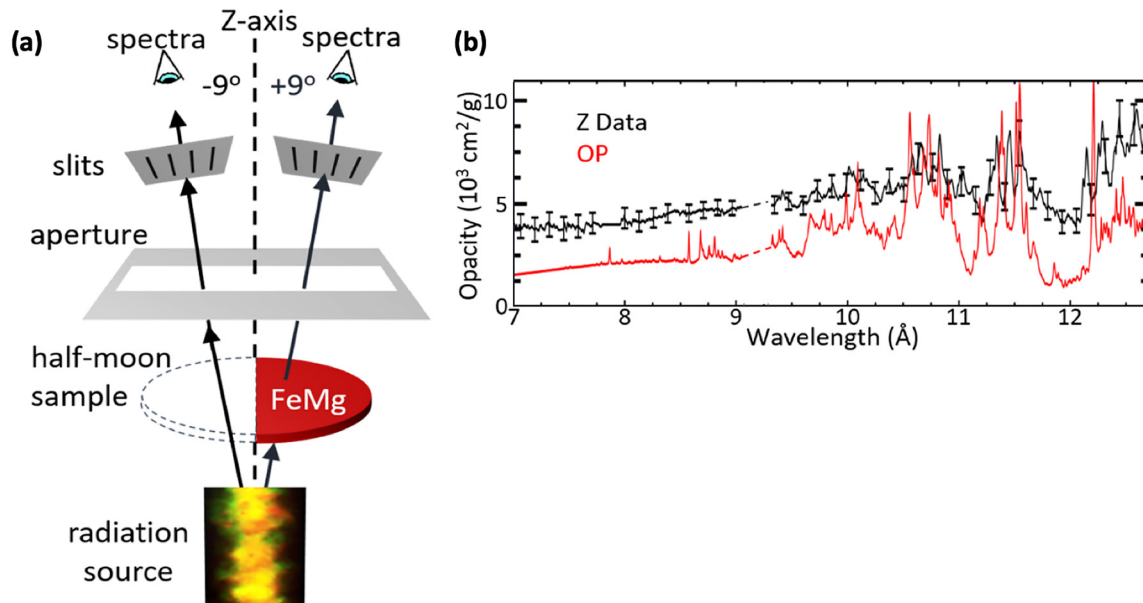


**FIG. 7.** (a) Z opacity experiments measure transmission through half-moon-shaped samples with multiple spectrometers. (b) Measured iron opacity (black) at  $T_e = 182$  eV and  $n_e = 3 \times 10^{22}/\text{cc}$  is generally higher than the Opacity Project (OP) model predictions (red), accounting for about half the increase needed to resolve the Standard Solar Model discrepancy. The OP opacity model [Badnell *et al.*, MNRAS **360**, 458 (2005)] is publicly available and widely used by astrophysicists for solar structure calculations.

opacity revisions will therefore lead to substantial changes in age estimates. Furthermore, if solar composition, opacity, and helioseismology inferences are found to be consistent, the soundness of the Standard Solar Model will be reinforced, but the composition and opacity used to model other Sun-like stars must be revised. On the other hand, if observations and solar model inputs cannot be reconciled, possible modifications to the solar model itself would be necessary.

Our present opacity research on Z focuses on testing hypotheses for the model-data discrepancy. One broad hypothesis category asks: Could the experiments be flawed? A second category asks: Does opacity theory include inaccurate or incomplete physics? A powerful strategy to address these questions is to obtain systematic opacity data as a function of temperature, density, and atomic number. Variations in each of these three key quantities cause testable opacity changes that provide insight into possible theory revisions and experimental flaws. Results of the first-ever systematic opacity study<sup>102</sup> reinforced our confidence in the experiments and suggested refinements to the opacity model. Nevertheless, a satisfactory resolution of the model-data discrepancy remains a topic for ongoing research.

Our Z opacity research illustrates how opportunities arise from the ability to heat, compress, and diagnose unprecedented macroscopic quantities of extreme HED matter. These radiation-heated matter investigations are examples of “benchmark” experiments that aspire to be a reliable reference point for models. A sound foundation for use-inspired or applied research is a major priority for such benchmark measurements, both for astrophysics and the HED research described elsewhere in this review paper. Meeting this need requires plasmas with parameters as close as possible to an intended application. Additional requirements include *reproducible and controlled* data on input quantities to make predictions and *reproducible and controlled* data on observables that a model predicts. Our x-ray-driven experiments on Z are well suited to such studies because we can produce the extreme conditions in plasmas of the size and duration commensurate with accurate data, all with demonstrated reproducibility.

### C. Dynamic material properties

Currents as high as 26 MA on Z, coupled to megagauss magnetic fields generated by those currents, produce enormous  $\mathbf{J} \times \mathbf{B}$  forces on current-carrying surfaces. Starting in the late 1990s, we used these forces to produce shockless compressions and quasi-isentropic loading on Z.<sup>103</sup> Those experiments reached 0.3 Mbar pressures and probed the kinetics of the  $\alpha$ - $\epsilon$  iron transition<sup>104</sup> and were followed by load designs and current pulse shapes configured to use the same  $\mathbf{J} \times \mathbf{B}$  forces to accelerate metal flyer plates magnetically to  $>20$  km/s.<sup>105</sup> The hypervelocity flyer plates imparted Mbar shock waves on impact, enabling exploration of the Hugoniot at ultra-high pressures. These advances provided critical HED material data on Z. Early success included the principal isentrope of the 6061-T6 aluminum alloy to 2.4 Mbar<sup>106</sup> and the Hugoniot of deuterium to 0.7 Mbar.<sup>107</sup> The principal isentrope and Hugoniot are key reference curves to construct equation-of-state (EOS) models. The data are used to validate theoretical methods for calculating thermodynamic and transport properties. We can also extract constitutive properties such as material strength at high pressures over a range of strain rates by innovative load designs and careful analysis of velocity profiles. For an extensive history of shock physics and dynamic materials research at Sandia, see the book

*Impactful Times: Memories of 60 Years of Shock Wave Research at Sandia National Laboratories.*<sup>108</sup>

The principal isentrope and the Hugoniot are important to understand dynamic material response, but many material phases, thermodynamic and transport properties, and associated phase transitions (e.g., solid–solid, solid–liquid, and liquid–liquid) are not probed by either curve. With advances in current pulse shaping and MHD simulations of Z load hardware in the last 15 years, we have dramatically increased the sophistication and versatility of the experimental platforms, going beyond pure ramp or shock to shock-ramp, or elevated temperature isentropes, as well as shock and release to greatly expand the breadth of the accessible thermodynamic phase space and interesting physical processes. In concert with these advances, we have developed a containment capability for hazardous materials such as plutonium and uranium. Meanwhile, advances occurred in diagnostics, wave analysis methods, accelerator modeling, pulse shaping, data analysis, large-scale MHD simulations, EOS and transport models, and first-principles theoretical methods. Tight coupling of the capabilities on Z with such advances have allowed us to address entirely new questions in dynamic compression science. Examples of these platforms and applications follow.

### 1. Improved capabilities for dynamic materials experiments at Z

In the last 15 years, the capability to shape the current pulse flexibly and reliably has vastly improved, beginning with refurbishment of Z in 2007, which introduced a topological change that quadrupled the number of gas-switch trigger times<sup>20,109</sup> along with many new capabilities. Today, various pulse shapes with rise times up to 1.4  $\mu$ s are possible thanks to (1) the 95-kV charge voltage, (2) two independent Marx trigger times, (3) independent laser triggering of 36 low-jitter, 6-MV gas switches,<sup>20,110</sup> (4) a detailed Z transmission line circuit model,<sup>111,112</sup> and (5) 2D load simulations. Figure 8 shows MITL current waveforms representing the range of possible pulse shapes, including double-ramp pulse shapes for shock-ramp experiments. The standard synchronous pulse shape for ICF is shown for comparison.<sup>113–115</sup>

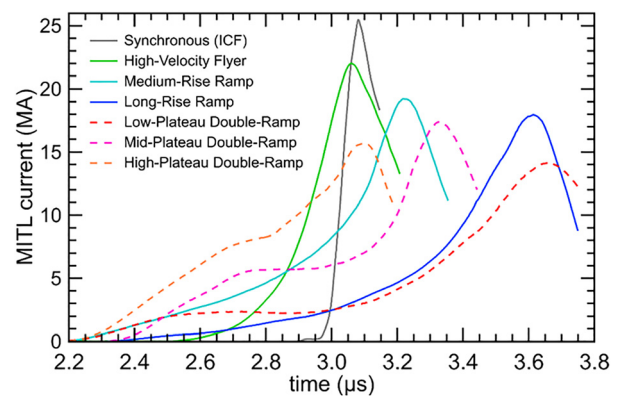


**FIG. 8.** Representative pulse shapes for Z dynamic materials experiments, compared to synchronous (non-shaped) pulse for ICF. Dual Marx triggers provide pulse shapes that peak late in time. Double-ramp pulse shapes are typically used to drive shock-ramp experiments, for which the plateau region of the pulse delays arrival of the post-shock ramp.



In 2008, a stripline load<sup>116</sup> significantly increased peak pressures and accuracy of our quasi-isentropic data. This advance enabled  $>4$  Mbar ramp compressions<sup>117</sup> and  $>40$  km/s Al flyer velocities.<sup>118</sup> A stripline load design requires modeling 2D MHD effects of magnetic scale length relating load current history to magnetic pressure loading history and time dependence of the load inductance caused by magnetic diffusion, motion, and electrode deformation. We use resistive-MHD codes such as ALEGRA<sup>119</sup> as predictive design tools and in post-shot analyses. These simulations require sophisticated EOS and electrical conductivity models of the electrode material.<sup>120</sup>

A limitation to using MHD simulations for design and analysis is that the 3D load geometries must be accurately represented by 1D simulations (with limited 2D simulations), given the prohibitive cost of 3D simulations as a design tool. We put considerable care into designing 3D load geometries that are amenable to accurate representation in 1D and 2D. Typical load designs begin with 1D Lagrangian simulations to determine the magnetic field drive, followed by 2D Eulerian simulations to determine the load current and associated inductance history. The magnetic field is not allowed to penetrate to the sample material, negating the need for detailed electrical conductivity models. We use simple analytical EOS models if little or no high-pressure data are available. Finally, a configuration is determined by adjusting the switch parameters in the circuit model to match the load current self-consistently to the inductance.<sup>112</sup>

## 2. Density functional theory equation-of-state and transport

*Ab initio* theory is vital to material modeling. Electronic structure calculations, primarily with density functional theory (DFT), provide complementary information about material conditions that are often exceedingly difficult to diagnose experimentally. Because of direct access to microstructure and temperature, *ab initio* molecular dynamics (AIMD) simulations frequently diagnose phase transitions such as critical points,<sup>121</sup> melt curves, and solid–solid phase transitions<sup>122</sup> and access thermodynamic states along the Hugoniot<sup>121–124</sup> and the principal isentrope,<sup>121</sup> allowing direct comparison with data while providing insight into behavior such as molecular dissociation.<sup>125</sup> The extreme conditions on Z, along with highly precise diagnostics, have allowed us to test approximations in *ab initio* theories. For instance, the choice of density functional approximation in DFT has a significant effect on the calculated state of singly- or multiply-shocked deuterium<sup>126</sup> and has led to research on alternative methods such as quantum Monte Carlo (MC).<sup>127,128</sup> Time-dependent DFT research has also allowed us to calculate the optical response of x-ray Thomson scattering.<sup>129</sup> With AIMD simulations, in conjunction with the Kubo–Greenwood formula, we can calculate the optical properties of materials. Simulations are initialized with desired temperature and density states and allowed to equilibrate, at which time the optical properties are calculated from multiple simulation time step snapshots as the domain oscillates around equilibrium. More snapshots are added until a canonical ensemble is produced. Arrays of conductivity values are created by simulating density-dependent isotherms. These arrays guide development of electrical conductivity models such as Lee–More–Desjarlais<sup>130</sup> for aluminum.<sup>131</sup> Once the EOS is validated, the conductivity model can be “tuned” with a Z experiment.<sup>120</sup>

## 3. Materials research diagnostic suite and data analysis

Virtually all pressure and density data are tied to the Velocity Interferometer System for Any Reflector (VISAR)<sup>132</sup> and/or photonic Doppler velocimetry (PDV).<sup>133</sup> The VISAR has measured flyer velocities, shock-wave speeds, and sample-interface motion since the Z dynamic material program began. PDV was deployed in the last decade, initially to support cylindrical implosions.<sup>134</sup> Both diagnostics are usually fielded simultaneously on material samples and as current monitors; PDV also monitors radiation and plasma production.<sup>135</sup>

Streaked visible spectroscopy (SVS)<sup>136</sup> provides time-resolved data on light emitted, absorbed, or reflected by shock fronts and surfaces within a sample. SVS consists of a fiber optic probe at the sample coupled to a grating spectrometer. A streak camera records the output vs time. SVS is typically used with transparent materials that become opaque under shock loading, such as liquid deuterium,<sup>137</sup> liquid xenon, or lithium deuteride.<sup>138</sup> Material states that exceed 5000 K produce ample light for fiber-coupled streak cameras, and temperatures as low as 3000 K are sometimes measurable. Peak emission occurs in the visible to ultraviolet range for temperatures high enough for SVS to observe, so the spectral shape does not strongly constrain the inferred temperature; sample emissivity is essential to determine temperature unambiguously. Emissivity can be estimated from reflectivity of the VISAR laser or calculated from first-principles. SVS also monitors changes in the electronic structure by measuring the reflectivity from a sample surface. In this manner, we have mapped the transition of deuterium from an insulator to a metal.<sup>139</sup>

Ramp compression produces lower temperatures than shock compression, reducing light emission below streaked spectroscopy capabilities. Temperatures as low as 1200 K have been measured via band pyrometry with InGaAs avalanche photodiodes ( $\sim 1000$  to 1700 nm). Shorter wavelength data are impractical because of substantial and poorly understood background radiation; longer wavelength data are prohibited by optical fiber absorption in the  $\sim 50$ -m relay between the samples and the diagnostic. Overcoming these spectral barriers and supporting temperature measurements  $< 1000$  K is an ongoing challenge.

## 4. X-ray diffraction on Z

Velocimetry diagnostics provide insight into material behavior in the continuum; macroscopic-scale, x-ray diffraction (XRD) opens the door to atomic-scale understanding to detect, identify, and quantify phase transitions by direct observation of compression and strain of the crystal lattice. Because of Z's destructive nature and the low XRD signal vs background emission levels, detecting an XRD pattern close to a sample and recovering the data are quite challenging. We are now fielding a Spherical Crystal Diffraction Imager (SCDI) (see Fig. 6 in Ref. 140) on Z that relays and images the XRD pattern away from the load debris field. That diagnostic uses the Z-Beamlet laser<sup>23</sup> to probe a shock-compressed sample with 6.2-keV Mn-He<sub>x</sub> x rays. A spherically bent crystal composed of highly oriented pyrolytic graphite collects and focuses the diffracted x rays into a 2.54-cm-thick tungsten housing, where an image plate records the data. Our SCDI diagnostic has measured XRD patterns of shock-compressed Be samples at pressures of 1.8–2.2 Mbar.<sup>141</sup>

### 5. Uncertainty analysis

Data uncertainties occur on every experiment. Over the last decade, we have developed methods to reduce and incorporate uncertainties in our data analysis. Monte Carlo (MC) methods easily incorporate uncertainties in calculations and account for correlated and uncorrelated errors in the data and models to provide confidence in the uncertainties. We have applied MC methods to impedance matching to calculate Hugoniot states<sup>122,124</sup> and to calculate temperatures from pyrometry data in Z shock experiments and in laser-driven decaying shock experiments<sup>142</sup> and from Z ramp compression data.<sup>143</sup> We have expanded MC methods to analyze Hugoniot data for phase transitions of materials such as carbon<sup>144</sup> and MgO.<sup>122</sup> Recently, we have been developing Bayesian methods to analyze properties under ramp compression.<sup>145</sup>

### 6. Improved shock impedance standards and application to deuterium experiments

We analyze most shock physics experiments by comparing the material shock response with that of a standard reference material, an approach known as impedance matching. For decades, aluminum was the predominant impedance match standard since it had been well characterized in numerous gas gun, explosive-driven, and nuclear-driven experiments. Because it is opaque, however, the shock speed must be determined by measuring the transit time through the Al standard. For small thicknesses and short transit times typical of multi-Mbar experiments, that combination severely limited the attainable precision. Precision can be improved by using impedance match standards amenable to direct shock velocity measurement with velocimetry. In the past decade, we have collected data on several more ideal impedance match standards:  $\alpha$ -quartz,<sup>146</sup> fused silica,<sup>147</sup> polymethylpentene (also known as TPX<sup>TM</sup>) plastic,<sup>148</sup> and silica aerogel.<sup>149</sup> These standards are initially transparent, but the shock fronts become reflective when shocked to high enough pressures. Velocimetry can directly and continuously measure the shock velocity with high precision as the shock transits the standard. The differing initial densities in these standards (2.65 g/cc for quartz to 0.1 g/cc for aerogel) allow probes at different pressures.

Today  $\alpha$ -quartz is the predominant standard for HED experiments on Z and laser facilities. We have accumulated hundreds of data points for its shock compression and high-pressure release response, initially from  $\sim 3$  to 12 Mbar; example shock and release measurements using TPX and two different initial density silica aerogels are shown in Fig. 9. Using Z data along with first-principles DFT calculations, we developed a simple analytical model in 2013 for  $\alpha$ -quartz that includes both precise Hugoniot<sup>146</sup> and isentropic release paths from the Hugoniot states<sup>150</sup> that account for all experimental uncertainties in that pressure range. We recently conducted  $\alpha$ -quartz release experiments at lower pressures and used first-principles calculations to extend our analytical model to 30 Mbar, well above the existing experimental data.<sup>151</sup> The high precision of the  $\alpha$ -quartz standard has reconciled two data sets for the liquid deuterium Hugoniot,<sup>146</sup> led to quick adoption of the new standard in the HED community, and proved critical to analyze 10 Mbar experiments of the deuterium Hugoniot.<sup>152</sup> This new standard would not have been possible without ultra-high-velocity flyers on Z. A similar analytical release model for Al<sup>153</sup>

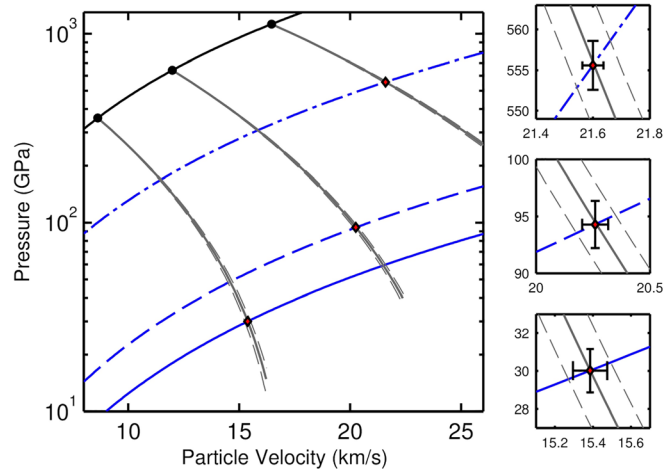


**FIG. 9.** Representative  $\alpha$ -quartz release measurements into TPX (dotted-dashed blue line), 190 mg/cc silica aerogel (dashed blue line), and 110 mg/cc silica aerogel (solid blue line). Black line,  $\alpha$ -quartz principal Hugoniot; black circles, initial shocked states; red diamonds, measured release states; solid (dashed) gray lines, release paths from the analytical release model (one-sigma standard deviation). Right panels shown for more details. Reproduced with permission from Knudson and Desjarlais, Phys. Rev. B **88**, 184107 (2013). Copyright 2013 American Physical Society.

improved the accuracy and precision of previous Al impedance matching studies, including early Z studies of liquid deuterium.<sup>126</sup>

An example of this increased precision is a recent study of the molecular-to-atomic transition of liquid deuterium along the principal Hugoniot.<sup>126</sup> Using a cryogenic cell with  $\alpha$ -quartz front and rear windows, we measured the flyer velocity from the initial motion to impact and the shock velocities in  $\alpha$ -quartz and deuterium, both of which became reflective. The  $\alpha$ -quartz model provided highly constrained adiabatic release paths and could be incorporated into an MC method to ensure propagation of all random and systematic errors in the standard (both for Hugoniot and release). The uncertainties in particle velocity, pressure, and density compression for deuterium were  $\sim 0.5\%$ ,  $\sim 0.6\%$ , and  $\sim 1.5$  to  $1.9\%$ , respectively—a significant increase in precision over previous data (see Fig. 10). This unprecedented precision enabled discrimination between subtle differences in first-principles theoretical predictions and provided an important benchmark for first-principles theory, a means for evaluation of future theoretical developments, and stringent constraints on the high-pressure response of hydrogen in a regime that is directly relevant to planetary interiors.

### 7. Shock experiments with beryllium

Our ability to fabricate and launch composite flyer plates has improved the Z shock platform. These flyer plates typically consist of an Al substrate with a somewhat thinner copper layer electroplated on the impact surface. Al acts as a sacrificial current-carrying layer that is largely consumed by the diffusing magnetic field, leaving the Cu layer at near ambient conditions upon impact. The large density discontinuity at the Cu/Al interface causes a rarefaction wave that propagates back toward the shock front, enabling measurement of sound velocity

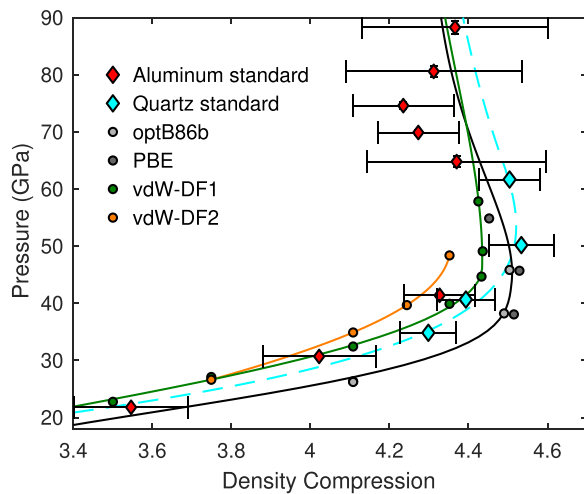


**FIG. 10.** Deuterium pressure–density compression Hugoniot (all relative to  $\rho_0 = 0.167$  g/cc) in the vicinity of the molecular-to-atomic transition. Cyan diamonds, individual plate impact experiments with the  $\alpha$ -quartz standard;<sup>150</sup> red diamonds, weighted average of plate impact with an aluminum standard,<sup>107</sup> reanalyzed using the recent aluminum release model<sup>153</sup> (weighted averages of up to seven individual experiments); colored circles, first-principles calculations using various exchange–correlation functionals. Reproduced with permission from Knudson and Desjarlais, Phys. Rev. Lett. 118, 035501 (2017). Copyright 2017 American Physical Society.

in the sample at high pressure to provide information beyond the shock Hugoniot that is sensitive to phase transitions and melt. We have used this capability to measure the beryllium Hugoniot and sound velocity from 0.90 to 3 Mbar.<sup>154</sup> The data agree with state-of-the-art LANL and LLNL EOS tables<sup>155,156</sup> but do not agree with earlier solid Be Hugoniot data at  $>0.90$  Mbar.<sup>157</sup> Onset of shock melting was seen at  $\sim 2$  Mbar, but we found no evidence of the proposed hcp–bcc transition, suggesting that Be melts directly from the hcp phase. The sound velocity data resolved questions about the location of the hcp–bcc transition and the pressure at which the Hugoniot crosses the melt curve. These results constrain the Be EOS at conditions relevant to ICF implosions and will aid future target designs.

### 8. Insulator–metal transition in deuterium

In 1935, Wigner and Huntington<sup>158</sup> suggested that hydrogen or its isotopes could become metallic at sufficiently high compression. In addition to being of fundamental interest to condensed matter theory, the planetary science community recently recognized that an insulator–metal transition in liquid hydrogen could have a direct bearing on conditions under which helium rain will form in a hydrogen–helium atmosphere<sup>159</sup> and on Saturn’s high thermal luminosity relative to its estimated age. Experimental demonstration of this metallization has been elusive, and theoretical predictions have depended sensitively on the framework used, varying from  $\sim 1$  Mbar to  $>3$  Mbar. In the early 2010s, we conducted experiments to probe this transition in collaboration with the University of Rostock in Germany as part of the Z Fundamental Science Program. Reaching these pressures while hydrogen remains a low-temperature liquid, just above melt, was not

possible with ramp or shock compression alone. Instead, we designed a shock-ramp platform with a small, prescribed gap between the electrode drive plate and a cryogenic sample. Using a carefully designed current profile, an initial rapid increase in current would drive the electrode across the gap to provide a small shock. The subsequent current increase then drove the sample along an isentrope to high pressure and density. We chose deuterium for these experiments because of its higher shock impedance, making the low temperatures for metallization easier to reach. By varying the initial shock strength, various isentropes could be accessed to sample the phase boundary at different temperatures. Our first experiments did not reach high enough pressures but showed that deuterium became absorptive at  $\sim 1$  to 1.5 Mbar by closing the bandgap, an essential precursor to metallization. Subsequent experiments used a stripline load<sup>116,118</sup> and reached higher pressures. These experiments demonstrated a density-driven, insulator–metal transition in liquid deuterium for the first time, with an abrupt transition to high reflectivity,  $\sim 60\%$  that of Al, at 2.8 to 3.0 Mbar pressures.<sup>139</sup>

### 9. Iron rain

Planetary accretion<sup>160</sup> and the Moon forming impact<sup>161</sup> involve high-velocity collisions among planetesimals to create HED matter. The impact velocity distribution in such collisions extends to 40 km/s and peaks at  $\sim 20$  km/s.<sup>160</sup> Z is ideal to measure key thermophysical properties accurately that determine the evolution of matter during accretion. One such property is the vaporization threshold (i.e., the shock pressure that vaporizes material upon impact). That threshold determines how much of a solid impacting object remains solid, melts, or is vaporized and thus decidedly affects the dynamics of a system after impact. In a collaboration among Sandia, Harvard, and UC Davis within the Z Fundamental Science Program, we developed a shock and deep-release platform to determine the critical point of iron.<sup>162</sup> Iron is of interest since its content differs in the Earth and Moon. We determined that the shock pressure to vaporize iron is  $\sim 5$  Mbar, which is significantly lower than the previous theoretical estimate. Such shock pressures are easily achieved by high velocity impacts at end stages of accretion, qualitatively changing the Earth–Moon system dynamics.<sup>162</sup> Through the Z Fundamental Science Program, Sandia also collaborates with university partners to measure thermophysical properties of minerals important to planetary science.<sup>122,142,163</sup>

### 10. Ramp compression and strength experiments

Ramp-compression experiments are a core component of our Z dynamic materials research. By tailoring the load design and current-pulse shape, we can smoothly compress a sample for hundreds of nanoseconds, mitigating the temperature increase associated with shock loading. Recent advances, such as new high-precision standards,<sup>117,164</sup> the stripline load,<sup>118</sup> and improved analyses,<sup>165,166</sup> have yielded data for multi-Mbar pressure–density quasi-isentropes to high precision (i.e., sub-1% density uncertainties). A notable feature of this compression to extreme pressures and relatively low temperatures is that most materials remain in the solid phase and support shear stress. As such, our Z platform has been adapted to study high-pressure strength using a release measurement in addition to the initial ramp (i.e., a ramp-release). The nature of the measured loading reversal has a strong sensitivity to strength, and we have developed an analysis



method to extract quantitative metrics of interest.<sup>167</sup> We have studied a variety of metals using ramp and ramp-release platforms, including Al, Cu, Be, Fe, Pb, Zr, Ta, Au, Pt, and Ir. Our Ta research is highlighted as an example in Fig. 11. As illustrated, we have obtained high-precision ramp-compression data<sup>165</sup> along with independent ramp-release strength estimates<sup>143</sup> to  $\sim 3$  Mbar. The data allow an unprecedented ability to predict the complete constitutive response of Ta under these conditions and have factored heavily in a collaborative effort among the three NNSA national security laboratories to understand material strength in the extremes.<sup>168</sup>

## 11. Containment experiments

In the early 2000s, we began to develop a containment system for dynamic compression experiments on hazardous materials without contaminating Z. The complicated architecture of the double-post-hole vacuum convolute, which combines current from four MITLs into a single feed gap near the load, necessitated the design of a cathode extension between the convolute and the load. This extension, essentially a metallic cylinder, provides a single feed gap long enough for an explosively driven closure system, referred to as the ultra-fast closure valve (UCV). Concurrent with firing of Z, the anode is explosively driven across the UCV feed gap, creating a hermetic seal along the cathode extension. An upper containment chamber (UCC) atop the UCV is protected by a stout baffle system to restrain the  $\sim 2$  MJ energy delivered to the load. The UCV, UCC, and baffle comprise a robust containment system that has allowed us to conduct  $>50$  dynamic compression experiments on hazardous materials beginning in 2006.

## D. Fusion science

The conventional approach to ICF relies on high implosion velocities ( $>350$  km/s) and spherical convergence to achieve the high fuel temperatures ( $>4$  keV) and areal densities ( $\rho R > 0.3$  g/cm<sup>2</sup>) required for ignition.<sup>169</sup> Such high velocities are achieved by heating the outside surface of a spherical capsule to generate ablation pressures as high as 150 Mbar. This heating is accomplished either directly with

many laser or ion beams (direct drive) or with x rays generated within a *Hohlraum* (indirect drive). From 1996 to 2006, the ICF program on Z focused on magnetic indirect drive approaches, where wire-array z-pinch implosions were used to create the x-ray drive pressure on a capsule. As discussed in two previous review articles,<sup>29,86</sup> considerable progress was made in these approaches and they remain viable paths to laboratory ICF on a larger pulsed power driver. The largest uncertainty was in the capsule physics, which is actively being studied today on the National Ignition Facility.

A much more energetically efficient approach is to use the magnetic pressure generated by a pulsed power accelerator to drive an implosion *directly*. In this approach, 5%–10% of the stored energy can be converted to the kinetic energy of an imploding metal tube, usually referred to as a “liner.” However, implosion velocities of only 70–150 km/s are attained when the liner thickness is sufficient to eliminate feedthrough of hydrodynamic instabilities. Numerical simulations and experiments<sup>170–175</sup> indicate that thick-walled liners with an aspect ratio ( $AR = R_{\text{outer}}/\Delta R_{\text{wall}} \sim 6$ –9) should be adequately robust. Magneto-inertial fusion concepts can relax the implosion velocity requirements while still achieving high temperatures by use of insulating magnetic fields to decrease thermal conductivity normal to the field and increase fusion product confinement.<sup>15,176,177</sup> Magnetized liner inertial fusion (MagLIF)<sup>29,170,178</sup> is a specific MIF concept that we are studying today at Z.

## 1. Implosion physics

Assembly of fusion fuel to high stagnation pressure can be achieved by magnetic acceleration of a metallic liner. The magnetic pressure applied to a current-carrying liner can be estimated with the formula<sup>29</sup>

$$P_{\text{mag}} = B^2/2\mu_0 = 105\{(I_{\text{MA}}/26)/R_{\text{mm}}\}^2(\text{Mbar}).$$

For a liner carrying 26 MA imploded to 1 mm radius, the magnetic pressure exerted is 105 Mbar. Ignition-relevant Gbar-scale magnetic pressures may be achieved on a future (e.g., 60–70 MA) pulsed power facility at mm-scale radii.

In an ICF system, magnetic pressure must be applied rapidly so the fuel heating rate exceeds radiation and conduction losses, and the implosion must remain highly symmetric. Fuel magnetization in MIF systems limits the fuel energy loss during an implosion, although liner velocities  $>100$  km/s are required. Higher implosion velocities are achieved by increasing the liner’s aspect ratio, but such liners are more likely to disassemble during an implosion because of MRT instability growth. The liner must stay intact through implosion and stagnation. A detailed understanding of the physics governing the stability is needed to optimize the performance of concepts such as MagLIF<sup>170</sup> and to determine the requirements of a next-generation pulsed power facility. To that end, Sandia’s magnetic direct drive ICF research has prioritized liner implosion stability physics studies on Z.

In advance of our first MagLIF experiments, we conducted liner implosion physics experiments on Z<sup>171,172</sup> to constrain the MRT instability data to validate the MHD packages in codes such as LASNEX,<sup>179</sup> HYDRA,<sup>180</sup> and GORGON.<sup>181</sup> We imploded aluminum liners with machined 25-to-400- $\mu\text{m}$ -wavelength sinusoidal surface perturbations on Z in 100 ns and quantified the MRT instability growth with

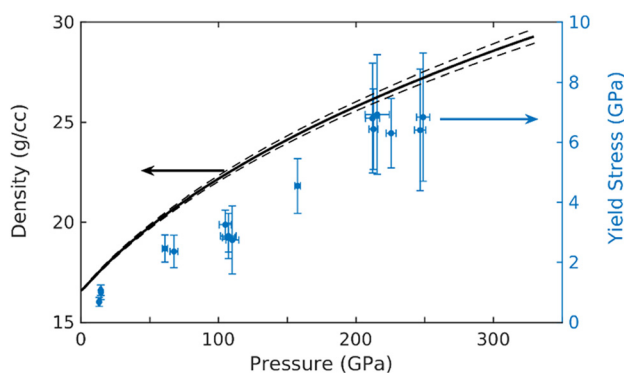


**FIG. 11.** Tantalum ramp [Davis *et al.*, *J. Appl. Phys.* **116**, 204903 (2014)] and ramp-release [Brown *et al.*, *J. Appl. Phys.* **115**, 043530 (2014)] results. Ramp compression path (smooth line) contains low standard errors (dashed lines), providing tight equation-of-state constraints. Each point is for strength estimated from the peak state in a ramp-release measurement; error bars represent standard errors.

radiography. Agreement between our experimental and simulated radiographs was remarkable for wavelengths down to  $50\ \mu\text{m}$  (Fig. 12).

Next, we diagnosed the implosion stability of cylindrical MagLIF-like Be liners through stagnation.<sup>173,174</sup> Relative to Al, Be liners are favorable since their lower density allows a higher implosion velocity from a lower aspect ratio (thicker walled) liner geometry that is more robust against MRT feedthrough. Beryllium's low atomic number also reduces radiative losses when mixed into the hot fuel.<sup>182</sup> The implosion morphology data of these liners have higher than expected azimuthal correlation of MRT structures through stagnation. Our simulations were a better match to the data when initialized with an azimuthal bias applied to the random surface generator at several axial locations. However, the simulations are not a rigorous implementation of the surface finish of the liners, which are normally turned on a lathe and result in highly azimuthally correlated structures with a 100–250 nm root mean square (rms) surface roughness. For additional experiments using liners with surface roughness smaller than 50 nm rms, we observed no changes in the imploding liner's instability growth. Further experiments using a different machining technique to produce axially oriented grooves (instead of azimuthally oriented ones) also resulted in no obvious impact on the observed instability growth.<sup>183</sup>

To determine what provides the primary seed for MRT instability growth, we began to study initiation and evolution of electrothermal instabilities (ETI). ETI is an Ohmic-heating-driven instability that relies on the feedback between temperature and conductivity in a metal.<sup>184–194</sup> Our simulations show that, as the surface temperature exceeds the melting point, ETI-driven temperature perturbations can generate non-uniform expansion on a liner's surface, resulting in a largely azimuthally correlated perturbation with orders of magnitude larger amplitude than the initial surface roughness. ETI-driven perturbations can therefore provide the dominant seed for MRT growth on ultra-smooth liners. Our simulations also predicted a dramatic reduction in instability growth on solid metal rods and liners when thick

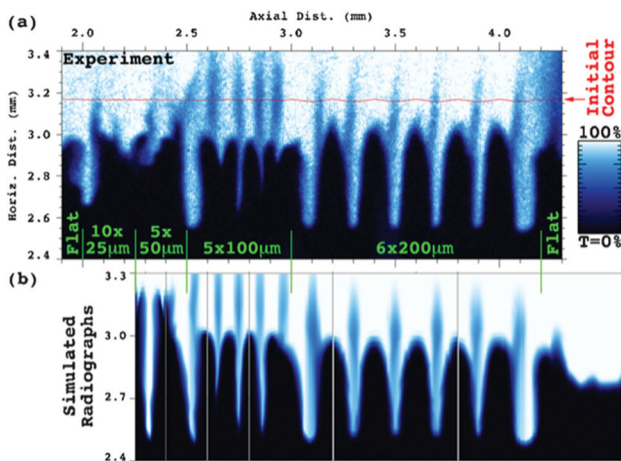


FIG. 12. (a) Experimental radiograph of the liner with pre-imposed sinusoidal perturbation; initial contour overlays radiograph. (b) Mosaic of simulated radiographs from six different LASNEX calculations. Modified with permission from Sinars *et al.*, Phys. Rev. Lett. **105**, 185001 (2010). Copyright 2010 Author(s), licensed under a Creative Commons Attribution 3.0 License.

dielectric coatings are applied to the current-carrying surface.<sup>195</sup> The dielectric damps growth of ETI-driven density perturbations, reducing the seed for subsequent MRT growth [Fig. 13(a)]. We demonstrated the efficacy of stabilizing dielectric coatings on Z [Fig. 13(b)] from radiography of high-current-density rods and imploding liners.<sup>196</sup>

To prepare for preheated and premagnetized MagLIF experiments, we developed external Helmholtz-like magnetic field coils for Z.<sup>197</sup> Surprisingly, the change in liner morphology for the additional 7-T axial magnetic field was dramatic. In premagnetized liner implosions, we observed helical instability formation.<sup>198,199</sup> Those instabilities were distinctly different from mostly azimuthally symmetric instabilities seen for unmagnetized liners. We explored causes for seeding and evolution of the helical instabilities, including axial flux compression by imploding plasmas generated outside the liner<sup>200</sup> and helical flow and energy deposition from particles originating in MITLs.<sup>201</sup> The helical instabilities have also been studied on university-scale drivers, providing an extensive data set to compare with simulations.<sup>202</sup>

Our MagLIF experiments generate enough x rays during stagnation for high-resolution imaging of the hot fuel column. Fuel convergence ratios are near 40, and the liner implosion dynamics clearly impact the structure of the fuel stagnation column.<sup>203</sup> The helical structure that develops on premagnetized liners results in a helical fuel column, as indicated by x-ray emissions [Fig. 14(a)]. Increasing the liner aspect ratio (i.e., decreasing the wall thickness) amplifies the helical feedthrough to the fuel, and the structure becomes more complicated, with many overlapping helical modes [Fig. 14(b)]. A dielectric coating increases the uniformity of the fuel column, as shown in Fig. 14(c), without diminishing the neutron yield.<sup>204</sup> A limited data set also suggests that coated liners have enhanced shot-to-shot reproducibility compared to uncoated ones.

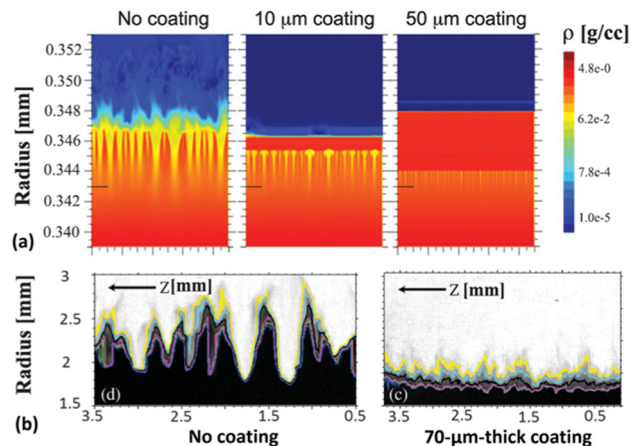
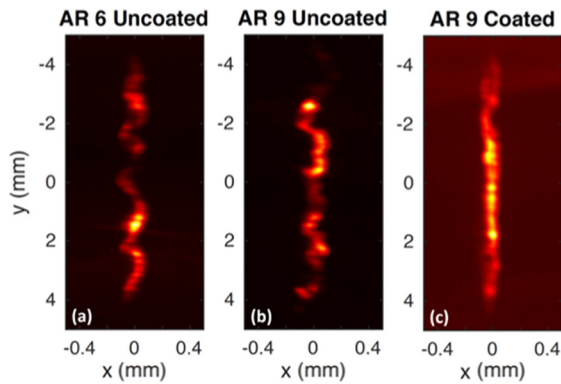


FIG. 13. (a) Simulated density contours showing difference in predicted perturbation growth for several thicknesses of dielectric coating on an Al rod at identical times for  $\sim 7$  MA. (b) Experimental radiographs of the current-carrying surface for both uncoated and dielectric-coated Al liners imploded on Z at nearly same current. Transmission contour percentages are 10% (blue), 15% (green), 20% (magenta), 40% (black), 60% (cyan), and 80% (yellow). (a) Adapted with permission from Peterson *et al.*, Phys. Rev. Lett. **112**, 135002 (2014). Copyrights 2014 American Physical Society. (b) Adapted with permission from Awe *et al.*, Phys. Rev. Lett. **116**, 065001 (2016). Copyrights 2014 American Physical Society.



**FIG. 14.** Comparison of x-ray emissions from the stagnation column in MagLIF experiments driven by (a) AR = 6 uncoated, (b) AR = 9 uncoated, and (c) AR = 9 dielectric coated liners.

Our implosion physics studies on Z continue to advance. Innovations, such as the dynamic screw pinch, may enhance liner stability by providing a magnetic drive with a tilted, dynamic polarization<sup>205</sup> that uses tilted or helical return-current posts.<sup>206</sup> Ongoing experimental<sup>207–209</sup> and computational ETI studies<sup>210</sup> are informing material choices and fabrication techniques for imploding liners and high-current-density electrodes. Detailed experimental studies of the underlying physics that drive implosion instabilities, coupled with detailed modeling and engineered mitigation strategies, will advance the target performance on Z and inform requirements for a next-generation pulsed power facility.

### 2. Magnetized liner inertial fusion

The MagLIF concept described in Ref. 170 has three important steps. The first is to apply an axial field of 10–30 T using capacitor-

bank-driven external Helmholtz-like coils positioned above and below the target.<sup>197</sup> Closed field lines are not required if the cylindrical liner is long enough to keep axial transport losses manageable. A 1-cm-long liner is sufficient for implosions driven by Z, which has a 100-ns current pulse. The second step is to preheat the deuterium (or deuterium–tritium) fuel to an average temperature of 100–200 eV using a laser beam. The 527-nm Z-Beamlet laser<sup>22,23</sup> has been used for fully integrated MagLIF experiments<sup>203,211</sup> and to study the preheating process.<sup>212,213</sup> The beam enters through a laser entrance hole (LEH) on top of the liner, which is covered with a thin (1.5–3.5 μm) polyimide foil to contain the fuel. The third step is to use the axially directed current from Z to generate a large azimuthal magnetic field on the outside of the liner to compress and further heat the fuel to fusion conditions at stagnation. The geometry used in many Z experiments is shown in Fig. 15. On the time scale of the implosion, the axial magnetic field is nearly frozen into both the fuel and the liner because of high conductivity and, hence, the magnetic field rises to very high values ( $\sim 10^4$  T) as the liner is compressed. The axial magnetic field inhibits radial electron thermal conduction loss throughout the implosion, particularly near stagnation when the losses would be the greatest because of the high temperatures.

Our MHD simulations indicate that the MagLIF concept can be scaled to achieve multi-MJ yields at currents significantly greater than what is possible on Z.<sup>170,178,182,214</sup> Gigajoule yields may even be possible by propagating the fusion burn into a layer of frozen deuterium–tritium (DT).<sup>178</sup>

We conducted the first Z experiments integrating all three steps of the MagLIF concept<sup>170</sup> in November 2013.<sup>203,211</sup> For these experiments, the applied magnetic field was 10 T, the initial deuterium gas density 0.7 mg/cc, the LEH foil thickness 3.5 μm, the laser preheat energy  $\sim 0.5$  kJ,<sup>212,213</sup> and the peak load current 16–18 MA. Although not optimal, the input parameters were sufficient to produce fusion conditions and demonstrate viability of MagLIF, key tenets of MIF concepts with primary deuterium–deuterium (DD) neutron yields of

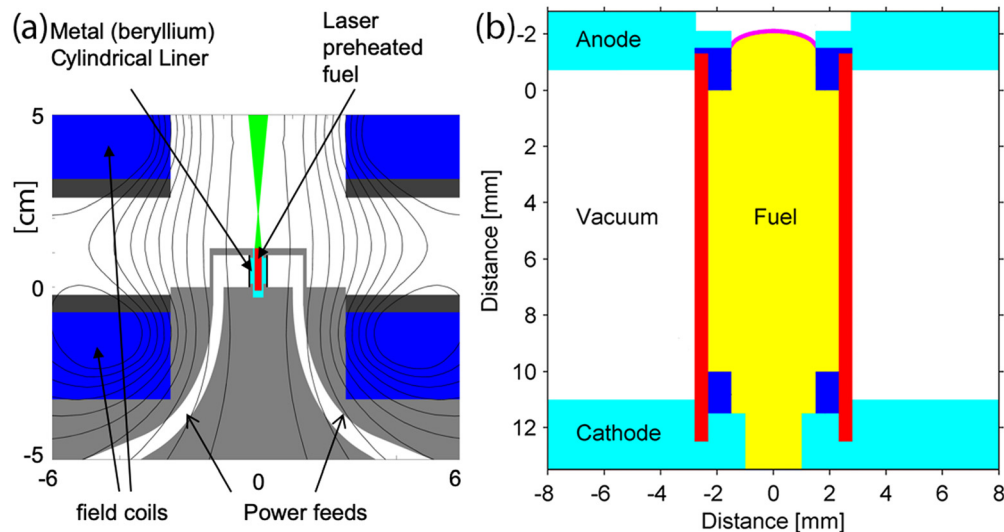


**FIG. 15.** (a) Example geometry for MagLIF experiments on Z, illustrating magnetic field lines, laser beam path, and final power flow feed gap topology. Dimensions are in cm. (b) Expanded view of an example MagLIF liner target.



$\sim 10^{12}$ , and multi-keV fuel temperatures.<sup>211,215,216</sup> The neutron spectra are isotropic and Gaussian, consistent with thermonuclear neutron production.<sup>211</sup> We observed significant secondary DT neutron production; the neutron spectra indicated a highly magnetized fuel column at stagnation of the fuel radius greater than the Larmor radius of tritons from DD fusion.<sup>217,218</sup>

So far, we have used Be liners 7.5–10 mm long with an outer diameter of 5.58 mm. Our numerical simulations<sup>219</sup> indicate this is near the optimum length for 100-ns implosions and the optimum diameter for 16–20 MA currents. The predicted optimum length increases with implosion time and the optimum diameter increases with drive current. The targets typically have AR = 6, but aspect ratios as low as 4.5 and as high as 9 have been tested,<sup>204</sup> with the lower aspect ratios producing more stable fuel columns, as expected. Targets with a 75- $\mu\text{m}$ -thick dielectric coating<sup>195</sup> produce more stable fuel columns,<sup>196,204</sup> even with AR = 9 liners.

We diagnose the fuel column structure at stagnation using spherically bent crystal imaging of the x-ray self-emission. A fuel column with a radius of 50–100  $\mu\text{m}$  and an axial extent of 7–9 mm has a complex morphology<sup>203,204,211,216</sup> suggestive of a helical structure with 1–2 mm wavelength and 0.1–0.2 mm amplitude. Magnetized liner implosions without a deuterium gas fill exhibit a helical structure<sup>198</sup> that apparently persists in MagLIF implosions. The small radius implies a high convergence ratio,  $\text{CR} = R_0/R_f > 40$  (where  $R_0$  is the initial radius and  $R_f$  is the final radius), that is particularly susceptible to instability. Our simulations<sup>219,220</sup> indicate that the convergence ratio can be reduced by increasing the fuel density and preheat energy, which is a goal of our future experiments.

We diagnose the burn-averaged ion temperature of the fuel column by neutron-time-of-flight spectra, with values between 1 and 3 keV inferred, depending on the experimental configuration.<sup>216</sup> Axially resolved x-ray spectrometers<sup>64,221</sup> assess electron temperatures as a function of axial position along the fuel column.<sup>76</sup> Electron temperatures can vary by  $>1$  keV over the column height, but the axially integrated, emissivity-weighted average electron temperatures are typically similar to the burn-averaged ion temperatures. The areal density of the Be tamper can be determined using the K-edge absorption of iron impurities in the Be alloy;<sup>76,222</sup> typically, the areal density is  $\sim 0.75$  g/cm<sup>2</sup>. We are developing a burn duration diagnostic based on nuclear measurements; at present, we use x-ray emission to approximate the burn duration. The typical MagLIF x-ray emission duration<sup>223</sup> is 1–2 ns. We infer stagnation pressures of  $\sim 1$  Gbar using a combination of the data.

Mix of high-atomic-number material with the fuel is a common concern for all concepts since enhanced radiative losses can degrade target performance. The main sources of mix in MagLIF are materials from the LEH window foil, the top and bottom end caps, and the inner surface of the liner. Understanding these sources of mix and the impact on fusion performance will allow us to target the dominant issues. To that end, we are developing an advanced time-resolved x-ray spectrometer to diagnose the origins and quantities of mix.

The LEH foil material can penetrate the fuel during laser preheat because the laser intensity is high enough to ablate the window and heat it to  $\sim 1$  keV. A portion of the window material gains momentum in the direction of the fuel through this process. We have applied spectroscopic dopants to the LEH foil to diagnose the axial penetration at stagnation. Several early laser configurations introduced significant

LEH foil material into the fuel. We reduced that foil mix below the detection threshold with a low energy (20 J) pulse  $\sim 20$  ns prior to the main preheat pulse.<sup>224</sup> The end cap material can also mix with the fuel during preheat. The laser spot size and pointing can be chosen to avoid interaction with the end caps but scattering and filamentation can cause the laser light to strike them directly and liberate that material. We have identified such mix through disproportionately high x-ray emission with the mid-Z end cap material. However, we can reduce that mix by a factor of 3 by switching from Al to Be for the end cap material, resulting in a 50% increase in fuel energy at stagnation and an order of magnitude increase in primary neutron yield. The material from the inner surface of the liner can also mix with the fuel by direct laser interaction, but this is less likely because of the greater distance from the nominal laser beam path. Instead, the main mechanism for liner material mixing is the deceleration instability that develops near the end of an implosion; that mixing does not reduce the performance as much as mix introduced early in an implosion.<sup>219</sup> Mix introduced during preheat has more time to radiate away energy, thereby counteracting the benefits of preheat.

We have significantly improved the MagLIF experiments. The fuel preheat energy was increased from 0.5 kJ to 1–2 kJ by using thinner (1.5- $\mu\text{m}$ ) LEH foils, random phase plates, and a prepulse to reduce the LEH foil density before the main laser pulse.<sup>215,223</sup> Higher initial deuterium fuel densities (1.05–1.45 mg/cc) have reduced the convergence. Improved magnetic field coils have enabled experiments at 15 T, and reduction of the transmission line inductance has increased the drive current from 16 MA to nearly 20 MA. Such improvements have increased the primary neutron yield by more than an order of magnitude (to  $\sim 2$  kJ DT-equivalent yields), consistent with predictions of 2D MHD simulations.<sup>216</sup> Our MHD simulations indicate that additional improvements should occur at 25–30 T, 4–6 kJ fuel preheat, and 21–22 MA peak load current.<sup>216,219</sup> These parameters should be achievable on Z in the next 5 years. With these increased capabilities, we can conduct experiments across a wider range of input parameters, enabling more rigorous testing of our scaling predictions with increasing drive current. Yields of up to 100 kJ DT-equivalent may eventually be possible, comparable to the 20–50 kJ obtained on the National Ignition Facility,<sup>225</sup> which is quite interesting given the two very different approaches (magneto-inertial fusion vs hot-spot ignition) and plasma pressures.

## E. Power flow physics

The MITLs deliver Z's electromagnetic power pulse to a z-pinch physics load. The MITL system<sup>226,227</sup> has operated on more than 3400 physics experiments and routinely delivers a nearly lossless 26-MA, 85-TW current pulse to a low-inductance ( $<3.0$  nH) z-pinch wire-array radiation source. However, as our target concepts have expanded over the past 20 years, not all load configurations are as well impedance-matched to Z. Hence, the electrical energy coupled to the physics load can be current limited for some loads. As an example, some Z experiments use electrical pulse shapes ranging from short ( $\sim 100$  ns) to long ( $>1000$  ns), with load inductances approaching 10–12 nH. Ultimately, the large voltages to drive such high inductances result in large electric fields across the anode–cathode (A–K) gaps in the MITLs, which then produce electrode plasmas that divert current away from the target. To improve current delivery to a wide variety of targets, we have invested a significant effort in the past 10 years

to improving our understanding of the physics associated with vacuum power flow on pulsed power accelerators. Detailed physics models suggest that heating the MITL electrodes as the current rises rapidly desorbs loosely bound contaminants, such as water and hydrocarbons. These contaminants subsequently become ionized low-density plasmas that expand into the A–K gaps. The physics challenge of understanding contaminant desorption that impacts performance over a range of spatial scales, from atomistic to micrometer scale to centimeter scale and larger, is outlined schematically in Fig. 16.

Our initial studies were targeted at understanding current loss and plasma expansion in the Z vacuum post-hole convolute,<sup>228</sup> a device that combines the current of four vacuum MITLs into a single radial inner MITL connected to a target; here, current loss is readily observed for high inductance loads. Several generations of 3D particle-in-cell (PIC) models have simulated the integrated device performance.<sup>73,229,230</sup> We have advanced these models to the point where approximate models have been implemented in 1D transmission line codes to predict Z's performance in a limited manner.<sup>112,231</sup>

We have improved our ability to measure electrode plasma properties in the last 10 years, producing high-quality data to validate the models in power flow design codes. Electrical monitors at the vacuum insulator stack<sup>232</sup> and the entrance to the radial inner MITL<sup>233</sup> have achieved an uncertainty of <5% for most load configurations. Load current inferences from velocimetry data<sup>234</sup> have similarly achieved an overall uncertainty of <5%, greatly improving our understanding of current delivery to targets. We have commissioned optical diagnostics to infer the presence of electrode plasmas ranging from optical emission spectroscopy in the post hole convolute<sup>228</sup> to chordal point interferometry near the target.<sup>235</sup>

We are developing hybrid kinetic-fluid models as a bridge toward integrated simulations that include coupled power flow and target physics models, scalable to the largest high-performance computing architectures. This effort is pushing hybrid PIC models of electrode plasmas to higher densities ( $10^{18}/\text{cc}$ ) in the radial inner MITL<sup>75</sup> to explore full-scale models of coupled convolute and radial inner MITL systems,<sup>74</sup> advance atomistic simulations of contaminant

desorption,<sup>236</sup> and develop models of highly enhanced ion current losses in the radial inner MITL.<sup>237</sup> These efforts, coupled with dedicated experiments to validate power flow models, will ultimately provide confidence in extrapolating Z performance to next-generation pulsed power accelerator architectures.

## IV. NEXT-GENERATION PULSED POWER

### A. Pulsed power technology development

We are evaluating various architectures for a next-generation pulsed power facility as a successor to Z that would produce  $\sim 60$  MA at about the same 100-ns rise time. Since 1995, a number of architectures have been proposed.<sup>238–243</sup> These architectures include the conventional Marx water-line (Z-like), induction voltage adder (HERMES III-like), fast Marx water-line, and linear transformer driver (LTD). All current designs use a modular architecture, and each has strengths, weaknesses, and research and development (R&D) requirements.

The electrical output parameters for each module are derived from the lumped inductance in the vacuum and the current rise time. Most designs use a transmission line transformer<sup>244,245</sup> to raise the impedance and voltage to drive the vacuum section. We did this for Saturn with a continual transformer and for the refurbished Z with a discrete stepped transformer. Other designs<sup>242</sup> have considered exponentially varying transformers.

The conventional Marx water-line architecture is a well understood option because of decades of experience at a comparable scale. This system uses relatively inexpensive and robust but large-energy storage capacitors in a Marx arrangement. Since the characteristic inductance–capacitance (LC) time is longer than the desired load current rise time, additional pulse compression is required. The first stage of additional compression is usually a water-insulated, low-impedance transmission line pulse charged by the Marx and discharged by a triggered switch. If that output switch must tolerate much higher voltage and current stress than the laser-triggered gas switch (LTGS) on Z, significant development could be required, as exemplified by the refurbishment of Z from July 2006 to September 2007.<sup>246</sup> LTGSs, however, provide useful flexibility for experiments that require shaped current pulses, such as for dynamic materials. A conceptual model of a conventional Marx-based, 50-MA accelerator is shown in Fig. 17(a).

Except for a vacuum induction voltage adder (IVA), concepts for a next-generation architecture use a large cylindrical water–vacuum insulator. The water–vacuum insulator (also known as the “vacuum stack”) of a >50-MA driver is estimated to be about double the height and diameter of the Z water–vacuum interface as the peak voltage would be nearly 20 MV. Performance scaling relations for vacuum-stack insulators are derived from much smaller scale experiments and may not be accurate in this regime. Obtaining Rexolite<sup>®</sup> insulating rings and anodized 6-m-diameter grading rings may also be a serious challenge.

An architecture consisting of many HERMES III-like IVA modules<sup>240</sup> in parallel eliminates all downstream pulse compression stages and the single, large water–vacuum interface that other architectures require. This architecture is ideal for high-impedance applications that require an output rise time of 50 ns or less. However, the IVA is inefficient in terms of energy delivered to the load and accelerator size when driving low-impedance, inductive loads with rise times of 100 ns or longer. Moreover, magnetic insulation of electron flow in the long vacuum lines and disk convolute is a potential concern.

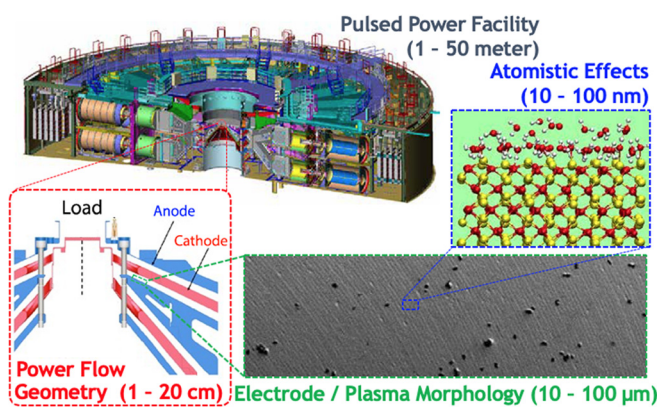


**FIG. 16.** Examples of spatial scales involved in calculating the detailed behavior of plasmas formed in the final power flow regions of the Z facility delivering electrical power to the target. Detailed models attempt to estimate plasma desorption at the atomistic level, plasma formation and expansion on realistic surfaces, and the flow of the plasmas in the complex geometry feeding electrical power to the target.

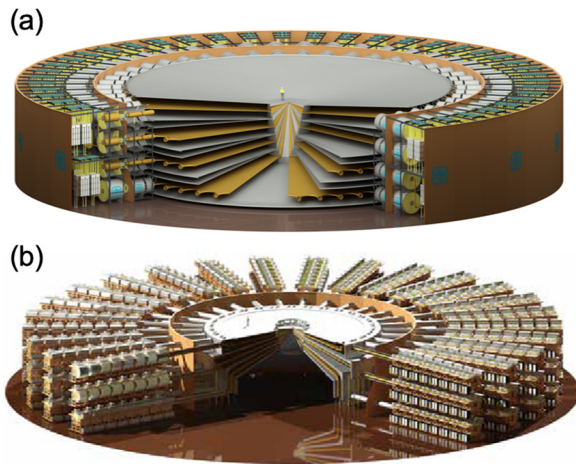


**FIG. 17.** Example diagrams of two possible architectures for next-generation pulsed power machines capable of coupling  $\sim 10$  MJ to fusion targets ( $\sim 30$  MJ to radiation science targets). (a) Marx water-line architecture similar to Z. (b) Linear transformer driver.

L-3 Harris (formerly Titan Pulse Sciences Division) has developed various fast Marx water-line architectures since the late 1990s.<sup>241,247–249</sup> This architecture is similar to the well-understood conventional Marx water-line system. The key benefit of the fast Marx is elimination of the intermediate store and triggered output switch characteristic of the conventional Marx architecture. However, most fast Marx systems built to date are optimized for high-impedance applications and are not operated above 2-MV output voltage; an efficient Z successor might require a Marx output voltage  $>5$  MV. Fast Marxes use small energy storage capacitors to reduce the LC time, so numerous capacitors and switches are needed. Most switches can be internally triggered from the Marx erection process, so triggering is relatively simple.

Like fast Marxes, linear transformer drivers eliminate both the intermediate storage capacitor and the high-voltage triggered output switch and use numerous small-energy storage capacitors and switches to achieve fast output pulses. The primary advantage of the LTD architecture is that downstream pulse compression is not required to achieve a 100-ns rise time. (A “very fast Marx”<sup>241</sup> could also accomplish this.) LTDs eliminate the risk associated with developing an output switch with higher voltage hold-off than the present LTGSs on Z. Eliminating all pulse compression stages also improves the electrical efficiency by about a factor of two, thereby reducing the stored energy requirement by  $\sim 50\%$ . Elimination of these pulse compression stages could yield a smaller system and reduced facility cost if the capacitor and system energy density and cost per Joule are comparable to the other architectures. Other potential benefits are detailed by Stygar *et al.*<sup>242</sup> The primary weaknesses of the LTD architecture are higher cost, trigger system complexity ( $\sim 10^5$  switches, each of which must be actively triggered), and a demanding reliability ( $\sim 10^{-7}$  failure rates). Moreover, we have only experimentally demonstrated the technology at about 1/1000th of a full-scale facility, so the technology readiness level could be higher. A conceptual model of an LTD-based, 50-MA facility is shown in Fig. 17(b).

For more than a decade, our research emphasis has been on maturing fast (100-ns), high-current (1 MA at 100-kV output per

cavity), LTD technology.<sup>250–254</sup> Our primary motivation has been to evaluate the viability of LTD technology for a next-generation pulsed power facility. In the past 15 years, we have significantly improved LTD reliability and performance at the single-cavity level. Our latest high-current LTD produces  $>1.1$ -MA peak current, has a switch pre-fire rate of  $\sim 10^{-5}$ , and is relatively compact with 2.2-m diameter.<sup>254</sup> While this progress is impressive and promising, scaling to a  $>50$ -MA driver will require substantial additional R&D.

## B. Scientific opportunities

We believe that it is possible to build a next-generation pulsed power facility capable of delivering 800–1000 TW of electrical power to the insulator stack. Circuit models suggest that such a facility could couple roughly 10 MJ to high-inductance fusion targets and could deliver factors of 2–3 times that energy to lower-inductance plasma radiation sources. With appropriate pulse shaping, it may be possible to generate  $>20$  Mbar pressures in mm-scale, high-Z material samples for dynamic material research and allow us to push the frontiers of highly accurate material data to include grain boundaries and material strength. Such a facility would be roughly three times the diameter of the existing Z and would likely require new operational concepts to reduce the manual labor and worker hazards involved with loading and unloading experimental hardware.

Wire-array plasma radiation sources on Z today are roughly 50% efficient at converting the energy delivered to the wire array into soft x-ray radiation (0.1–1 keV). Hence, such a facility should be readily capable of producing  $>10$  MJ soft x-ray radiation sources, as compared to  $\sim 2.5$  MJ on Z today). This increased yield would provide new opportunities for radiation science experiments, such as higher-Z and higher-temperature opacity research, as well as higher-performing multi-frequency x-ray radiation sources.

Fusion experiments with MagLIF targets are continuing to demonstrate favorable scaling with currents, initial magnetic fields, and laser preheat. We will continue this research over the next several years to increase the credibility of extrapolating our MagLIF results from  $\sim 20$  MA to  $\sim 60$  MA on a future pulsed power accelerator. Our computational predictions for MagLIF at that scale, based on extrapolations from the results that we expect to demonstrate on Z in the next few years, suggest that  $>5$  MJ of fusion yield should be possible without alpha-particle energy deposition. Significantly higher yields (tens of MJ) are predicted in volume-burning targets that include alpha heating.<sup>220</sup> A facility at this scale should also be able to test ideas involving radially propagating burn in DT-ice-containing targets, which might eventually lead to still higher yields.<sup>178</sup>

In addition to magnetic direct drive fusion targets, such a facility may also be capable of creating high temperature, large-scale *Hohlraums* for indirect-drive fusion capsule research.<sup>255</sup> More work would be needed on this facility to demonstrate the appropriate x-ray radiation pulse shapes to drive a capsule and the appropriate radiation symmetry in the case of a dynamic *Hohlraum* geometry.<sup>29,256</sup> Nonetheless, such *Hohlraums* could complement those being produced today on the National Ignition Facility in that they would be radiation-driven rather than laser-driven and, hence, the significantly greater x-ray energy could allow larger-diameter capsules.

Higher fusion yields offer a potential energy source to create even brighter plasma radiation sources, as illustrated by the curves overlaid in Fig. 5. Since the largest laboratory driver that we can imagine



building today would be limited to tens of MJ energy coupled to targets, the energy released from fusion targets is the only practical way to create plasmas with more energy than that delivered by the driver. Even at tens of MJ yields, fusion sources offer an exciting means to create 10–100 keV x-ray sources that far exceed anything possible today.

## V. CONCLUSION

Z has been an “engine of discovery”<sup>257</sup> for a wide range of high energy density science, as illustrated by examples in this review paper and in the references. A key point is that most scientific breakthroughs on the facility have been opportunistic, rather than being planned in advance during the design phase for Z. When Z was converted to a z-pinch facility in 1996, nearly 100% of the shots used wire arrays of one form or another; these shots were intended to build upon the success of breakthrough experiments on the Saturn facility<sup>16,17</sup> and, in this respect, Z was highly successful.<sup>18</sup> Today, however, we use wire arrays on fewer than 10% of the experiments.

Now, about one third of our Z shots are dynamic materials experiments that were not envisioned in 1996. Moreover, the direction of our ICF experiments on Z transformed from magnetic indirect drive to magnetic direct drive in 2007, after we realized that magneto-inertial fusion targets offer a potentially revolutionary path to significant fusion yields and extreme conditions on Z. Indeed, our first MagLIF experiments on Z in late 2013 were pivotal in demonstrating the prospects for magneto-inertial fusion and led to new investment in such ideas by the Department of Energy.<sup>258</sup> We created the Z Fundamental Science Program in the late 2000s to encourage an influx of novel ideas using plasma radiation sources and dynamic materials platforms. Because of breakthroughs in the design of containment systems, today we can conduct experiments on virtually any hazardous material in the nuclear stockpile, and we have conducted over 50 such experiments to date. While our plasma radiation source research has been a key part of Z from the beginning, we have innovated continually throughout Z’s life and we are continuing to set x-ray and neutron yield facility records after more than 20 years of operation.

The potential for additional scientific innovation on Z over the next decade is high. We have achieved new facility records for the peak pressure in dynamic materials during the preparation of this manuscript that are allowing us to probe new material physics regimes. We might reach the DT-equivalent yield of up to 100 kJ in MagLIF targets on Z over the next 5 years on new experimental platforms. We intend to test new ideas to control z-pinch physics implosion stability on Z over the next few years. These new concepts could lead to further advances in radiation and fusion physics. Our investment in new diagnostics, experimental techniques, and analyses should enable improved scientific understanding based upon precision data from Z.

Our advances in pulsed power technology and architectures could provide an order of magnitude increase in power and energy delivered to targets. As with Z today, we expect that technical innovation will occur on a new facility over the full range of basic, use-inspired, and applied science. The history of Z and its predecessors is replete with surprises in materials, radiation, and fusion science models, thereby illustrating our challenge of making predictive calculations in high energy density physics. A next-generation pulsed power facility will doubtless result in discoveries and innovations as we access new physics regimes.

## ACKNOWLEDGMENTS

The work described in this manuscript would not have been possible without the contributions of hundreds of technologists and other staff members as well as our external collaborators over the past 23 years of Z operations, particularly those from Los Alamos and Lawrence Livermore National Laboratories on NNSA mission science not described here. We would especially like to acknowledge Yitzhak Maron of Weizmann Institute in Israel for his active multi-year support of several Z programs (e.g., x-ray spectroscopy, power flow, and visible spectroscopy). We would also like to thank Tara Camacho-Lopez and Michael Church for their contributions to the narrative and graphics. We would like to honor the contributions of Carlos Cox, now deceased, to the radiography diagnostics developed for Z. Finally, we would also like to acknowledge the many additional retirees and other alumni from Sandia who made contributions over the past 15 years, whom we were unable to contact to add as coauthors but who are represented in the citations herein. Sandia National Laboratories is a multi-mission laboratory managed and operated by National Technology and Engineering Solutions of Sandia LLC, a wholly owned subsidiary of Honeywell International Inc. for the U.S. Department of Energy’s National Nuclear Security Administration under Contract No. DE-NA0003525. This paper reviews objective technical results and analysis. Any subjective views or opinions that might be expressed do not necessarily represent the views of the U.S. Department of Energy or the U.S. Government.

## DATA AVAILABILITY

Data sharing is not applicable to this article as no new data were created or analyzed in this study.

## REFERENCES

- <sup>1</sup>J. C. “Charlie” Martin and his AWRE co-workers, *J. C. Martin on Pulsed Power*, edited by T. H. Martin, A. H. Guenther, and M. Kristiansen, *Advances in Pulsed Power Technologies* Vol. 3 (Plenum Press, New York, 1996). The notes and lectures prepared by “Charlie” Martin and his co-workers at the Atomic Weapons Research Establishment (now the Atomic Weapons Establishment) in Aldermaston, Reading UK are a primer for modern experimental pulsed power.
- <sup>2</sup>K. R. Prestwich, “Electron and ion beam accelerators,” *AIP Conf. Proc.* **249**(2), 1725–1793 (1992).
- <sup>3</sup>M. E. Savage, L. F. Bennett, D. E. Bliss, W. T. Clark, R. S. Coats, J. M. Elizondo, K. R. LeChien, H. C. Harjes, J. M. Lehr, J. E. Maenchen *et al.*, “An overview of pulsed compression and power flow in the upgraded Z pulsed power driver,” in 16th IEEE International Pulsed Power Conference (2007), Vol. 2, pp. 979–984.
- <sup>4</sup>J. C. Martin, P. Champney, and T. Storr, “Lecture notes prepared for a visit of Sandia corporation,” AWRE, Aldermaston, England, Publication (1964).
- <sup>5</sup>“Sandia Laboratory team develops new flash-x ray machine—World’s largest,” *Sandia Lab News* **17**(2), 1 (1965).
- <sup>6</sup>M. C. Jones, D. J. Ampleford, M. E. Cuneo, R. Hohlfelder, C. A. Jennings, D. W. Johnson, B. Jones, M. R. Lopez, J. MacArthur, J. A. Mills *et al.*, “X-ray power and yield measurements at the refurbished Z machine,” *Rev. Sci. Instrum.* **85**, 083501 (2014).
- <sup>7</sup>D. J. Ampleford, B. Jones, C. A. Jennings, S. B. Hansen, M. E. Cuneo, A. J. Harvey-Thompson, G. A. Rochau, C. A. Coverdale, A. R. Laspe, T. M. Flanagan *et al.*, “Contrasting physics in wire array z pinch sources of 1–20 keV emission on the Z facility,” *Phys. Plasmas* **21**, 056708 (2014).
- <sup>8</sup>D. D. Bloomquist, R. W. Stinnett, D. H. McDaniel, J. R. Lee, A. W. Sharpe, J. A. Halbleib, L. G. Schlitt, P. W. Spence, P. Corcoran *et al.*, “Saturn, a large

- area x-ray simulation accelerator,” in Proceedings of the Sixth IEEE Pulsed Power Conference (1987), pp. 310–317.
- <sup>9</sup>T. W. L. Sanford, “Dynamics of electron flows and radiation fields produced by electron-beam diodes on the HERMES III accelerator,” *Phys. Fluids B* **3**, 2387 (1991).
- <sup>10</sup>G. Yonas, K. R. Prestwich, J. W. Poukey, and J. R. Freeman, “Electron beam focusing using current-carrying plasmas in high- $\beta$  diodes,” *Phys. Rev. Lett.* **30**, 164 (1973).
- <sup>11</sup>M. J. Clouser, “Targets for electron-beam fusion,” *Phys. Rev. Lett.* **34**, 570 (1975).
- <sup>12</sup>M. A. Sweeney and M. J. Clouser, “Low-Z ablator targets for electron beam fusion,” *Appl. Phys. Lett.* **27**, 483 (1975).
- <sup>13</sup>J. Chang, M. M. Widner, A. V. Farnsworth, R. J. Leeper, T. S. Prevender, L. Baker, and J. N. Olsen, “Neutron production from advanced REB fusion targets,” in Second International Topical Conference on Electron Beam Research and Technology (1977), Vol. 1, pp. 195–205.
- <sup>14</sup>M. J. Clouser, “Ion-beam implosion of fusion targets,” *Phys. Rev. Lett.* **35**, 848 (1975).
- <sup>15</sup>M. A. Sweeney and A. V. Farnsworth, Jr., “High-gain, low-intensity ICF targets for a charged particle beam fusion driver,” *Nucl. Fusion* **21**, 41 (1981).
- <sup>16</sup>T. W. L. Sanford, G. O. Allshouse, B. M. Marder, T. J. Nash, R. C. Mock, R. B. Spielman, J. F. Seaman, J. S. McGurn, D. Jobe, T. L. Gilliland *et al.*, “Improved symmetry greatly increases x-ray power from wire-array z-pinch,” *Phys. Rev. Lett.* **77**, 5063 (1996).
- <sup>17</sup>C. Deeney, T. J. Nash, R. B. Spielman, J. F. Seaman, G. A. Chandler, K. W. Struve, J. L. Porter, W. A. Stygar, J. S. McGurn, D. O. Jobe *et al.*, “Power enhancement by increasing the initial array radius and wire number of tungsten Z pinches,” *Phys. Rev. E* **56**, 5945 (1997).
- <sup>18</sup>R. B. Spielman, C. Deeney, G. A. Chandler, M. R. Douglas, D. L. Fehl, M. K. Matzen, D. H. McDaniel, T. J. Nash, J. L. Porter, T. W. L. Sanford *et al.*, “Tungsten wire-array Z-pinch experiments at 200 TW and 2 MJ,” *Phys. Plasmas* **5**, 2105 (1998).
- <sup>19</sup>M. K. Matzen, M. A. Sweeney, R. G. Adams, J. R. Asay, J. E. Bailey, G. R. Bennett, D. E. Bliss, D. D. Bloomquist, T. A. Brunner, R. B. Campbell *et al.*, “Pulsed-power-driven high energy density physics and inertial confinement fusion research,” *Phys. Plasmas* **12**, 055503 (2005).
- <sup>20</sup>M. E. Savage, K. R. LeChien, M. R. Lopez, B. S. Stoltzfus, W. A. Stygar, D. S. Artery, J. A. Lott, and P. A. Corcoran, “Status of the Z pulsed power driver,” in Proceedings of the 18th IEEE Pulsed Power Conference (2011), pp. 983–990.
- <sup>21</sup>D. V. Rose, D. R. Welch, E. A. Madrid, C. L. Miler, R. E. Clark, W. A. Stygar, M. E. Savage, G. A. Rochau, J. E. Bailey, T. J. Nash *et al.*, “Three-dimensional electromagnetic model of the pulsed-power z-pinch accelerator,” *Phys. Rev. Accel. Beams* **13**, 010402 (2010).
- <sup>22</sup>P. K. Rambo, I. C. Smith, J. L. Porter, M. J. Hurst, C. S. Speas, R. G. Adams, A. J. Garcia, E. Dawson, B. D. Thurston, C. Wakefield *et al.*, “Z-Beamlet: A multikilojoule, terawatt-class laser system,” *Appl. Opt.* **44**, 2421 (2005).
- <sup>23</sup>P. Rambo, J. Schwarz, M. Schollmeier, M. Geissel, I. Smith, M. Kimmel, C. Speas, J. Shores, D. Armstrong, J. Bellum, E. Field, D. Kletecka, and J. Porter, “Sandia’s Z-backlighter laser facility,” *Proc. SPIE* **10014**, 100140Z (2016).
- <sup>24</sup>G. R. Bennett, I. C. Smith, J. E. Shores, D. B. Sinars, G. Robertson, B. W. Atherton, M. C. Jones, and J. L. Porter, “2–20 ns interframe time 2-frame 6.151 keV x-ray imaging on the recently upgraded Z accelerator: A progress report,” *Rev. Sci. Instrum.* **79**, 10E914 (2008).
- <sup>25</sup>D. B. Sinars, G. R. Bennett, D. F. Wenger, M. E. Cuneo, and J. L. Porter, “Evaluation of bent-crystal x-ray backlighting and microscopy techniques for the Sandia Z machine,” *Appl. Opt.* **42**, 4059 (2003).
- <sup>26</sup>M. S. Schollmeier, P. F. Knapp, D. J. Ampleford, E. C. Harding, C. A. Jennings, D. C. Lamppa, G. P. Loisel, M. R. Martin, G. K. Robertson, J. E. Shores, I. C. Smith, C. S. Speas, M. R. Weis, J. L. Porter, and R. D. McBride, “A 7.2 keV spherical x-ray crystal backlighter for two-frame, two-color backlighting at Sandia’s Z Pulsed Power Facility,” *Rev. Sci. Instrum.* **88**, 103503 (2017).
- <sup>27</sup>M. Schollmeier, T. Ao, E. S. Field, B. R. Galloway, P. Kalita, M. W. Kimmel, D. V. Morgan, P. K. Rambo, J. Schwarz, J. E. Shores, I. C. Smith, C. S. Speas, J. F. Benage, and J. L. Porter, “Polycapillary x-ray lenses for single-shot, laser-driven powder diffraction,” *Rev. Sci. Instrum.* **89**, 10F102 (2018).
- <sup>28</sup>D. E. Stokes, *Pasteur’s Quadrant—Basic Science and Technological Innovation* (Brookings Institution Press, 1997).
- <sup>29</sup>M. E. Cuneo, M. C. Herrmann, D. B. Sinars, S. A. Slutz, W. A. Stygar, R. A. Vesey, A. B. Sefkow, G. A. Rochau, G. A. Chandler, J. E. Bailey *et al.*, “Magnetically driven implosions for inertial confinement fusion at Sandia National Laboratories,” *IEEE Trans. Plasma Sci.* **40**, 3222 (2012).
- <sup>30</sup>C. Deeney, C. A. Coverdale, and M. R. Douglas, “A review of long-implosion-time z pinches as efficient and high-power radiation sources,” *Laser Part. Beams* **19**, 497 (2001).
- <sup>31</sup>T. W. L. Sanford, R. C. Mock, R. B. Spielman, D. L. Peterson, D. Mosher, and N. F. Roderick, “Symmetric aluminum-wire arrays generate high-quality z pinches at large array radii,” *Phys. Plasmas* **5**, 3737 (1998).
- <sup>32</sup>C. A. Coverdale, B. M. Jones, D. J. Ampleford, J. Chittenden, C. Jennings, J. W. Thornhill, J. P. Apruzese, R. W. Clark, K. G. Whitney, A. Dasgupta *et al.*, “K-shell x-ray sources at the Z accelerator,” *High Energy Density Phys.* **6**, 143 (2010).
- <sup>33</sup>G. A. Rochau, J. E. Bailey, R. E. Falcon, G. P. Loisel, T. Nagayama, R. C. Mancini, I. Hall, D. E. Winget, M. H. Montgomery, and D. A. Liedahl, “ZAPP: The Z Astrophysical Plasma Properties collaboration,” *Phys. Plasmas* **21**, 056308 (2014).
- <sup>34</sup>J. W. Thornhill, A. L. Velikovich, R. W. Clark, J. P. Apruzese, J. Davis, K. G. Whitney, P. L. Coleman, C. A. Coverdale, C. Deeney, B. M. Jones, and P. D. LePell, “Assessing the ZR machine’s potential for producing multi-keV x-rays in K-shell line and free-bound continuum radiation,” *IEEE Trans. Plasma Sci.* **34**, 2377 (2006).
- <sup>35</sup>B. Jones, C. Deeney, C. A. Coverdale, P. D. LePell, J. L. McKenney, J. P. Apruzese, J. W. Thornhill, K. G. Whitney, R. W. Clark, A. L. Velikovich *et al.*, “K-shell radiation physics in low- to moderate-atomic-number z-pinch plasmas on the Z accelerator,” *J. Quant. Spectrosc. Radiat. Transfer* **99**, 341 (2006).
- <sup>36</sup>B. M. Jones, C. A. Coverdale, C. Deeney, D. B. Sinars, E. M. Waisman, M. E. Cuneo, D. J. Ampleford, P. D. LePell, K. R. Cochrane, J. W. Thornhill *et al.*, “Implosion dynamics and K-shell x-ray generation in large diameter stainless steel wire array z-pinch with various array nesting configurations,” *Phys. Plasmas* **15**, 122703 (2008).
- <sup>37</sup>J. W. Thornhill, J. L. Giuliani, A. Dasgupta, J. P. Apruzese, J. Davis, Y. K. Chong, C. A. Jennings, D. J. Ampleford, B. Jones, C. A. Coverdale *et al.*, “2D radiation MHD K-shell modeling of stainless-steel double wire array experiments on the refurbished Z machine,” *IEEE Trans. Plasma Sci.* **38**, 606 (2010).
- <sup>38</sup>J. W. Thornhill, J. L. Giuliani, B. Jones, J. P. Apruzese, A. Dasgupta, Y. K. Chong, A. J. Harvey-Thompson, D. J. Ampleford, S. B. Hansen, C. A. Coverdale *et al.*, “Two-dimensional RMHD modeling assessment of current flow, plasma conditions, and Doppler effects in recent Z argon experiments,” *IEEE Trans. Plasma Sci.* **43**, 2480 (2015).
- <sup>39</sup>C. A. Jennings, M. E. Cuneo, E. M. Waisman, D. B. Sinars, D. J. Ampleford, G. R. Bennett, W. A. Stygar, and J. P. Chittenden, “Simulations of the implosion and stagnation of compact wire arrays,” *Phys. Plasmas* **17**, 092703 (2010).
- <sup>40</sup>C. A. Jennings, D. J. Ampleford, D. C. Lamppa, S. B. Hansen, B. Jones, A. J. Harvey-Thompson, M. Jobe, T. Strizic, J. Reneker, G. A. Rochau, and M. E. Cuneo, “Computational modeling of krypton gas puffs with tailored mass density profiles on Z,” *Phys. Plasmas* **22**, 056316 (2015).
- <sup>41</sup>K. Killebrew, A. Maurer, D. J. Ampleford, C. A. Coverdale, D. Schroen, R. R. Holt, G. A. Rochau, J. E. Bailey, B. Jones, M. E. Savage, and D. A. Graham, “Characterization of fine metallic wires for wire array z-pinch experiments,” *IEEE Trans. Plasma Sci.* **40**, 3372 (2012).
- <sup>42</sup>M. Krishnan, K. W. Elliott, R. E. Madden, P. L. Coleman, J. R. Thompson, A. Bixler, D. C. Lamppa, J. L. McKenney, T. Strizic, D. Johnson *et al.*, “Architecture, implementation and testing of a multiple-shell gas injection system for high current implosions on the Z accelerator,” *Rev. Sci. Instrum.* **84**, 063504 (2013).
- <sup>43</sup>B. M. Jones, C. A. Jennings, D. C. Lamppa, S. B. Hansen, A. J. Harvey-Thompson, D. J. Ampleford, M. E. Cuneo, T. Strizic, D. Johnson, M. C. Jones *et al.*, “A renewed capability for gas puff science on Sandia’s Z machine,” *IEEE Trans. Plasma Sci.* **42**, 1145 (2014).

- <sup>44</sup>P. L. Coleman, D. C. Lamppa, R. E. Madden, K. Wilson-Elliott, B. Jones, D. J. Ampleford, D. E. Bliss, C. Jennings, A. Bixler, and M. Krishnan, "Development and use of a 2D interferometer to measure mass flow from a multi-shell z-pinch gas puff," *Rev. Sci. Instrum.* **83**, 083116 (2012).
- <sup>45</sup>C. A. Coverdale, C. Deeney, M. R. Douglas, J. P. Apruzese, K. G. Whitney, J. W. Thornhill, and J. Davis, "Optimal wire-number range for high x-ray power in long-implosion-time aluminum z pinches," *Phys. Rev. Lett.* **88**, 065001 (2002).
- <sup>46</sup>B. Jones, C. A. Jennings, J. E. Bailey, G. A. Rochau, Y. Maron, C. A. Coverdale, E. P. Yu, S. B. Hansen, D. J. Ampleford, P. W. Lake *et al.*, "Doppler measurement of implosion velocity in fast z-pinch x-ray sources," *Phys. Rev. E* **84**, 056408 (2011).
- <sup>47</sup>D. J. Ampleford, S. B. Hansen, C. A. Jennings, B. Jones, C. A. Coverdale, A. J. Harvey-Thompson, G. A. Rochau, G. Dunham, N. W. Moore, M. E. Cuneo *et al.*, "Opacity and gradients in aluminum wire array z pinch implosions on the Z pulsed power facility," *Phys. Plasmas* **21**, 031201 (2014).
- <sup>48</sup>C. A. Coverdale, C. Deeney, P. D. LePell, B. Jones, J. Davis, R. W. Clark, J. P. Apruzese, J. W. Thornhill, and K. G. Whitney, "Large diameter (45–80 mm) nested stainless steel wire arrays at the Z accelerator," *Phys. Plasmas* **15**, 023107 (2008).
- <sup>49</sup>B. M. Jones, D. J. Ampleford, C. A. Jennings, E. M. Waisman, S. B. Hansen, C. A. Coverdale, M. E. Cuneo, J. P. Apruzese, J. W. Thornhill, J. L. Giuliani *et al.*, "Wire array z-pinch length variations for K-shell x-ray generation on Z," *IEEE Trans. Plasma Sci.* **43**, 2509 (2015).
- <sup>50</sup>D. J. Ampleford, C. A. Jennings, B. Jones, S. B. Hansen, M. E. Cuneo, C. A. Coverdale, M. C. Jones, T. M. Flanagan, M. Savage, W. A. Stygar *et al.*, "K-shell emission trends from 60–130 cm/ $\mu$ s stainless steel implosions," *Phys. Plasmas* **20**, 103116 (2013).
- <sup>51</sup>S. B. Hansen, B. M. Jones, J. L. Giuliani, J. P. Apruzese, J. W. Thornhill, H. A. Scott, D. J. Ampleford, C. A. Jennings, C. A. Coverdale, M. E. Cuneo *et al.*, "Doppler effects on 3D non-LTE radiation transport and emission spectra," *High Energy Density Phys.* **7**, 303 (2011).
- <sup>52</sup>A. Dasgupta, R. W. Clark, N. D. Ouart, J. L. Giuliani, W. Thornhill, J. Davis, B. Jones, D. J. Ampleford, S. B. Hansen, and C. A. Coverdale, "Spectroscopic analysis of Cu wire array implosions on the refurbished Z generator," *High Energy Density Phys.* **8**, 284 (2012).
- <sup>53</sup>A. Dasgupta, R. W. Clark, J. L. Giuliani, N. D. Ouart, B. Jones, D. J. Ampleford, and S. B. Hansen, "K- $\alpha$  emission spectroscopic analysis from a Cu z-pinch," *High Energy Density Phys.* **9**, 347 (2013).
- <sup>54</sup>J. P. Apruzese, J. L. Giuliani, J. W. Thornhill, C. A. Coverdale, B. Jones, and D. J. Ampleford, "Analysis of spatially resolved z-pinch spectra to investigate the nature of bright spots," *Phys. Plasmas* **20**, 022707 (2013).
- <sup>55</sup>J. W. Thornhill, J. L. Giuliani, Y. K. Chong, A. L. Velikovich, A. Dasgupta, J. P. Apruzese, B. Jones, D. J. Ampleford, C. A. Coverdale, C. A. Jennings *et al.*, "Two-dimensional radiation MHD modeling assessment of designs for argon gas puff distributions for future experiments on the refurbished Z machine," *High Energy Density Phys.* **8**, 197 (2012).
- <sup>56</sup>B. M. Jones, J. P. Apruzese, A. J. Harvey-Thompson, D. J. Ampleford, C. A. Jennings, S. B. Hansen, N. W. Moore, D. C. Lamppa, D. Johnson, M. C. Jones *et al.*, "Effect of gradients at stagnation on K-shell x-ray yield in reproducible, high-current, fast Ar gas puff implosions," *Phys. Plasmas* **22**, 020706 (2015).
- <sup>57</sup>H. Sze, J. S. Levine, J. Banister, B. H. Failor, N. Qi, P. Steen, A. L. Velikovich, J. Davis, and A. Wilson, "Magnetic Rayleigh-Taylor instability mitigation and efficient radiation production in gas puff Z-pinch implosions," *Phys. Plasmas* **14**, 056307 (2007).
- <sup>58</sup>A. J. Harvey-Thompson, C. A. Jennings, B. Jones, J. P. Apruzese, D. J. Ampleford, D. C. Lamppa, C. A. Coverdale, M. E. Cuneo, J. L. Giuliani, S. B. Hansen *et al.*, "Investigating the effect of adding an on-axis jet to Ar gas puff z pinches on Z," *Phys. Plasmas* **23**, 101203 (2016).
- <sup>59</sup>J. P. Apruzese, J. L. Giuliani, N. D. Ouart, V. Tangri, A. J. Harvey-Thompson, B. Jones, C. A. Jennings, S. B. Hansen, D. J. Ampleford, G. A. Rochau *et al.*, "Effects of a Xe dopant on an Ar gas-puff implosion on Z," *Phys. Plasmas* **23**, 123303 (2016).
- <sup>60</sup>J. L. Giuliani and R. J. Commisso, "A review of the gas-puff z-pinch as an x-ray and neutron source," *IEEE Trans. Plasma Sci.* **43**, 2385 (2015).
- <sup>61</sup>J. H. Hammer, J. L. Eddleman, P. T. Springer, M. Tabak, A. Toor, K. L. Wong, G. B. Zimmerman, C. Deeney, R. Humphreys, T. J. Nash *et al.*, "Two-dimensional radiation-magnetohydrodynamic simulations of Saturn imploding z pinches," *Phys. Plasmas* **3**, 2063 (1996).
- <sup>62</sup>A. Dasgupta, R. W. Clark, N. Ouart, J. Giuliani, A. Velikovich, D. J. Ampleford, S. B. Hansen, C. Jennings, A. J. Harvey-Thompson, B. Jones *et al.*, "A non-LTE analysis of high energy density Kr plasmas on Z and NIF," *Phys. Plasmas* **23**, 101208 (2016).
- <sup>63</sup>S. B. Hansen, D. J. Ampleford, M. E. Cuneo, N. Ouart, B. Jones, C. A. Jennings, A. Dasgupta, C. A. Coverdale, G. A. Rochau, G. Dunham *et al.*, "Signatures of hot electrons and fluorescence in Mo K $\alpha$  emission on Z," *Phys. Plasmas* **21**, 031202 (2014).
- <sup>64</sup>D. B. Sinars, D. F. Wenger, S. A. Pikuz, B. Jones, M. Geissel, S. B. Hansen, C. A. Coverdale, D. J. Ampleford, M. E. Cuneo, L. A. McPherson, and G. A. Rochau, "Compact, rugged in-chamber transmission spectrometers (7–28 keV) for the Sandia Z facility," *Rev. Sci. Instrum.* **82**, 063113 (2011).
- <sup>65</sup>P. F. Knapp, C. Ball, K. Austin, S. B. Hansen, M. D. Kernaghan, P. W. Lake, D. J. Ampleford, L. A. McPherson, D. Sandoval, P. Gard *et al.*, "A new time and space resolved transmission spectrometer for inertial confinement fusion and radiation source development research," *Rev. Sci. Instrum.* **88**, 013504 (2017).
- <sup>66</sup>Q. Looker, M. G. Wood, P. W. Lake, J. K. Kim, and D. K. Serkland, "GaAs x-ray detectors with sub-nanosecond temporal response," *Rev. Sci. Instrum.* **90**, 113505 (2019).
- <sup>67</sup>L. A. McPherson, D. J. Ampleford, C. A. Coverdale, J. W. Argo, A. C. Owen, and D. M. Jaramillo, "High energy x-ray imaging at the Z facility," *Rev. Sci. Instrum.* **87**, 063502 (2016).
- <sup>68</sup>J. R. Fein, D. J. Ampleford, J. K. Vogel, B. Koziolowski, C. C. Walton, M. Wu, C. R. Ball, A. Ames, J. Ayers, P. Bell *et al.*, "Wolter imager on the Z machine to diagnose warm x-ray sources," *Rev. Sci. Instrum.* **89**, 10G115 (2018).
- <sup>69</sup>J. K. Vogel, M. J. Pivovarov, B. Koziolowski, C. C. Walton, J. Ayers, P. Bell, D. Bradley, M.-A. Descalle, S. Hau-Riege, L. A. Pickworth *et al.*, "Design and raytrace simulations of a multilayer-coated Wolter x-ray optic for SNL's Z machine," *Rev. Sci. Instrum.* **89**, 10G113 (2018).
- <sup>70</sup>M. Wu, B. Koziolowski, J. K. Vogel, P. Lake, J. R. Fein, D. J. Ampleford, C. J. Bourdon, J. Ayers, P. Bell, D. K. Bradley *et al.*, "Characterizations and calibrations of multilayer coated Wolter optic for Z-diagnostic at SNL," *Rev. Sci. Instrum.* **89**, 10G114 (2018).
- <sup>71</sup>K. S. Bell, C. A. Coverdale, D. J. Ampleford, J. E. Bailey, G. Loisel, V. Harper-Slaboszewicz, J. Schwarz, and K. Moy, "The differential absorption hard x-ray (DAHx) spectrometer at the Z facility," *IEEE Trans. Plasma Sci.* **45**, 2393 (2017).
- <sup>72</sup>V. J. Harper-Slaboszewicz, B. A. Ulmen, C. T. Parzyck, D. J. Ampleford, A. L. McCourt, K. S. Bell, and C. A. Coverdale, "Coarse spectral characterization of warm x-rays at the Z facility using a filtered thermoluminescent dosimeter array," *Rev. Sci. Instrum.* **88**, 043501 (2017).
- <sup>73</sup>D. V. Rose, E. A. Madrid, D. R. Welch, R. E. Clark, C. B. Mstrom, W. A. Stygar, and M. E. Cuneo, "Computational analysis of current-loss mechanisms in a post-hole convolute driven by magnetically insulated transmission lines," *Phys. Rev. Accel. Beams* **18**, 030402 (2015).
- <sup>74</sup>N. Bennett, D. R. Welch, C. A. Jennings, E. Yu, M. H. Hess, B. T. Hutsel, G. Laity, J. K. Moore, D. V. Rose, K. Peterson, and M. E. Cuneo, "Current transport and loss mechanisms in the Z accelerator," *Phys. Rev. Accel. Beams* **22**, 120401 (2019).
- <sup>75</sup>D. R. Welch, N. Bennett, T. C. Genoni, D. V. Rose, C. Thoma, C. Miller, and W. A. Stygar, "Electrode contaminant plasma effects in  $10^7$ -A Z pinch accelerators," *Phys. Rev. Accel. Beams* **22**, 070401 (2019).
- <sup>76</sup>S. B. Hansen, E. C. Harding, P. F. Knapp, M. R. Gomez, T. Nagayama, and J. E. Bailey, "Changes in the electronic structure of highly compressed iron revealed by x-ray fluorescence lines and absorption edges," *High Energy Density Phys.* **24**, 39 (2017).
- <sup>77</sup>F. J. Rogers and C. A. Iglesias, *Science* **263**, 50 (1994).
- <sup>78</sup>J. E. Bailey, G. A. Rochau, R. C. Mancini, C. A. Iglesias, J. J. MacFarlane, I. E. Golovkin, C. Blancard, P. Cosse, and G. Faussurier, "Experimental investigation of opacity models for stellar interior, inertial fusion, and high energy density plasmas," *Phys. Plasmas* **16**, 058101 (2009).
- <sup>79</sup>R. E. Falcon, G. A. Rochau, J. E. Bailey, J. L. Ellis, A. L. Carlson, T. A. Gomez, M. H. Montgomery, D. E. Winget, E. Y. Chen, M. R. Gomez, and T. J. Nash,



- "An experimental platform for creating white dwarf photospheres in the laboratory," *High Energy Density Phys.* **9**, 82 (2013).
- <sup>80</sup>S. B. Hansen, E. C. Harding, P. F. Knapp, M. R. Gomez, T. Nagayama, and J. E. Bailey, "Fluorescence and absorption spectroscopy for warm dense matter studies and ICF plasma diagnostics," *Phys. Plasmas* **25**, 056301 (2018).
- <sup>81</sup>C. B. Tarter, W. H. Tucker, and E. E. Salpeter, "The interaction of x-ray sources with optically thin environments," *Astrophys. J.* **156**, 943 (1969).
- <sup>82</sup>D. A. Liedahl, "X-ray photoionized plasmas in space and in the laboratory," *Astrophys. Space Sci.* **336**, 251 (2011).
- <sup>83</sup>M. E. Foord, R. F. Heeter, P. A. M. Van Hoof, R. S. Thoe, J. E. Bailey, M. E. Cuneo, H.-K. Chung, D. A. Liedahl, K. B. Fournier, G. A. Chandler *et al.*, "Charge-state distribution and Doppler effect in an expanding photoionized plasma," *Phys. Rev. Lett.* **93**, 055002 (2004).
- <sup>84</sup>T. Nagayama, J. E. Bailey, G. P. Loisel, G. A. Rochau, J. J. MacFarlane, and I. Golovkin, "Calibrated simulations of Z opacity experiments that reproduce the experimentally measure plasma conditions," *Phys. Rev. E* **93**, 023202 (2016).
- <sup>85</sup>T. Nagayama, J. E. Bailey, G. P. Loisel, G. A. Rochau, J. J. MacFarlane, and I. Golovkin, "Numerical investigations of potential systematic uncertainties in iron opacity measurements at solar interior temperatures," *Phys. Rev. E* **95**, 063206 (2017).
- <sup>86</sup>M. K. Matzen, "Z pinches as intense x-ray sources for high-energy density physics applications," *Phys. Plasmas* **4**, 1519 (1997).
- <sup>87</sup>T. J. Nash, M. S. Derzon, G. A. Chandler, R. Leeper, D. Fehl, J. Lash, C. Ruiz, G. Cooper, J. F. Seaman, J. McGurn *et al.*, "High-temperature dynamic hohlraums on the pulsed power driver Z," *Phys. Plasmas* **6**, 2023 (1999).
- <sup>88</sup>T. W. L. Sanford, R. E. Olson, R. L. Bowers, G. A. Chandler, M. S. Derzon, D. E. Hebrun, R. J. Leeper, R. C. Mock, T. J. Nash, D. L. Peterson, L. E. Ruggles, W. W. Simpson, K. W. Struve, and R. A. Vesey, "Z-pinch-generated x-rays demonstrate potential for indirect-drive ICF experiments," *Phys. Rev. Lett.* **83**, 5511 (1999).
- <sup>89</sup>J. E. Bailey, T. Nagayama, G. P. Loisel, G. A. Rochau, C. Blancard, J. Colgan, P. Cosse, G. Faussurier, C. J. Fontes, F. Gilleron *et al.*, "A higher-than-predicted measurement of iron opacity at solar interior temperatures," *Nature* **517**, 56 (2015).
- <sup>90</sup>R. C. Mancini, J. E. Bailey, J. F. Hawley, T. Kallman, M. Witthoef, S. J. Rose, and H. Takabe, "Accretion disk dynamics, photoionized plasmas, and stellar opacities," *Phys. Plasmas* **16**, 041001 (2009).
- <sup>91</sup>I. M. Hall, T. Durmaz, R. C. Mancini, J. E. Bailey, G. A. Rochau, I. E. Golovkin, and J. J. MacFarlane, "Absorption spectroscopy of a laboratory photoionized plasma experiment at Z," *Phys. Plasmas* **21**, 031203 (2014).
- <sup>92</sup>G. P. Loisel, J. E. Bailey, D. A. Liedahl, C. J. Fontes, T. R. Kallman, T. Nagayama, S. B. Hansen, G. A. Rochau, R. C. Mancini, and R. W. Lee, "Benchmark experiment for photoionized plasma emission from accretion-powered x-ray sources," *Phys. Rev. Lett.* **119**, 075001 (2017).
- <sup>93</sup>R. E. Falcon, G. A. Rochau, J. E. Bailey, T. A. Gomez, M. H. Montgomery, D. E. Winget, and T. Nagayama, "Laboratory measurements of white dwarf photospheric spectral lines: H $\beta$ ," *Astrophys. J.* **806**, 214 (2015).
- <sup>94</sup>M. H. Montgomery, R. E. Falcon, G. A. Rochau, J. E. Bailey, T. A. Gomez, A. L. Carlson, D. E. Bliss, T. Nagayama, M. Stein, and D. E. Winget, "An experimental platform for creating white dwarf photospheres in the laboratory: Preliminary results," *High Energy Density Phys.* **17**, 168 (2015).
- <sup>95</sup>M.-A. Schaeuble, T. Nagayama, J. E. Bailey, T. A. Gomez, M. H. Montgomery, and D. E. Winget, "H $\beta$  and H $\gamma$  absorption-line profile inconsistencies in laboratory experiments performed at white dwarf photosphere conditions," *Astrophys. J.* **885**, 86 (2019).
- <sup>96</sup>M. Asplund, N. Grevesse, A. J. Sauval, C. A. Prieto, and D. Kiselman, "Line formation in solar granulation IV. [O1], O1 and OH lines and the photospheric O abundance," *Astron. Astrophys.* **417**, 751 (2004).
- <sup>97</sup>S. Basu and H. M. Antia, "Helioseismology and solar abundances," *Phys. Rep.* **457**, 217 (2008); see also D. B. Guenther, P. Demarque, U.-C. Kim, and M. H. Pinsonneault, "Standard solar model," *Astrophys. J.* **387**, 372 (1992) and the references therein.
- <sup>98</sup>A. M. Serenelli, S. Basu, J. W. Ferguson, and M. Asplund, "New solar composition: The problem with solar models revisited," *Astrophys. J.* **705**, L123 (2009).
- <sup>99</sup>S. J. Davidson, J. M. Foster, C. C. Smith, and K. A. Warburton, "Investigation of the opacity of hot, dense aluminum in the region of its K edge," *Appl. Phys. Lett.* **52**, 847 (1988).
- <sup>100</sup>T. S. Perry, P. T. Springer, D. F. Fields, D. R. Bach, F. J. D. Serduke, C. A. Iglesias, F. J. Rogers, J. K. Nash, M. H. Chen, B. G. Wilson *et al.*, "Absorption experiments on x-ray-heated mid-Z constrained samples," *Phys. Rev. E* **54**, 5617 (1996).
- <sup>101</sup>J. E. Bailey, G. A. Rochau, C. A. Iglesias, J. Abdallah, Jr., J. J. MacFarlane, I. Golovkin, P. Wang, R. C. Mancini, P. W. Lake, T. C. Moore, M. Bump, O. Garcia, and S. Mazevet, "Iron-plasma transmission measurements at temperatures above 150 eV," *Phys. Rev. Lett.* **99**, 265002 (2007).
- <sup>102</sup>T. Nagayama, J. E. Bailey, G. P. Loisel, G. S. Dunham, G. A. Rochau, C. Blancard, J. Colgan, P. Cosse, G. Faussurier, C. J. Fontes *et al.*, "Systematic study of L-shell opacity at stellar interior temperatures," *Phys. Rev. Lett.* **122**, 235001 (2019).
- <sup>103</sup>J. R. Asay, "Isentropic compression experiments on the Z accelerator," *AIP Conf. Proc.* **505**, 261 (2000).
- <sup>104</sup>J. R. Asay, C. A. Hall, K. G. Holland, M. A. Bernard, W. A. Stygar, R. B. Spielman, S. E. Rosenthal, D. H. McDaniel, and D. B. Hayes, "Isentropic compression of iron with the Z Accelerator," *AIP Conf. Proc.* **505**, 1151 (2000).
- <sup>105</sup>R. W. Lemke, M. D. Knudson, C. A. Hall, T. A. Haill, M. P. Desjarlais, J. R. Asay, and T. A. Mehlhorn, "Characterization of magnetically accelerated flyer plates," *Phys. Plasmas* **10**, 1092 (2003).
- <sup>106</sup>J.-P. Davis, "Experimental measurement of the principal isentrope for aluminum 6061-T6 to 240 GPa," *J. Appl. Phys.* **99**, 103512 (2006).
- <sup>107</sup>M. D. Knudson, D. L. Hanson, J. E. Bailey, C. A. Hall, J. R. Asay, and W. W. Anderson, "Equation of state measurements in liquid deuterium to 70 GPa," *Phys. Rev. Lett.* **87**, 225501 (2001).
- <sup>108</sup>J. R. Asay, L. C. Chhabildas, R. Jeffery Lawrence, and M. A. Sweeney, *Impactful Times: Memories of 60 Years of Shock Wave Research at Sandia National Laboratories* (Springer, Cham, Switzerland, 2017).
- <sup>109</sup>J.-P. Davis, C. Deeney, M. D. Knudson, R. W. Lemke, T. D. Pointon, and D. E. Bliss, "Magnetically driven isentropic compression to multi-megabar pressures using shaped current pulses on the Z accelerator," *Phys. Plasmas* **12**, 056310 (2005).
- <sup>110</sup>K. R. LeChien, W. A. Stygar, M. E. Savage, P. E. Wakeland, V. Anaya, D. S. Artery, M. J. Baremore, D. E. Bliss, R. Chavez, G. D. Coombs *et al.*, "6.1-MV, 0.79-MA laser-triggered gas switch for multimodule, multiterawatt pulsed-power accelerators," *Phys. Rev. Accel. Beams* **13**, 030401 (2010).
- <sup>111</sup>P. A. Corcoran, B. A. Whitney, V. L. Bailey, I. D. Smith, W. A. Stygar, M. E. Savage, G. A. Rochau, J. E. Bailey, B. M. Jones, T. J. Nash *et al.*, "Circuit modeling techniques applied to ZR," in Proceedings of the 17th IEEE International Pulsed Power Conference (2009), pp. 150-155.
- <sup>112</sup>B. T. Hutsel, P. A. Corcoran, M. E. Cuneo, M. R. Gomez, M. H. Hess, D. D. Hinshelwood, C. A. Jennings, G. R. Laity, D. C. Lamppa, R. D. McBride *et al.*, "Transmission-line-circuit model of an 85-TW, 25-MA pulsed-power accelerator," *Phys. Rev. Accel. Beams* **21**, 030401 (2018).
- <sup>113</sup>C. T. Seagle, J.-P. Davis, M. R. Martin, and H. L. Hanshaw, "Shock-ramp compression: Ramp compression of shock-melted tin," *Appl. Phys. Lett.* **102**, 244104 (2013).
- <sup>114</sup>C. T. Seagle, J.-P. Davis, and M. D. Knudson, "Mechanical response of lithium fluoride under off-principal dynamic shock-ramp loading," *J. Appl. Phys.* **120**, 165902 (2016).
- <sup>115</sup>A. J. Porwitzky, C. T. Seagle, and B. J. Jensen, "Zero to 1,600 m/s in 40 microns: Sensitive pulse shaping for materials characterization on Z," *Proc. Eng.* **204**, 337 (2017).
- <sup>116</sup>D. B. Seidel, W. L. Langston, R. S. Coats, M. D. Knudson, R. W. Lemke, J.-P. Davis, and T. D. Pointon, "An optimization study of stripline loads for isentropic compression experiments," in IEEE Pulsed Power Conference (2009), pp. 1165-1170.
- <sup>117</sup>R. G. Kraus, J.-P. Davis, C. T. Seagle, D. E. Fratanduono, D. C. Swift, J. L. Brown, and J. H. Eggert, "Dynamic compression of copper to over 450 GPa: A high-pressure standard," *Phys. Rev. B* **93**, 134105 (2016).
- <sup>118</sup>R. W. Lemke, M. D. Knudson, and J.-P. Davis, "Magnetically driven hypervelocity launch capability at the Sandia Z accelerator," *Int. J. Impact Eng.* **38**, 480 (2011).

- <sup>119</sup>A. C. Robinson, T. A. Brunner, and S. Carroll, "ALEGRA: An arbitrary Lagrangian-Eulerian multimaterial, multiphysics code," AIAA Paper No. 2008-1235, 2008.
- <sup>120</sup>K. R. Cochrane, R. W. Lemke, Z. Riford, and J. H. Carpenter, "Magnetically launched flyer plate technique for probing electrical conductivity of compressed copper," *J. Appl. Phys.* **119**, 105902 (2016).
- <sup>121</sup>M. P. Desjarlais, "Quantum molecular dynamics simulations for generating equation of state data," *AIP Conf. Proc.* **1161**, 32 (2009).
- <sup>122</sup>S. Root, L. Shulenberg, R. W. Lemke, D. H. Dolan, T. R. Mattsson, and M. P. Desjarlais, "Shock response and phase transitions of MgO at planetary impact conditions," *Phys. Rev. Lett.* **115**, 198501 (2015).
- <sup>123</sup>T. R. Mattsson, J. M. D. Lane, K. R. Cochrane, M. P. Desjarlais, A. P. Thompson, F. Pierce, and G. S. Grest, "First-principles and classical molecular dynamics simulation of shocked polymers," *Phys. Rev. B* **81**, 054103 (2010).
- <sup>124</sup>S. Root, R. J. Magyar, J. H. Carpenter, D. L. Hanson, and T. R. Mattsson, "Shock compression of a fifth period element: Liquid xenon to 840 GPa," *Phys. Rev. Lett.* **105**, 085501 (2010).
- <sup>125</sup>T. R. Mattsson, K. R. Cochrane, J. M. D. Lane, and S. Root, "Simulations of hydrocarbon polymers related to compression experiments on Sandia's Z machine," in *Computational Approaches for Chemistry under Extreme Conditions*, edited by N. Goldman (Springer, 2019).
- <sup>126</sup>M. D. Knudson and M. P. Desjarlais, "High-precision shock wave measurements of deuterium: Evaluation of exchange-correlation functionals at the molecular-to-atomic transition," *Phys. Rev. Lett.* **118**, 035501 (2017).
- <sup>127</sup>L. Shulenberg and T. R. Mattsson, "Quantum Monte Carlo applied to solids," *Phys. Rev. B* **88**, 245117 (2013).
- <sup>128</sup>R. C. Clay, M. P. Desjarlais, and L. Shulenberg, "Deuterium Hugoniot: Pitfalls of thermodynamic sampling beyond density functional theory," *Phys. Rev. B* **100**, 075103 (2019).
- <sup>129</sup>A. D. Baczewski, L. Shulenberg, M. P. Desjarlais, S. B. Hansen, and R. J. Magyar, "X-ray Thomson scattering in warm dense matter without the Chihara decomposition," *Phys. Rev. Lett.* **116**, 115004 (2016).
- <sup>130</sup>M. P. Desjarlais, "Practical improvements to the Lee-More conductivity near the metal-insulator transition," *Contrib. Plasma Phys.* **41**, 267 (2001).
- <sup>131</sup>M. P. Desjarlais, J. D. Kress, and L. A. Collins, "Electrical conductivity for warm, dense aluminum plasmas and liquids," *Phys. Rev. E* **66**, 025401 (2002).
- <sup>132</sup>L. M. Barker and R. E. Hollenbach, "Laser interferometer for measuring high velocities of any reflective surface," *J. Appl. Phys.* **43**, 4669 (1972).
- <sup>133</sup>O. T. Strand, D. R. Goosman, C. Martinez, and T. L. Whitworth, "Compact system for high-speed velocimetry using heterodyne techniques," *Rev. Sci. Instrum.* **77**, 83108 (2006).
- <sup>134</sup>D. H. Dolan, R. W. Lemke, R. D. McBride, M. R. Martin, E. Harding, D. G. Dalton, B. E. Blue, and S. S. Walker, "Tracking an imploding cylinder with photonic Doppler velocimetry," *Rev. Sci. Instrum.* **84**, 55102 (2013).
- <sup>135</sup>D. H. Dolan, K. Bell, B. Fox, S. C. Jones, P. Knapp, M. R. Gomez, M. Martin, A. Porwitzky, and G. Laity, "Plasma and radiation detection via fiber interferometry," *J. Appl. Phys.* **123**, 034502 (2018).
- <sup>136</sup>G. Dunham, J. E. Bailey, A. Carlson, P. Lake, and M. D. Knudson, "Diagnostic methods for time-resolved optical spectroscopy of shocked liquid deuterium," *Rev. Sci. Instrum.* **75**, 928 (2004).
- <sup>137</sup>J. E. Bailey, M. D. Knudson, A. L. Carlson, G. S. Dunham, M. P. Desjarlais, D. L. Hanson, and J. R. Asay, "Time-resolved optical spectroscopy measurements of shocked liquid deuterium," *Phys. Rev. B* **78**, 144107 (2008).
- <sup>138</sup>M. D. Knudson, M. P. Desjarlais, and R. W. Lemke, "Shock compression experiments on lithium deuteride (LiD) single crystals," *J. Appl. Phys.* **120**, 235902 (2016).
- <sup>139</sup>M. D. Knudson, M. P. Desjarlais, A. Becker, R. W. Lemke, K. R. Cochrane, M. E. Savage, D. E. Bliss, T. R. Mattsson, and R. Redmer, "Direct observation of an abrupt insulator-to-metal transition in dense liquid deuterium," *Science* **348**, 1455 (2015).
- <sup>140</sup>T. Ao, M. S. Schollmeier, P. Kalita, P. D. Gard, J. R. Williams, C. B. Blada, H. L. Hanshaw, I. C. Smith, J. E. Shores, C. S. Speas, and C. T. Seagle, "A spherical crystal diffraction imager for Sandia's Z pulsed power facility," *Rev. Sci. Instrum.* **91**, 043106 (2020).
- <sup>141</sup>T. Ao, M. S. Schollmeier, P. Kalita, P. D. Gard, J. R. Williams, C. B. Blada, H. L. Hanshaw, I. C. Smith, J. E. Shores, C. S. Speas, and C. T. Seagle, "X-ray diffraction of dynamically compressed matter on Sandia's Z pulsed power facility," Report No. SAND2019-11868, 2019.
- <sup>142</sup>S. Root, J. P. Townsend, E. Davies, R. W. Lemke, D. E. Bliss, D. E. Fratanduono, R. G. Kraus, M. Millot, D. K. Spaulding, L. Shulenberg, S. T. Stewart, and S. B. Jacobsen, "The principal Hugoniot of forsterite to 950 GPa," *Geophys. Res. Lett.* **45**, 3865, <https://doi.org/10.1029/2017GL076931> (2018).
- <sup>143</sup>J. L. Brown, C. S. Alexander, J. R. Asay, T. J. Vogler, D. H. Dolan, and J. L. Belof, "Flow strength of tantalum under ramp compression to 250 GPa," *J. Appl. Phys.* **115**, 043530 (2014).
- <sup>144</sup>M. D. Knudson, M. P. Desjarlais, and D. H. Dolan, "Shock-wave exploration of the high-pressure phases of carbon," *Science* **322**, 1822 (2008).
- <sup>145</sup>J. L. Brown and L. B. Hund, "Estimating material properties under extreme conditions by using Bayesian model calibration with functional output," *J. R. Stat. Soc., Ser. C-Appl. Stat.* **67**, 1023-1045 (2018).
- <sup>146</sup>M. D. Knudson and M. P. Desjarlais, "Shock compression of quartz to 1.6 TPa: Redefining a pressure standard," *Phys. Rev. Lett.* **103**, 225501 (2009).
- <sup>147</sup>S. Root, J. P. Townsend, and M. D. Knudson, "Shock compression response of fused silica: An impedance matching standard," *J. Appl. Phys.* **126**, 165901 (2019).
- <sup>148</sup>S. Root, T. R. Mattsson, K. Cochrane, R. W. Lemke, and M. D. Knudson, "Shock response of poly(4-methyl-1-pentene) (PMP) to 985 GPa," *J. Appl. Phys.* **118**, 205901 (2015).
- <sup>149</sup>M. D. Knudson and R. W. Lemke, "Shock response of low-density silica aerogel in the multi-Mbar regime," *J. Appl. Phys.* **114**, 053510 (2013).
- <sup>150</sup>M. D. Knudson and M. P. Desjarlais, "Adiabatic release measurements in  $\alpha$ -quartz between 300 and 1200 GPa: Characterization of  $\alpha$ -quartz as a shock standard in the multi-megabar regime," *Phys. Rev. B* **88**, 184107 (2013).
- <sup>151</sup>M. P. Desjarlais, M. D. Knudson, and K. R. Cochrane, "Extension of the Hugoniot and analytical release model of  $\alpha$ -quartz to 0.2-3 TPa," *J. Appl. Phys.* **122**, 035903 (2017).
- <sup>152</sup>A. Fernandez-Pañella, M. Millot, D. E. Fratanduono, M. P. Desjarlais, S. Hamel, M. C. Marshall, D. J. Erskine, P. A. Sterne, S. Haan, T. R. Boehly, G. W. Collins, J. H. Eggert, and P. M. Celliers, "Shock compression of liquid deuterium up to 1 TPa," *Phys. Rev. Lett.* **122**, 255702 (2019).
- <sup>153</sup>M. D. Knudson, M. P. Desjarlais, and A. Pribram-Jones, "Adiabatic release measurements in aluminum between 400 and 1200 GPa: Characterization of aluminum as a shock standard in the multi-megabar regime," *Phys. Rev. B* **91**, 224105 (2015).
- <sup>154</sup>C. A. McCoy, M. D. Knudson, and M. P. Desjarlais, "Sound velocity, shear modulus, and shock melting of beryllium along the Hugoniot," *Phys. Rev. B* **100**, 054107 (2019).
- <sup>155</sup>S. P. Lyon and J. D. Johnson, "SESAME: The Los Alamos National Laboratory equation of state database," Report No. LA-UR-92-3407, Los Alamos National Laboratory, 1992.
- <sup>156</sup>L. X. Benedict, T. Ogitsu, A. Trave, C. J. Wu, P. A. Sterne, and E. Schwegler, "Calculations of high-pressure properties of beryllium: Construction of a multiphase equation of state," *Phys. Rev. B* **79**, 064106 (2009).
- <sup>157</sup>W. M. Isbell, F. H. Shipman, and A. H. Jones, "Hugoniot equation of state measurements for eleven materials to five megabars," Report No. MSL-68-13, General Motors Corporation Materials and Structures Laboratory, 1968.
- <sup>158</sup>E. Wigner and H. B. Huntington, "On the possibility of a metallic modification of hydrogen," *J. Chem. Phys.* **3**, 764 (1935).
- <sup>159</sup>W. Lorenzen, B. Holst, and R. Redmer, "Metallization in hydrogen-helium mixtures," *Phys. Rev. B* **84**, 235109 (2011).
- <sup>160</sup>S. N. Raymond, D. P. O'Brien, A. Morbidelli, and N. A. Kaib, "Building the terrestrial planets: Constrained accretion in the inner solar system," *Icarus* **203**, 644 (2009).
- <sup>161</sup>M. Cuk and S. T. Stewart, "Making the Moon from a fast-spinning Earth: A giant impact followed by resonant despinning," *Science* **338**, 1047 (2012).
- <sup>162</sup>R. G. Kraus, S. Root, R. W. Lemke, S. T. Stewart, S. B. Jacobsen, and T. R. Mattsson, "Impact vaporization of planetesimal cores in the late stages of planet formation," *Nat. Geosci.* **8**, 269 (2015).
- <sup>163</sup>E. J. Davies, P. J. Carter, S. Root, R. G. Kraus, D. K. Spaulding, S. T. Stewart, and S. B. Jacobsen, "Silicate melting and vaporization during rocky planet formation," *J. Geophys. Res.* **125**, e2019JE006227, <https://doi.org/10.1029/2019JE006227> (2020).

- <sup>164</sup>J.-P. Davis, M. D. Knudson, L. Shulenburg, and S. D. Crockett, "Mechanical and optical response of [100] lithium fluoride to multi-megabar dynamic pressures," *J. Appl. Phys.* **120**, 165901 (2016).
- <sup>165</sup>J.-P. Davis, J. L. Brown, M. D. Knudson, and R. W. Lemke, "Analysis of shockless dynamic compression data on solids to multi-megabar pressures: Application to tantalum," *J. Appl. Phys.* **116**, 204903 (2014).
- <sup>166</sup>J. L. Brown and L. B. Hund, "Estimating material properties under extreme conditions by using Bayesian model calibration with functional outputs," *J. R. Stat. Soc., Ser. C* **67**, 1023 (2018).
- <sup>167</sup>J. L. Brown, C. S. Alexander, J. R. Asay, T. J. Vogler, and J. L. Ding, "Extracting strength from high pressure ramp-release experiments," *J. Appl. Phys.* **114**, 223518 (2013).
- <sup>168</sup>D. G. Flicker, T. A. Arsenlis, R. Austin, N. R. Barton, J. F. Benage, C. A. Bronkhorst, J. L. Brown, S. L. Brown, W. T. Buttler, S.-R. Shen *et al.*, "The tri-lab tantalum strength consortium," in APS Shock Compression of Condensed Matter Meeting Abstracts (2017).
- <sup>169</sup>J. Lindl, "Development of the indirect-drive approach to inertial confinement fusion and the target physics basis for ignition and gain," *Phys. Plasmas* **2**, 3933 (1995).
- <sup>170</sup>S. A. Slutz, M. C. Herrmann, R. A. Vesey, A. B. Sefkow, D. B. Sinars, D. C. Rovang, K. J. Peterson, and M. E. Cuneo, "Pulsed-power-driven cylindrical liner implosions of laser preheated fuel magnetized with an axial field," *Phys. Plasmas* **17**, 056303 (2010).
- <sup>171</sup>D. B. Sinars, S. A. Slutz, M. C. Herrmann, R. D. McBride, M. E. Cuneo, K. J. Peterson, R. A. Vesey, C. Nakhleh, B. E. Blue, K. Killebrew *et al.*, "Measurements of magneto-Rayleigh-Taylor instability growth during the implosion of initially solid Al tubes driven by the 20-MA, 100-ns Z facility," *Phys. Rev. Lett.* **105**, 185001 (2010).
- <sup>172</sup>D. B. Sinars, S. A. Slutz, M. C. Herrmann, R. D. McBride, M. E. Cuneo, C. A. Jennings, J. P. Chittenden, A. L. Velikovich, K. J. Peterson, R. A. Vesey *et al.*, "Measurements of magneto-Rayleigh-Taylor instability growth during the implosion of initially solid metal liners," *Phys. Plasmas* **18**, 056301 (2011).
- <sup>173</sup>R. D. McBride, S. A. Slutz, C. A. Jennings, D. B. Sinars, M. E. Cuneo, M. C. Herrmann, R. W. Lemke, M. R. Martin, R. A. Vesey, K. J. Peterson *et al.*, "Penetrating radiography of imploding and stagnating beryllium liners on the Z accelerator," *Phys. Rev. Lett.* **109**, 135004 (2012).
- <sup>174</sup>R. D. McBride, M. R. Martin, R. W. Lemke, J. B. Greenly, C. A. Jennings, D. C. Rovang, D. B. Sinars, M. E. Cuneo, M. C. Herrmann, S. A. Slutz *et al.*, "Beryllium liner implosion experiments on the Z accelerator in preparation for magnetized liner inertial fusion," *Phys. Plasmas* **20**, 056309 (2013).
- <sup>175</sup>T. J. Awe, C. A. Jennings, R. D. McBride, M. E. Cuneo, D. C. Lamppa, M. R. Martin, D. C. Rovang, D. B. Sinars, S. A. Slutz, A. C. Owen *et al.*, "Modified helix-like instability structure on imploding z-pinch liners that are pre-implosion with a uniform axial magnetic field," *Phys. Plasmas* **21**, 056303 (2014).
- <sup>176</sup>I. R. Lindemuth and R. C. Kirkpatrick, "Parameter space for magnetized fuel targets in inertial confinement fusion," *Nucl. Fusion* **23**, 263 (1983).
- <sup>177</sup>I. R. Lindemuth and M. M. Widner, "Magnetohydrodynamic behavior of thermonuclear fuel in a preconditioned electron beam imploded target," *Phys. Fluids* **24**, 746 (1981).
- <sup>178</sup>S. A. Slutz and R. A. Vesey, "High-gain magnetized inertial fusion," *Phys. Rev. Lett.* **108**, 025003 (2012).
- <sup>179</sup>G. B. Zimmerman and W. L. Krueger, "Numerical simulation of laser-initiated fusion," *Comments Plasma Phys. Controlled Fusion* **2**, 51 (1975).
- <sup>180</sup>M. M. Marinak, R. E. Tipton, O. L. Landen, T. J. Murphy, P. Amendt, S. W. Haan, S. P. Hatchett, C. J. Keane, R. McEachern, and R. Wallace, "Three-dimensional simulations of Nova high growth factor capsule implosion experiments," *Phys. Plasmas* **3**, 2070 (1996).
- <sup>181</sup>J. P. Chittenden, S. V. Lebedev, C. A. Jennings, S. N. Bland, and A. Ciardi, "X-ray generation mechanisms in three-dimensional simulations of wire array Z-pinch," *Plasma Phys. Controlled Fusion* **46**, B457 (2004).
- <sup>182</sup>A. B. Sefkow, S. A. Slutz, J. M. Koning, M. M. Marinak, K. J. Peterson, D. B. Sinars, and R. A. Vesey, "Design of magnetized liner inertial fusion experiments using the Z facility," *Phys. Plasmas* **21**, 072711 (2014).
- <sup>183</sup>D. B. Sinars, K. J. Peterson, R. A. Vesey, C. Jennings, M. C. Herrmann, R. D. McBride, M. R. Martin, S. A. Slutz, E. P. Yu, B. E. Blue, and K. Tomlinson, "Fundamental magneto-Rayleigh-Taylor instability growth experiments on Z," in *55th Annual Meeting of American Physical Society Division of Plasma Physics* [Bull. Am. Phys. Soc. **58**(16), BP8.00120 (2013)].
- <sup>184</sup>D. D. Ryutov, M. S. Derzon, and M. K. Matzen, "The physics of fast z pinches," *Rev. Mod. Phys.* **72**, 167–223 (2000).
- <sup>185</sup>A. H. Nelson and M. G. Haines, "Analysis of the nature and growth of electrothermal waves," *Plasma Phys.* **11**, 811 (1969).
- <sup>186</sup>E. P. Velikhov, I. V. Novobrantsev, V. D. Pis'mennyi, A. T. Rakhimov, and A. N. Starostin, "Combined pumping of gas lasers," *Sov. Phys. Dokl.* **17**, 772 (1973).
- <sup>187</sup>M. G. Haines, "An electron thermal instability in a resistive non-equilibrium fully-ionized plasma," *J. Plasma Phys.* **12**, 1 (1974).
- <sup>188</sup>K. J. Peterson, D. B. Sinars, E. P. Yu, M. C. Herrmann, M. E. Cuneo, S. A. Slutz, I. C. Smith, B. W. Atherton, M. D. Knudson, and C. Nakhleh, "Electrothermal instability growth in magnetically driven pulsed power liners," *Phys. Plasmas* **19**, 092701 (2012).
- <sup>189</sup>V. I. Oreshkin, R. Baksht, N. Ratakhin, and A. V. Shishlov, "Wire explosion in vacuum: Simulation of as striation appearance," *Phys. Plasmas* **11**, 4771 (2004).
- <sup>190</sup>V. I. Oreshkin, "Overheat instabilities in the electric explosion of wires," *Tech. Phys. Lett.* **35**, 36 (2009).
- <sup>191</sup>V. I. Oreshkin, "Thermal instability during an electrical wire explosion," *Phys. Plasmas* **15**, 092103 (2008).
- <sup>192</sup>A. G. Roussikh, V. I. Oreshkin, S. A. Chaikovskiy, N. A. Labetytskaya, A. V. Shishlov, I. I. Beillis, and R. B. Baksht, "Study of the strata formation during the explosion of a wire in vacuum," *Phys. Plasmas* **15**, 102706 (2008).
- <sup>193</sup>K. J. Peterson, E. P. Yu, D. B. Sinars, M. E. Cuneo, S. A. Slutz, J. M. Koning, M. M. Marinak, C. Nakhleh, and M. C. Herrmann, "Simulations of electrothermal instability growth in solid aluminum rods," *Phys. Plasmas* **20**, 056305 (2013).
- <sup>194</sup>J. D. Pever and J. P. Chittenden, "Instability growth for magnetized liner inertial fusion seeded by electro-thermal, electro-choric, and material strength effects," *Phys. Plasmas* **22**, 102701 (2015).
- <sup>195</sup>K. J. Peterson, T. J. Awe, E. P. Yu, D. B. Sinars, E. S. Field, M. E. Cuneo, M. C. Herrmann, M. Savage, D. Schroen, K. Tomlinson, and C. Nakhleh, "Electrothermal instability mitigation by using thick dielectric coatings on magnetically imploded conductors," *Phys. Rev. Lett.* **112**, 135002 (2014).
- <sup>196</sup>T. J. Awe, K. J. Peterson, E. P. Yu, R. D. McBride, D. B. Sinars, M. R. Gomez, C. A. Jennings, M. R. Martin, S. E. Rosenthal, D. G. Schroen, A. B. Sefkow, S. A. Slutz, K. Tomlinson, and R. A. Vesey, "Experimental demonstration of the stabilizing effect of dielectric coatings on magnetically accelerated imploding metallic liners," *Phys. Rev. Lett.* **116**, 065001 (2016).
- <sup>197</sup>D. C. Rovang, D. C. Lamppa, M. E. Cuneo, A. C. Owen, J. McKenney, D. W. Johnson, S. Radovich, R. J. Kaye, R. D. McBride, C. S. Alexander *et al.*, "Pulsed-coil magnet system for applying uniform 10–30 T fields to centimeter-scale targets on Sandia's Z facility," *Rev. Sci. Instrum.* **85**, 124701 (2014).
- <sup>198</sup>T. J. Awe, R. D. McBride, C. A. Jennings, D. C. Lamppa, M. R. Martin, D. C. Rovang, S. A. Slutz, M. E. Cuneo, A. C. Owen, D. B. Sinars *et al.*, "Observations of modified three-dimensional instability structure for imploding z-pinch liners that are premagnetized with an axial field," *Phys. Rev. Lett.* **111**, 235005 (2013).
- <sup>199</sup>D. D. Ryutov, T. J. Awe, S. B. Hansen, R. D. McBride, K. J. Peterson, D. B. Sinars, and S. A. Slutz, "Effect of axial magnetic flux compression on the helical mode of the magnetic Rayleigh-Taylor instability (theory)," *AIP Conf. Proc.* **1639**, 63–66 (2014).
- <sup>200</sup>C. E. Seyler, M. R. Martin, and N. D. Hamlin, "Helical instability in MagLIF due to axial flux compression by low-density plasma," *Phys. Plasmas* **25**, 062711 (2018).
- <sup>201</sup>A. B. Sefkow, "On the helical instability and efficient stagnation pressure production in thermonuclear magnetized inertial fusion," invited talk at *58th Annual Meeting of American Physical Society Division of Plasma Physics* [Bull. Am. Phys. Soc. **61**(18), UI3.00006 (2016)].
- <sup>202</sup>D. A. Yager-Elorriaga, Y. Y. Lau, P. Zhang, P. C. Campbell, A. M. Steiner, N. M. Jordan, R. D. McBride, and R. M. Gilgenbach, "Evolution of sausage and helical modes in magnetized thin-foil cylindrical liners driven by a Z-pinch," *Phys. Plasmas* **25**, 056307 (2018).



- <sup>203</sup>M. R. Gomez, S. A. Slutz, A. B. Sefkow, D. B. Sinars, K. D. Hahn, S. B. Hansen, E. C. Harding, P. F. Knapp, P. F. Schmit, C. A. Jennings *et al.*, “Experimental demonstration of fusion-relevant conditions in magnetized liner inertial fusion,” *Phys. Rev. Lett.* **113**, 155003 (2014).
- <sup>204</sup>D. J. Ampleford, C. A. Jennings, E. C. Harding *et al.*, “Improved stability and reproducibility of magnetized liner inertial fusion experiments,” invited talk at the *60th Annual Meeting of American Physical Society Division of Plasma Physics* [Bull. Am. Phys. Soc. **63**(11), KI3.00001 (2018)].
- <sup>205</sup>P. F. Schmit, A. L. Velikovich, R. D. McBride, and G. K. Robertson, “Controlling Rayleigh-Taylor instabilities in magnetically driven solid metal shells by means of a dynamic screw pinch,” *Phys. Rev. Lett.* **117**, 205001 (2016).
- <sup>206</sup>G. A. Shipley, C. A. Jennings, and P. F. Schmit, “Design of dynamic screw pinch experiments for magnetized liner inertial fusion,” *Phys. Plasmas* **26**, 102702 (2019).
- <sup>207</sup>T. J. Awe, E. P. Yu, K. C. Yates, W. G. Yelton, B. S. Bauer, T. M. Hutchinson, S. Fuelling, and B. B. McKenzie, “On the evolution from micrometer-scale inhomogeneity to global overheated structure during the intense Joule heating of a z-pinch rod,” *IEEE Trans. Plasma Sci.* **45**, 584 (2017).
- <sup>208</sup>T. M. Hutchinson, T. J. Awe, B. S. Bauer, K. C. Yates, E. P. Yu, W. G. Yelton, and S. Fuelling, “Experimental observation of the stratified electrothermal instability on aluminum with thickness greater than a skin depth,” *Phys. Rev. E* **97**, 053208 (2018).
- <sup>209</sup>A. M. Steiner, P. C. Campbell, D. A. Yager-Elorriaga, K. R. Cochrane, T. R. Mattsson, N. M. Jordan, R. D. McBride, Y. Y. Lau, and R. M. Gilgenbach, “The electro-thermal stability of tantalum relative to aluminum and titanium in cylindrical liner ablation experiments at 550 kA,” *Phys. Plasmas* **25**, 032701 (2018).
- <sup>210</sup>E. P. Yu, T. J. Awe, K. R. Cochrane, K. C. Yates, T. M. Hutchinson, K. J. Peterson, and B. S. Bauer, “Use of hydrodynamic theory to estimate electrical current redistribution in metals,” *Phys. Plasmas* **27**, 052703 (2020).
- <sup>211</sup>M. R. Gomez, S. A. Slutz, A. B. Sefkow, K. D. Hahn, S. B. Hansen, P. F. Knapp, P. F. Schmit, C. L. Ruiz, D. B. Sinars, E. C. Harding *et al.*, “Demonstration of thermonuclear conditions in magnetized liner inertial fusion experiments,” *Phys. Plasmas* **22**, 056306 (2015).
- <sup>212</sup>M. Geissel, A. J. Harvey-Thompson, T. J. Awe, D. E. Bliss, M. E. Glinsky, M. R. Gomez, E. Harding, S. B. Hansen, C. Jennings, M. Kimmel *et al.*, “Minimizing scatter-losses during pre-heat for magneto-inertial fusion targets,” *Phys. Plasmas* **25**, 022706 (2018).
- <sup>213</sup>A. J. Harvey-Thompson, M. Geissel, C. A. Jennings, M. R. Weis, M. R. Gomez, J. R. Fein, D. J. Ampleford, G. A. Chandler, M. E. Glinsky, K. D. Hahn *et al.*, “Constraining preheat energy deposition in MagLIF experiments with multi-frame shadowgraphy,” *Phys. Plasmas* **26**, 032707 (2019).
- <sup>214</sup>S. A. Slutz, W. A. Stygar, M. R. Gomez, K. J. Peterson, A. B. Sefkow, D. B. Sinars, R. A. Vesey, E. M. Campbell, and R. Betti, “Scaling magnetized liner inertial fusion on Z and future pulsed-power accelerators,” *Phys. Plasmas* **23**, 022702 (2016).
- <sup>215</sup>S. B. Hansen, M. R. Gomez, A. B. Sefkow, S. A. Slutz, D. B. Sinars, K. D. Hahn, E. C. Harding, P. F. Knapp, P. F. Schmit, T. J. Awe *et al.*, “Diagnosing magnetized liner inertial fusion experiments on Z,” *Phys. Plasmas* **22**, 056313 (2015).
- <sup>216</sup>M. R. Gomez, S. A. Slutz, C. A. Jennings *et al.*, “Performance scaling in magnetized liner inertial fusion experiments” (unpublished).
- <sup>217</sup>P. F. Schmit, P. F. Knapp, S. B. Hansen, M. R. Gomez, K. D. Hahn, D. B. Sinars, K. J. Peterson, S. A. Slutz, A. B. Sefkow, T. J. Awe *et al.*, “Understanding fuel magnetization and mix using secondary nuclear reactions in magneto-inertial fusion,” *Phys. Rev. Lett.* **113**, 155004 (2014).
- <sup>218</sup>P. F. Knapp, P. F. Schmit, S. B. Hansen, M. R. Gomez, K. D. Hahn, D. B. Sinars, K. J. Peterson, S. A. Slutz, A. B. Sefkow, T. J. Awe *et al.*, “Effects of magnetization on fusion product trapping and secondary neutron spectra,” *Phys. Plasmas* **22**, 056312 (2015).
- <sup>219</sup>S. A. Slutz, M. R. Gomez, S. B. Hansen, E. C. Harding, B. T. Hutsel, P. F. Knapp, D. C. Lampapa, T. J. Awe, D. J. Ampleford, D. E. Bliss *et al.*, “Enhancing performance of magnetized liner inertial fusion at the Z facility,” *Phys. Plasmas* **25**, 112706 (2018).
- <sup>220</sup>S. A. Slutz, “Scaling of magnetized inertial fusion with drive current rise-time,” *Phys. Plasmas* **25**, 082707 (2018).
- <sup>221</sup>E. C. Harding, T. Ao, J. E. Bailey, G. Loisel, D. B. Sinars, M. Geissel, G. A. Rochau, and I. C. Smith, “Analysis and implementation of a space resolving spherical crystal spectrometer for x-ray Thomson scattering experiments,” *Rev. Sci. Instrum.* **86**, 043504 (2015).
- <sup>222</sup>M. R. Gomez, S. A. Slutz, P. F. Knapp, K. D. Hahn, M. R. Weis, E. C. Harding, M. Geissel, J. R. Fein, M. E. Glinsky, S. B. Hansen *et al.*, “Assessing stagnation conditions and identifying trends in magnetized liner inertial fusion,” *IEEE Trans. Plasma Sci.* **47**, 2081 (2019).
- <sup>223</sup>P. F. Knapp, M. R. Gomez, S. B. Hansen, M. E. Glinsky, C. A. Jennings, S. A. Slutz, E. C. Harding, K. D. Hahn, M. R. Weis, M. Evans *et al.*, “Origins and effects of mix on magnetized liner inertial fusion target performance,” *Phys. Plasmas* **26**, 012704 (2019).
- <sup>224</sup>A. J. Harvey-Thompson, M. R. Weis, E. C. Harding, M. Geissel, D. J. Ampleford, G. A. Chandler, J. R. Fein, M. E. Glinsky, M. R. Gomez, K. D. Hahn *et al.*, “Diagnosing and mitigating laser preheat induced mix in MagLIF,” *Phys. Plasmas* **25**, 112705 (2018).
- <sup>225</sup>O. A. Hurricane, D. A. Callahan, D. T. Casey, P. M. Celliers, C. Cerjan, E. L. Dewald, T. R. Dittrich, T. Doppner, D. E. Hinkel, L. F. Berzak-Hopkins *et al.*, “Fuel gain exceeding unity in an inertially confined fusion implosion,” *Nature* **506**, 343–349 (2014).
- <sup>226</sup>W. A. Stygar, P. A. Corcoran, H. C. Ives, R. B. Spielman, J. W. Douglas, B. A. Whitney, M. A. Mostrom, T. C. Wagoner, C. S. Speas, T. L. Gilliland *et al.*, “55-TW magnetically insulated transmission line system: Design, simulations, and performance,” *Phys. Rev. Accel. Beams* **12**, 120401 (2009).
- <sup>227</sup>For a history of studies and usage of MITLs to deliver power to the load in pulsed power drivers, see the following paper as well as references therein: J. P. VanDevender, T. D. Pointon, D. B. Seidel, K. W. Struve, C. Jennings, B. V. Oliver, and L. X. Schneider, “Requirements for self-magnetically insulated transmission lines,” *Phys. Rev. Accel. Beams* **18**, 030401 (2015).
- <sup>228</sup>M. R. Gomez, R. M. Gilgenbach, M. E. Cuneo, C. A. Jennings, R. D. McBride, E. M. Waisman, B. T. Hutsel, W. A. Stygar, D. V. Rose, and Y. Maron, “Experimental study of current loss and plasma formation in the Z-machine post hole convolute,” *Phys. Rev. Accel. Beams* **20**, 010401 (2017).
- <sup>229</sup>T. D. Pointon, W. A. Stygar, R. B. Spielman, H. C. Ives, and K. W. Struve, “Particle-in-cell simulations of electron flow in the post-hole convolute of the Z accelerator,” *Phys. Plasmas* **8**, 4534 (2001).
- <sup>230</sup>D. V. Rose, D. R. Welch, T. P. Hughes, R. E. Clark, C. B. Mostrom, and W. A. Stygar, “Plasma evolution and dynamics in high power vacuum transmission line post hole convolutes,” *Phys. Rev. Accel. Beams* **11**, 060401 (2008).
- <sup>231</sup>C. A. Jennings, J. P. Chittenden, M. E. Cuneo, W. A. Stygar, D. J. Ampleford, E. M. Waisman, M. Jones, M. E. Savage, K. R. LeChien, and T. C. Wagoner, “Circuit model for driving three-dimensional resistive MHD wire array z-pinch calculations,” *IEEE Trans. Plasma Sci.* **38**, 529 (2010).
- <sup>232</sup>T. C. Wagoner, W. A. Stygar, H. C. Ives, T. L. Gilliland, R. B. Spielman, M. F. Johnson, P. G. Reynolds, J. K. Moore, R. L. Mourning, D. L. Fehl *et al.*, “Differential-output B-dot and D-dot monitors for current and voltage measurements on a 20-MA, 3-MV pulsed power accelerator,” *Phys. Rev. Accel. Beams* **11**, 100401 (2008).
- <sup>233</sup>D. V. Rose, D. R. Welch, C. L. Miller, R. E. Clark, E. A. Madrid, C. B. Mostrom, T. C. Wagoner, J. K. Moore, W. A. Stygar, J. E. Bailey *et al.*, “10<sup>7</sup>-A load current B-dot monitor: Simulations, design, and performance,” *Phys. Rev. Accel. Beams* **13**, 040401 (2010).
- <sup>234</sup>A. Porwitzky and J. Brown, “Uncertainties in cylindrical anode current inferences on pulsed power drivers,” *Phys. Plasmas* **25**, 063102 (2018).
- <sup>235</sup>A. Porwitzky, D. H. Dolan, M. R. Martin, G. Laity, R. W. Lemke, and T. R. Mattsson, “Direct measurements of anode/cathode gap plasma in cylindrically imploding loads on the Z machine,” *Phys. Plasmas* **25**, 063110 (2018).
- <sup>236</sup>J. M. D. Lane, K. Leung, A. P. Thompson, and M. E. Cuneo, “Water desorption from rapidly heated metal oxide surfaces—First principles, molecular dynamics, and the Temkin isotherm,” *J. Phys.: Condens. Matter* **30**, 465002 (2018).
- <sup>237</sup>E. M. Waisman, M. P. Desjarlais, and M. E. Cuneo, “Ion current losses in the convolute and inner magnetically insulated transmission line on the Z machine,” *Phys. Rev. Accel. Beams* **22**, 030402 (2019).
- <sup>238</sup>J. J. Ramirez, “The Jupiter program,” in *10th IEEE International Pulsed Power Conference, Digest of Technical Papers* (1995), Vol. 1, pp. 91–98.

- <sup>239</sup>D. L. Cook, “Z, ZX, and X-1: A realistic path to high fusion yield,” in 12th IEEE International Pulsed Power Conference, Digest of Technical Papers (1999), Vol. 1, pp. 33–37.
- <sup>240</sup>K. W. Struve, J. P. Corley, D. L. Johnson, D. H. McDaniel, R. B. Spielman, and W. A. Stygar, “ZX pulsed-power design,” in 12th IEEE International Pulsed Power Conference, Digest of Technical Papers (1999), Vol. 1, pp. 493–496.
- <sup>241</sup>I. Smith, P. Corcoran, A. R. Miller, V. Carboni, P. Sincerny, P. Spence, C. Gilbert, W. Rix, E. Waisman, L. Schlitt, and D. Bell, “Pulse power for future and past X-ray simulators,” *IEEE Trans. Plasma Sci.* **30**, 1746 (2002).
- <sup>242</sup>W. A. Stygar, M. E. Cuneo, D. I. Headley, H. C. Ives, R. J. Leeper, M. G. Mazarakis, C. L. Olson, J. L. Porter, T. C. Wagoner, and J. R. Woodworth, “Architecture of petawatt-class z-pinch accelerators,” *Phys. Rev. Accel. Beams* **10**, 030401 (2007).
- <sup>243</sup>W. A. Stygar, T. J. Awe, J. E. Bailey, N. L. Bennett, E. W. Breden, E. M. Campbell, R. E. Clark, R. A. Cooper, M. E. Cuneo, J. B. Ennis *et al.*, “Conceptual designs of two petawatt-class pulsed-power accelerators for high-energy-density-physics experiments,” *Phys. Rev. Accel. Beams* **18**, 110401 (2015).
- <sup>244</sup>E. M. Williams and E. R. Schatz, “Design of exponential-line pulse transformers,” *Proc. IRE* **39**, pp. 84–86 (1951).
- <sup>245</sup>R. E. Matick, “Transmission line pulse transformers—Theory and applications,” *Proc. IEEE* **56**, pp. 47–62 (1968).
- <sup>246</sup>K. R. LeChien, M. E. Savage, V. Anaya, D. E. Bliss, W. T. Clark, J. P. Corley, G. Feltz, J. E. Garrity, D. W. Guthrie, K. C. Hodge *et al.*, “Development of a 5.4 MV laser triggered gas switch for multimodule, multimegampere pulsed power drivers,” *Phys. Rev. Accel. Beams* **11**, 060402 (2008).
- <sup>247</sup>P. Sincerny, M. Danforth, C. Gilbert, A. R. Miller, T. Naff, W. Rix, C. Stallings, E. Waisman, and L. Schlitt, “Concepts for an affordable high current imploding plasma generator,” in 12th IEEE International Pulsed Power Conference, Digest of Technical Papers (1999), Vol. 1, pp. 479–483.
- <sup>248</sup>P. Corcoran, I. Smith, P. Spence, A. R. Miller, E. M. Waisman, C. Gilbert, W. Rix, P. Sincerny, L. Schlitt, and D. Bell, “Pulse power for future x-ray simulators,” in 13th IEEE International Pulsed Power Conference, Digest of Technical Papers (2001), Vol. 1, pp. 577–581.
- <sup>249</sup>S. K. Lam, A. R. Miller, L. L. Sanders, P. Sincerny, and T. Tucker, “Fast discharge energy storage development for advanced x-ray simulators,” *IEEE Trans. Plasma Sci.* **33**, 982 (2005).
- <sup>250</sup>M. G. Mazarakis, W. E. Fowler, A. A. Kim, V. A. Sinebryukhov, S. T. Rogowski, R. A. Sharpe, D. H. McDaniel, C. L. Olson, J. L. Porter, K. W. Struve, W. A. Stygar, and J. R. Woodworth, “High current, 0.5-MA, fast, 100-ns, linear transformer driver experiments,” *Phys. Rev. Accel. Beams* **12**, 050401 (2009).
- <sup>251</sup>M. G. Mazarakis, M. E. Savage, W. E. Fowler, L. F. Bennett, M. Jones, F. W. Long, M. K. Matzen, D. H. McDaniel, R. G. McKee, J. L. McKenney *et al.*, “Experimental validation of the first 1-MA water-insulated MYKONOS LTD voltage adder,” in IEEE Pulsed Power Conference (2011), pp. 625–628.
- <sup>252</sup>J. R. Woodworth, W. E. Fowler, B. S. Stoltzfus, W. A. Stygar, M. E. Sceiford, M. G. Mazarakis, H. D. Anderson, M. J. Harden, J. R. Blickem, R. White, and A. A. Kim, “Compact 810 kA linear transformer driver cavity,” *Phys. Rev. Accel. Beams* **14**, 040401 (2011).
- <sup>253</sup>J. Leckbee, S. Cordova, B. Oliver, T. Webb, M. Toury, M. Caron, R. Rosol, B. Bui, T. Romero, and D. Ziska, “Linear transformer driver (LTD) research for radiographic applications,” in IEEE Pulsed Power Conference (2011), pp. 614–618.
- <sup>254</sup>J. D. Douglass, B. T. Hutsel, J. J. Leckbee, T. D. Mulville, B. S. Stoltzfus, M. L. Wisher, M. E. Savage, W. A. Stygar, E. W. Breden, and J. D. Calhoun, “100 GW linear transformer driver cavity: Design, simulations, and performance,” *Phys. Rev. Accel. Beams* **21**, 120401 (2018).
- <sup>255</sup>R. A. Vesey, M. C. Herrmann, R. W. Lemke, M. P. Desjarlais, M. E. Cuneo, W. A. Stygar, G. R. Bennett, R. B. Campbell, P. J. Christenson, T. A. Mehlhorn, J. L. Porter, and S. A. Slutz, “Target design for high fusion yield with the double z-pinch-driven hohlraum,” *Phys. Plasmas* **14**, 056302 (2007).
- <sup>256</sup>M. K. Matzen, C. Deeney, R. J. Leeper, J. L. Porter, R. B. Spielman, G. A. Chandler, M. S. Derzon, M. R. Douglas, D. L. Fehl, D. E. Hebron *et al.*, “Fast z-pinch as dense plasma, intense x-ray sources for plasma physics and fusion applications,” *Plasma Phys. Controlled Fusion* **41**, A175–A184 (1999).
- <sup>257</sup>A. Sessler and E. Wilson, *A Century of Particle Accelerators* (World Scientific Press, Singapore, 2007).
- <sup>258</sup>C. L. Nehl, R. J. Umstadtd, W. R. Regan, S. C. Hsu, and P. B. McGrath, “Retrospective of the ARPA-E ALPHA fusion program,” *J. Fusion Energy* **38**, 506 (2019).